České vysoké učení technické v Praze
Fakulta jaderná a fyzikálně inženýrská

Katedra fyziky
Obor: Fyzika a technika termojaderné fúze

Generace, ztráty a diagnostika ubíhajících elektronů v tokamacích

Generation, losses and detection of runaway electrons in tokamaks

MASTER'S THESIS

Author: Bc. Ondřej Ficker
Supervisor: Doc. RNDr. Jan Mlynář, Ph.D.
Year: 2015

Před svázáním místo téhle stránky vložíte zadání práce s podpisem děkana (bude to jediný oboustranný list ve Vaší práci) !!!!

Prohlášení

Prohlašuji, že jsem svou diplomovou práci vypracoval samostatně a použil jsem pouze podklady (literaturu, projekty, SW atd.) uvedené v přiloženém seznamu.

Nemám závažný důvod proti použití tohoto školního díla ve smyslu § 60 zákona č. 121/2000 Sb., o právu autorském, o právech souvisejících s právem autorským a o změně některých zákonů (autorský zákon).

V Praze dne .....

.....
Bc. Ondřej Ficker

Poděkování

Děkuji vedoucímu své diplomové práce doc. RNDr. Janu Mlynářovi, Ph.D. především za uvedení do světa experimentální práce na zařízeních fúzního výzkumu a za podnětné diskuze, které mou práci obohatily. Dále děkuji celému týmu tokamaku COMPASS, který svou pilnou prací zajišťuje stabilní provoz tohoto tokamaku. Jmenovitě děkuji dalším členům Runaway electron týmu, který vznikl v rámci MST2-9 projektu na tokamaku COMPASS - Mgr. Oleně Hronové, Ph.D., Mgr. Richardu Papřokovi a našemu srbskému kolegovi MSc. Miloši Vlainičovi, ale musím zmínit také další kolegy Ing. Martina Imríška, Mgr. Vladimíra Weinzettla, PhD. a RNDr. Jana Stöckela, CSc. Dále děkuji Ing. Vojtěchu Svobodovi, CSc. a týmu tokamaku Golem za možnost zkoušet nepříliš oblíbené výboje s produkcí ubíhajících elektronů i na tomto unikátním školním zařízení. Děkuji také profesoru RNDr. Petru Kulhánkovi, CSc. za nápady, které obhatily teoretickou část a našim zahraničním kolegům z CEA Cadarache i odjinud děkuji za komentáře k některým výsledkům uvedeným v této práci. V neposlední řadě děkuji také všem členům své rodiny, kteří mě celou dobu podporovali ve studiu.

Bc. Ondřej Ficker

Název práce:
Generace, ztráty a diagnostika ubíhajících elektronů v tokamacích

Autor: Bc. Ondřej Ficker

Obor: Fyzika a technika termojaderné fúze
Druh práce: Diplomová práce

Vedoucí práce: Doc. RNDr. Jan Mlynář, Ph.D.
Ústav fyziky plazmatu AV ČR

Abstrakt: Tato práce se věnuje tzv. ubíhajícím elektronům, které za určitých okolností vznikají v zařízeních typu tokamak určených pro výzkum termojaderné fúze s magnetickým udržením. Tyto energetické elektrony jsou urychlovány v elektrickém poli tokamaku takřka bez interakce s ostatními částicemi plazmatu, dosahují relativistických rychlostí a mohou způsobit značné poškození nejrůznějších komponent uvnitř vakuové nádoby tokamaku. Práce stručně shrnuje teoretické odvození ubíhajícího řešení kinetické rovnice a další fyzikální vlastnosti ubíhajících elektronů. Teoretické vztahy jsou následně aplikovány na konkrétní parametry tokamaků COMPASS a Golem. Interpretace dat naměřených na těchto zařízeních se soustředí především na objasnění souvislosti mezi procesy magnetické rekonekce při tzv. pilové nestabilitě a výtrysky ubíhajících elektronů. Podle výsledků z tokamaku COMPASS jsou energetické elektrony při těchto jevech pouze vyvrhovány a ne generovány.

Klíčová slova: ubíhající elektrony, tokamak, diagnostika plazmatu, tvrdé rentgenové záření, pilová nestabilita

Title:
Generation, losses and detection of runaway electrons in tokamaks

Author: Bc. Ondřej Ficker

Abstract: This thesis is focused on the so called runaway electrons that are generated in tokamaks under particular conditions. These energetic electrons are accelerated in the electric field of tokamak almost without collisions with thermal plasma particles and may cause large damage to the components inside the vacuum vessel. The brief derivation of runaway solution is given in the thesis and other properties of runaway electrons are summarised. The theoretical relations are subsequently applied to plasmas of COMPASS and Golem tokamaks. The analysis of data measured on COMPASS is focused namely on the investigation of the link between the processes of magnetic reconnection during the saw-tooth instability and bursts of runaway electrons. According to the COMPASS results, the energetic electrons are just ejected and not generated during these phenomena.

Key words: runaway electrons, tokamak, plasma diagnostics, HXR radiation, saw-tooth instability

Contents

Introduction

The rising demand for the energy

During the last decade, the age-long rising demand for the energy may have seemed to be stagnant or even satisfied. Energy consumption in Europe and North America is stable or even slightly decreasing as a part of the industrial infrastructure was moved to the cheaper regions. The situation is so comfortable that some of the most advanced economies intend to leave one of the most important achievements of the 20^{th} century - nuclear fission power plants. The trigger of this decision was the Fukushima Daichi disaster, severe, albeit caused namely by local tectonic conditions and failure of human factor. Some European countries, e. g. Germany responded to this disaster with huge investments into renewable energy and other, not so popular steps - development of coal power technologies and massive evolution of the distribution network. So far it seems that Germany copes with its "Energiewende" quite well, but most of the nuclear power plants are still working. There is a question, how the electricity supplies to regions far from the winds of Northern Sea will be secured. One thing is certain, it would not be possible without coal and gas, the fuels with limited reserves.

On the other hand, there are quickly developing countries, e. g. China. This rising giant has been building tens of nuclear reactors and consuming more than one third of world coal production. India may soon reach similar numbers. Furthermore, according to the International Energy Agency, there are still 1.3 billion people without access to electrical energy in the world [61]. The expected rise in developing countries will definitely overcome any possible decrease of energy consumption in the developed countries due to the increased efficiency of electricity usage. The US could serve as an example of such developed country with stable and predictable electricity production. Despite this, slow increase of electricity generation is predicted (see Figure 1). The growth in China and other expanding economies would be much more desperate.

If we take into account that the electricity will conquer new sectors of energy market via utilisation of electric cars, it is obvious that humankind will need a strong energy source not based on the fossil fuels. Renewable sources of energy are suitable for small production and remote regions but it will hardly ever be the only source of energy. Renewable sources fail to power the industry and megapoles as they work only under proper circumstances and will always need giant energy-storing facilities.

Nuclear fission could solve the energy problem for many centuries. Unfortunately, western civilisation tends to fear fission technologies. This situation leaves a single possible long-term solution - the fusion.

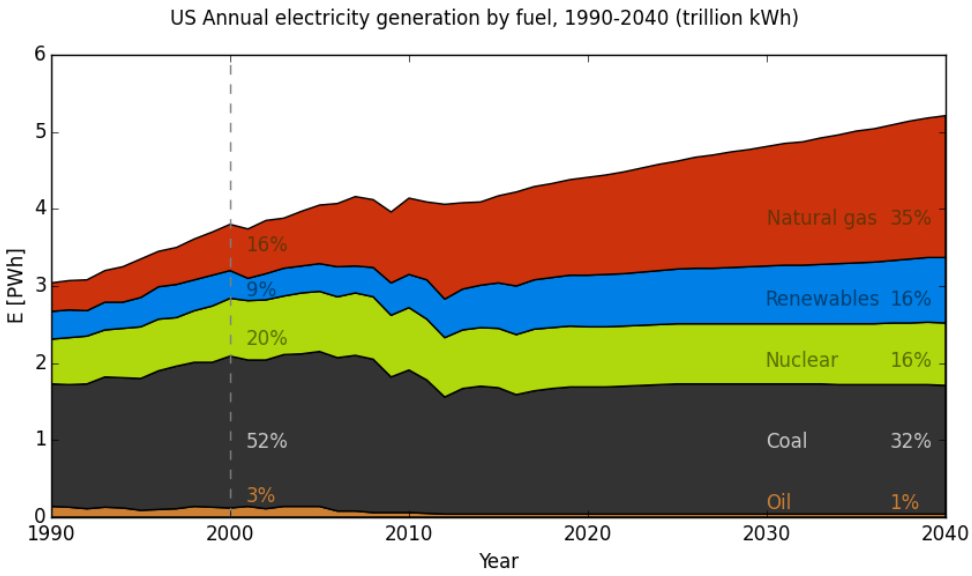

Figure 1: Historical development and prediction of the electricity generation by source in the US. Shell gas will take dominant role in next decades and the overall electricity generation will be rising. Source of data: EIA.

Fusion

Sun is a shining example of a working fusion reactor that has by far the main contribution to our own existence. Similar reactions, that power our star, are feasible on smaller scales and there is enough fuel for billions of years just on Earth. Fusion is inherently safe, it produces no radioactive waste and the activation of the reactor components can be made significantly lower than in fission power plants. Moreover, the sources of the fusion fuel are well distributed around the globe, namely in comparison with oil and uranium.

The benefits of fusion are large, however, it is a difficult way to go. The devices called "fusion reactors for energy generation" were continuously developed and even patented since the WWII albeit after seventy years of research we do not have a single device worth this name. The challenge of harnessing the fusion power is among those that are well defined and seem so hard to reach. Some very old goals of this kind have been finally conquered in the 20$^{\text{th}}$ century, but even more of them have arisen.

People, by their nature, prefer simple solutions and so far it is obvious that the controlled fusion does not offer such a solution. Large fusion experiments are extreme jigsaws uniting the high-end technologies with the state-of-the-art physics. None of the "easier alternative ways" seem to work so we have to carry on this expensive research before it is too late. We can not afford not to try.

Tokamaks and runaway electrons

Current research of fusion plasma confinement is focused on tokamaks, the devices with long history and best experimental results among all concepts of magnetic confinement fusion. The word tokamak is an abbreviation of the Russian term for the toroidal chamber

with magnetic coils (see Figure). In these devices, the plasma is confined by the dominant toroidal magnetic field and primarily heated by current flowing in the toroidal direction. This current is generated by an external electric field. The tokamak community currently looks up to the final stage of the fusion research - the ITER (International Thermonuclear Experimental Reactor) project. This large reactor is designed to finally reach the break-even. This means that the energy generated by the fusion reactions balances the energy supplied by the heating systems. In fact, in ITER the former overcomes the latter by ten times. This would be an important step on the way to the power plant, although it does not mean net electricity generation, yet.

Unfortunately the plasma tends to be unstable in many ways. A large group of instabilities is connected with plasma due to its nature of a conductive fluid in a magnetic field. In such a fluid, various kinds of unstable waves, local isolated regions (magnetic islands) and other phenomena (magnetohydrodynamic - MHD - instabilities in general) may occur. These instabilities are usually degrading the confinement and fusion power. Except of these fluid instabilities, there is another group connected to the velocity distribution of plasma particles. These instabilities are called kinetic instabilities and uncontrolled acceleration of fast electrons is among them. Indeed, the toroidal electric field - if large enough - could raise problems by overcoming the collisional drag and accelerating some of the plasma electrons to relativistic energies. The beam of so called runaway electrons (RE) presents one of the most dangerous issues to the plasma facing components (PFC) due to its ability to deposit large power into a small area.

The conditions for the RE beam creation in large tokamaks are not fulfilled during normal operation, albeit in smaller tokamaks the beam may arise during the plasma breakdown (at the beginning of the discharge). The fields sufficient for the RE beam generation may also arise due to some plasma instabilities and namely due to the sudden termination of the plasma current - the disruption. The number of RE created by an over-critical electric field could be multiplied by the avalanche mechanism: fast electrons knock on thermal electrons and make them runaway, while staying in the runaway region of velocity space. The mechanisms of the RE generation will be detailed in the chapter 2.

The RE may stay confined and interact with plasma instabilities. However, the RE beam is hard to control and it eventually crashes into PFC. The consequences of such impact would be tremendous in ITER as the predicted RE current is up to 12 MA. Therefore, it is necessary to stop the RE generation or mitigate the beam in the early stages. Due to these facts, intensive experimental efforts are focused on RE in many tokamaks, including the Czech tokamak COMPASS as a part of coordinated European research. For the author of this thesis, participation in this project is a great opportunity to gain experience in the field of fusion research and contribute to this important topic.

This thesis summarises the basic theoretical models and issues connected with runaway electrons (chapters 1 and 2), the recent experimental results of COMPASS and Golem tokamaks are described and analysed in chapter 3. However, the main effort of this thesis is focused on correlation of RE bursts with magnetic reconnection phenomena (chapter 4).

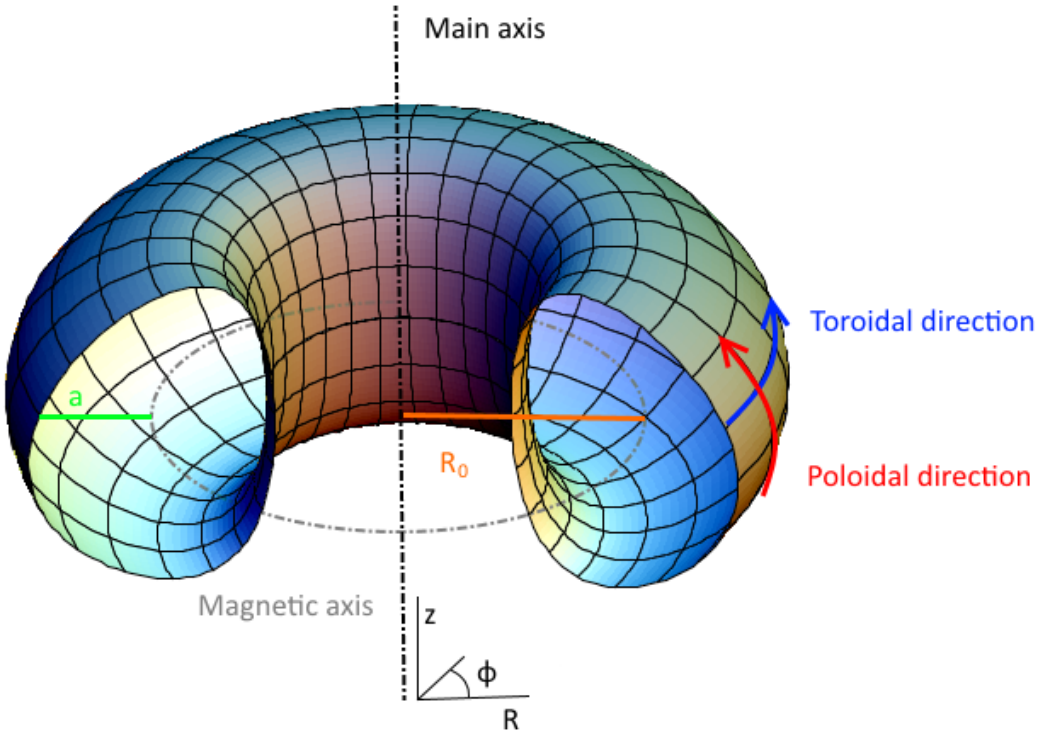

Figure 2: The cut of the toroid with the D-shape cross-section, a typical shape of tokamak vacuum chamber. Toroidal and poloidal directions that correspond to main components of magnetic field in tokamak are displayed. Also main (major) axis of symetry and so called magnetic axis are visualised together with major radius R_0 and minor radius a. The deifnition of these quantities is not so clear as for standard torus. Magnetic axis is not fixed during the experiments and R_0 is correctly defined as the distance between main axis and geometrical centre of poloidal cross-section and for minor radius $a = R_{max} - R_0$, where R_{max} is the radial coordinate of the point most distant from the major axis. To describe the shape of the non-circular cross-section completly, two additional parameters - elongation κ and triangularity δ - must be defined. The cylindrical coordinated system (R, z, ϕ) drawed in the bottom is one of the options, however radial coordinate r related to magntic axis and minor radius and poloidal angle θ may be used in toroidal system (r, θ, ϕ). The best way to describe the tokamak plasma is probably the utisilation of magnetic flux surfaces Ψ of arbitrary shape instead of r in (Ψ, θ, ϕ) coordinate system. Image generated by '3D-XplorMath-J' software and ajusted in Paint.NET.

Chapter 1

Physics background

1.1 Plasma

The fusion fuel in a thermonuclear reactor is confined in the form of a plasma. Plasma is by the definition a **quasi-neutral system** of charged (and neutral) particles that **behaves collectively**. The first term in bold means that the electrical charge of every macroscopic volume is zero. The collective behaviour is possible because of the long range Coulomb interaction between the particles. Plasma interacts with external electromagnetic fields and the particles are affected by fields generated by other particles. Therefore, plasma is a self-consistent system and it is difficult to find numerical solution describing various processes in plasma.
The most important plasma parameters are electron density n_e, electron temperature T_e and the same quantities n_i, T_i describing ions. Furthermore, the plasma in tokamak is affected by the magnitude of the magnetic field B and plasma current I_p. The values of these parameters define the time and space scale of the plasma processes. The three most important characteristic frequencies of magnetised plasma are

$$\omega_{p\alpha}^2 = \frac{Q_\alpha^2 n_\alpha}{\epsilon_0 m_\alpha} \qquad \omega_{c\alpha} = \frac{Q_\alpha B}{m_\alpha} \qquad \nu_{\alpha\beta} = \frac{n_e Q_\alpha^2 Q_\beta^2 \ln(\lambda)}{4\pi\epsilon_0^2 m_e^2 * c^3}, \tag{1.1}$$

which corresponds to plasma frequency (frequency of plasma oscillations), cyclotron frequency (gyration around the vector of the magnetic field) and collisional frequency, respectively. Indices α, β mark the type of the plasma particles - electrons or ions of fuel or impurity isotopes in arbitrary ionisation states, Q is the charge of the particle, m is the mass of the particle and ϵ_0 is the permittivity of vacuum.
Complementary characteristic lengths may be defined to these characteristic frequencies

$$\lambda_D^2 = \frac{\epsilon_0 m_\alpha}{\sum_\alpha Q_\alpha^2 n_\alpha / T_\alpha} \qquad r_{L\alpha} = \frac{m_\alpha \mathrm{v}_\perp}{Q_\alpha B} \qquad \lambda_\alpha = \frac{\mathrm{v}_{T\alpha}}{\nu_{\alpha\beta}}, \tag{1.2}$$

the first quantity is the Debye length (a shielding length of a charge in a plasma), the second quantity is the Larmor radius (a radius of a cyclic motion of a particle with a perpendicular component of velocity $\mathrm{v}_\perp$ around the magnetic field line) and the last one is the mean free path of particle that is a function of a thermal velocity $\mathrm{v}_{T\alpha}$. Notice that

the mean free path in plasma is defined as the length of path of particle corresponding to the change of direction of motion by 90°. The particle interacts with many other particles simultaneously, therefore, the traditional understanding of collisional frequency can not be used. However, the runaway electrons could not be treated the same way as the background plasma. These electrons have kinetic energy that can overcome their rest energy many times and the collisional interaction between these particles and the background plasma is weak. Therefore, description of the RE physics should start with the relativistic equation of motion in external magnetic and electric fields. In fact, as will be shown in further text, low density tokamak plasma with strong runaway electron beam can be compared to betatron operation.

1.2 Relativistic single particle motion in external fields

The relativistic equation of motion

$$\frac{\mathrm{d}\mathbf{p}}{\mathrm{d}t} = e(\mathbf{E} + \mathbf{v} \times \mathbf{B}) \tag{1.3}$$

is the relation between the time evolution of the relativistic particle momentum $\mathbf{p}$ and applied electric ($\mathbf{E}$) and magnetic ($\mathbf{B}$) fields. The relativistic momentum is defined

$$\mathbf{p} = \gamma m_0 \mathbf{v} \qquad \gamma = \sqrt{1 - \frac{\mathrm{v}^2}{c^2}} = \sqrt{1 + \left(\frac{p}{m_e c}\right)^2}, \tag{1.4}$$

where m_0 is the rest mass, $\mathbf{v}$ is the velocity of the particle and γ is the Lorentz factor. In order to find solutions of relativistic problems, the definition of relativistic energy is useful

$$\mathcal{E} = \sqrt{m_0^2 c^4 + \mathbf{p}^2 c^2} \qquad \mathbf{v}_\perp = \frac{\mathbf{p}_\perp c^2}{\mathcal{E}} \tag{1.5}$$

Let the relativistic particle with random initial velocity move along a line with parallel electric and magnetic fields. This may serve as the very basic model of runaway electron acceleration in tokamak without considering the friction force and effects of the toroidal geometry. This situation may be solved analytically component by component or by some specialised numerical solver. In this simple single particle case we could use high precision energy conserving algorithms, e. g. relativistic Boris-Buneman (BB) solver that was developed specially for this type of problems. This attitude is necessary in situations with fast temporal evolution or strong spatial dependence of fields, e. g. for particles moving across the reconnection region.
Analytical solution for constant $\mathbf{B} = (0, 0, B)$, $\mathbf{E} = (0, 0, E)$ is summarised below according to the reference [10]. Using the the small initial momentum $\mathbf{p} = (0, m\mathrm{v}_\perp, 0)$ The components of (1.3) are:

$$\frac{\mathrm{d}p_x}{\mathrm{d}t} = e\mathrm{v}_y B; \qquad \frac{\mathrm{d}p_y}{\mathrm{d}t} = -e\mathrm{v}_x B; \qquad \frac{\mathrm{d}p_z}{\mathrm{d}t} = eE. \tag{1.6}$$

This issue is often solved in educational materials (e.g. lectures [10]) with assumption that the perpendicular component of momentum $p_\perp$ is constant. This condition is satisfied

for small electric fields and short time-scales and it leads to the solution for Cartesian components in the form

$$x(\phi) = r_L - r_L \cos(\phi) \tag{1.7}$$

$$y(\phi) = r_L \sin(\phi) \tag{1.8}$$

$$z(\phi) = \frac{\mathcal{E}_i}{eE}\left(\cosh\left(\frac{E\phi}{cB}\right) - 1\right), \tag{1.9}$$

where r_L is classic Larmor radius, $\mathcal{E}_i$ is the initial energy of the particle and ϕ is the angular displacement related to the relativistic cyclotron frequency $\dot{\phi}(t) = \omega_{CR}(t) = \frac{eB}{m_0\gamma}$. It is obvious, that the equation (1.9) is a catenary and the solution in cyclic coordinate ϕ is the same as it would be in x, y-plane without the magnetic field. The only relativistic effect in the perpendicular direction according to this solution is the change of the cyclotron frequency. However, this solution is valid only for small changes of the Lorentz factor as all the components of the equation of motion are connected via this parameter and therefore the radius of gyration is affected. The third graph of figure 1.1 also indicates the relativistic expansion of the Larmor radius. Furthermore, for very high energies the relativistic Lorentz equation should be replaced by the Lorentz-Dirac equation that incorporates relativistic radiation processes and the self-consistent reaction of the particle to the electromagnetic fields.

1.2.1 Boris-Buneman algorithm for the full particle motion

The other way to solve this problem is to use a numerical solver. The iterative equations of relativistic the Boris-Buneman (BB) algorithm are in the following table, where n is the time index and Δt is a properly chosen time step.

$$\gamma_n = \frac{1}{\sqrt{1 - \mathbf{v}_n^2/c^2}} \tag{1.10}$$

$$\tilde{\mathbf{E}} = \frac{Q}{m_0}\frac{\Delta t}{2}\mathbf{E} \qquad \tilde{\mathbf{B}} = \frac{Q}{m_0}\frac{\Delta t}{2}\mathbf{B} \tag{1.11}$$

$$\mathbf{u}_n = \gamma_n \mathbf{v}_n \tag{1.12}$$

$$\tilde{\mathbf{u}} = \mathbf{u}_n + \tilde{\mathbf{E}} \tag{1.13}$$

$$\widehat{\mathbf{u}} = \tilde{\mathbf{u}} + 2\frac{(\tilde{\mathbf{u}} + \tilde{\mathbf{u}} \times \tilde{\mathbf{B}}) \times \tilde{\mathbf{B}}}{1 + \tilde{\mathbf{B}}^2} \tag{1.14}$$

$$\mathbf{u}_{n+1} = \widehat{\mathbf{u}} + \tilde{\mathbf{E}} \tag{1.15}$$

$$\mathbf{v}_{n+1} = \frac{\mathbf{u}_{n+1}}{\sqrt{1 - \mathbf{u}_{n+1}^2/c^2}} \tag{1.16}$$

$$\mathbf{x}_{n+1} = \mathbf{x}_n + \mathbf{v}_{n+1}\Delta t \tag{1.17}$$

This quite complicated second-order algorithm has been shown to be stable and energy-conserving under various conditions. The left-hand side of the equation of motion is

linearised by the substitution (1.12) that hides the relativistic factor. The influence of the fields is divided to four phases:

- Half of the acceleration caused by the electric field (1.13)
- Part of the direction change caused by the magnetic field (inner vector product in (1.14))
- Rest of the direction change caused by the magnetic field (outer vector product in (1.14))
- The second half of the acceleration caused by the electric field. (1.15)

The algorithm was implemented in a simple Python program in the framework of this project (see the cloud link in Appendix). The most interesting results of this simple model are displayed in figure 1.1. The first graph in the figure may serve for quick determination of the time scale necessary for gaining a particular kinetic energy. The electron is accelerated without any drag in a electrical field 3 V/m which is a value often accessed in some phase of discharges in smaller tokamaks. Notice that the kinetic energy 1 MeV would be achieved in 3 ms in the vacuum. Acceleration of RE in tokamak plasma is always slower in the given field albeit its usually of a similar order of magnitude. The second graph demonstrates the relativistic behaviour of the algorithm. The maximum speed is limited by the speed of light.
The third graph shows interesting behaviour with increasing Larmor radius. The magnetic field is 1 T and the parallel electric field is 10 kV in this case. The Larmor radius - quantity connected with motion perpendicular to the magnetic field - seems to be rising during the parallel acceleration in these high fields and this behaviour is surprisingly resistant to refinements of time step. This behaviour is in disagreement with the analytical solution given in [10], however it seems that it is reasonable as it follows the relation for relativistic Larmor radius (green curve in the figure 1.1). The process of gyration is very fast and computationally expensive, however, the computation of the full particle motion is unavoidable in some situations.

1.2.2 Relativistic Lagrangian and Hamiltonian

Sometimes it is not possible to apply the equation of motion (1.3) directly. In this case the Lagrangian or the Hamiltonian of the system of particles and electromagnetic field have to be used. For this application, the scalar potential φ and the vector potential $\mathbf{A}$ are particularly useful. The relations between the fields and potentials are described by these equations

$$\mathbf{E} = -\nabla\varphi - \frac{\partial \mathbf{A}}{\partial t} \qquad \mathbf{B} = \mathrm{rot}\mathbf{A}. \tag{1.18}$$

Using these potentials, the relativistic Lagrangian of particle in an electromagnetic field is [29]

$$L(\mathbf{r}, \dot{\mathbf{r}}, t) = -m_0 c^2 \sqrt{1 - \mathrm{v}^2/c^2} - e\varphi + e\mathbf{A} \cdot \dot{\mathbf{r}}. \tag{1.19}$$

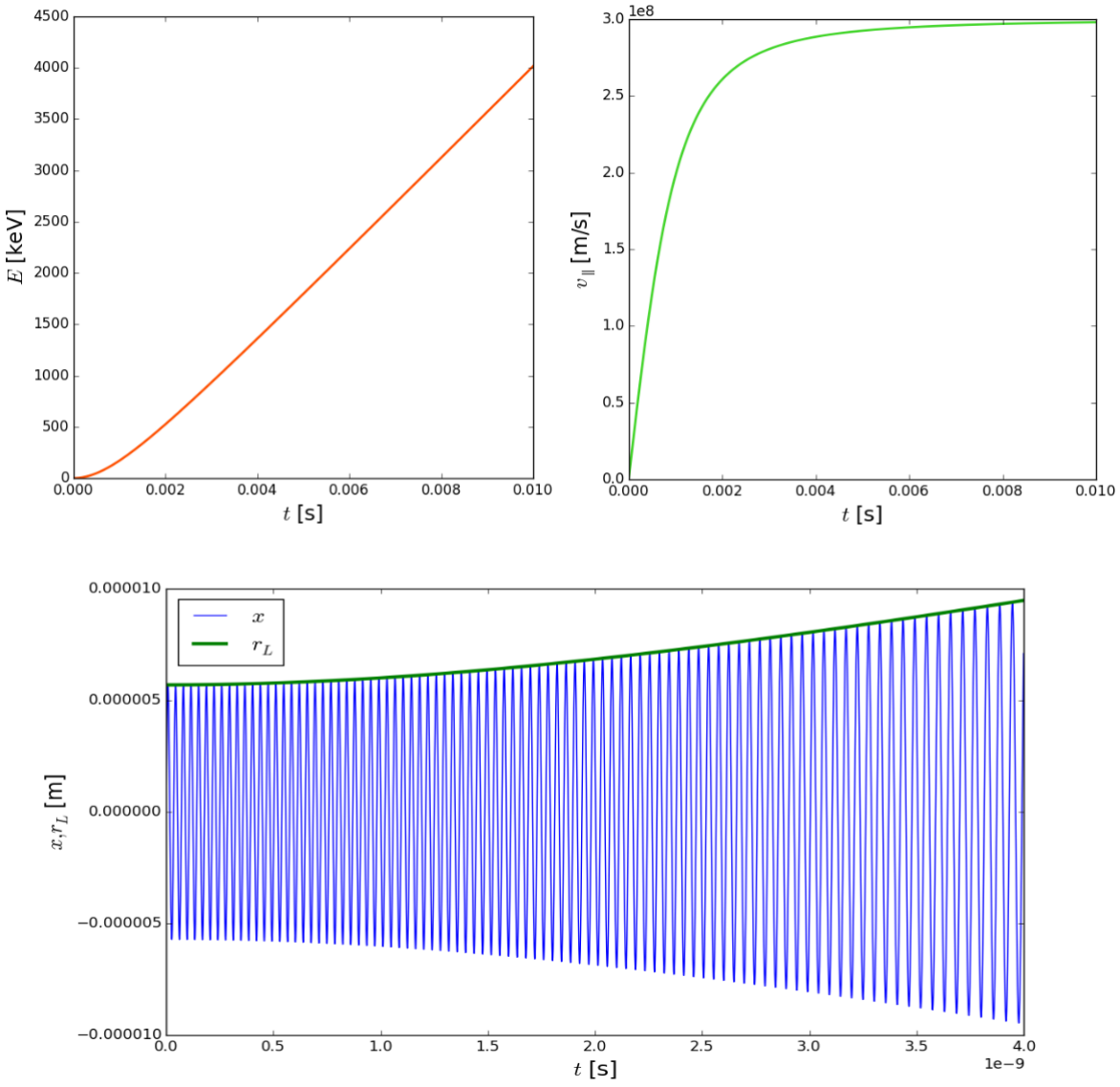

Figure 1.1: The results of the Boris-Buneman (BB) algorithm for a simple particle acceleration, top left: relativistic kinetic energy of an electron as a function of time in electric field $\mathbf{E} = 3\mathrm{V/m}$, top right: velocity of electron in accelerating electric field, bottom: the rising value of the Larmor radius in the very high electric field.

Furthermore, the relativistic Hamiltonian [29] takes a form

$$H(\mathbf{r},\mathbf{p},t) = c^2\sqrt{m_0^2c^2 + (\mathbf{p} - e\mathbf{A})^2} + e\varphi. \tag{1.20}$$

1.2.3 Relativistic drift equation

The description of full particle motion is not necessary (gyroradius in the order of tenths of milimeter and frequency in the order of THz) and almost impossible for runaway electrons on larger time scales. The required time step to track the full particle motion is many orders of magnitude smaller than typical time scale of disruption or plasma instabilities in tokamak. Therefore, the first simplification is the relativistic drift equation (RDE) that omits the gyro-motion. This is possible only in magnetic fields with small time and space variations

$$|\frac{\partial B_k}{\partial x_j}| \ll \frac{B}{r_L} \qquad |\frac{\partial B_k}{\partial t}| \ll \omega_C B, \qquad \forall k,j. \tag{1.21}$$

The derivation of this equation follows.
For the purpose of RDE, the relativistic Lagrangian formalism (1.19) is used in [41]. The particle position $\mathbf{r}$ is the sum of the position of the guiding center $\mathbf{R}$ and the circular motion with the gyroradius ρ

$$\mathbf{r} = \mathbf{R} + \rho(\hat{x}\cos\theta + \hat{y}\sin\theta), \tag{1.22}$$

where $(\hat{x},\hat{y},\hat{b})$ defines an orthonormal basis determined by the direction of the magnetic field $\mathbf{B} = B\hat{b}$ and we suppose $\dot{\mathbf{R}} = (\hat{b}\cdot\dot{\mathbf{R}})\hat{b}$. The derivative of the position vector is

$$\mathbf{v} = \dot{\mathbf{R}} + \rho\dot{\theta}(-\hat{x}\sin\theta + \hat{y}\cos\theta). \tag{1.23}$$

For derivation of the gyro-averaged Lagrangian we also need an approximate value of magnetic potential at point $\mathbf{r}$ using expansion

$$\mathbf{A}(\mathbf{r}) = \mathbf{A}(\mathbf{R}) + \rho\left(\frac{\partial\mathbf{A}}{\partial x}\cos\theta + \frac{\partial\mathbf{A}}{\partial y}\sin\theta\right). \tag{1.24}$$

Using this expression, the last term in equation (1.19) is adjusted and averaged over θ. Finally, the gyro-average of the Lagrangian is

$$L(\mathbf{R},\rho,\theta,\dot{\mathbf{R}},\dot{\rho},\dot{\theta}) = -mc^2\sqrt{1 - [(\hat{b}\cdot\dot{\mathbf{R}})^2 + \rho^2\dot{\theta}^2]/c^2} - e\phi + e(\mathbf{A}\dot{\mathbf{R}}) + \frac{eB\rho^2\dot{\theta}}{2}. \tag{1.25}$$

From this function, the guiding-center equation is derived using the well-know relation for Euler-Lagrange equations

$$\frac{\mathrm{d}}{\mathrm{d}t}\left(\frac{\partial L}{\partial\dot{\mathbf{R}}}\right) = \left(\frac{\partial L}{\partial\mathbf{R}}\right). \tag{1.26}$$

This relation leads to the equation for the guiding center motion in the form

$$m\frac{\mathrm{d}(\gamma v_\parallel)}{\mathrm{d}t} = e(\mathbf{E} + \dot{\mathbf{R}}\times\mathbf{B}) - \mu\nabla B - \gamma m v_\parallel^2\kappa, \tag{1.27}$$

where $\mathrm{v}_\parallel = \dot{\mathbf{R}}\hat{b}$, $\mu = \frac{m_e \mathrm{v}_\perp^2}{2B}$ is the magnetic moment and $\kappa = \hat{b} \cdot \nabla\hat{b} (= -\hat{b} \times (\nabla \times \hat{b}))$ is the curvature of magnetic field lines. The magnetic moment appeared in the equation after using relations for Larmor radius ($\rho = r_L$) and cyclotron frequency ($\dot{\theta} = \omega_C$) The parallel component of this equation is

$$\frac{\mathrm{d}(m\gamma \mathrm{v}_\parallel)}{\mathrm{d}t} = e\mathbf{E}_\parallel - \mu(\nabla_\parallel B). \tag{1.28}$$

This component is related to the effect of magnetic mirrors that is important in tokamaks for trapped particles. The perpendicular component, i. e. RDE, is derived by adjusting the vector product of equation (1.27) with $\hat{b}$

$$\dot{\mathbf{R}}_\perp = \dot{\mathbf{R}} - \mathrm{v}_\parallel \hat{b} = \frac{\mathbf{E} \times \hat{b}}{B} + \frac{\mu}{eB}\hat{b} \times \nabla B + \frac{m\gamma \mathrm{v}_\perp^2}{eB}\hat{b} \times \kappa. \tag{1.29}$$

The three terms in this equation corresponds to three types of drift motions most important for stationary tokamak plasma, described below.

1.2.4 Drifts

Drift motion, i. e. motion of the gyro-center perpendicular to the magnetic field lines. Is quite important for RE in low density and post-disruption plasmas. As the change of momentum due to the collisions is small, the drift effects dominate. Notice that it is slow in comparison to the cyclotron frequency.

$\mathbf{E} \times \mathbf{B}$ drift

This drift is well known from tokamak plasmas. It is independent on the particle charge and therefore the direction of the drift velocity for electrons and ions is the same, resulting in a flux of plasma. The drift velocity is

$$\mathrm{v}_{E\times B} = \frac{\mathbf{E} \times \mathbf{B}}{B^2}. \tag{1.30}$$

This motion would lead to expansion of the plasma torus outwards in case of the vertical separation of charges (creates $\mathbf{E}$) and toroidal magnetic field. To make the tokamak resistant to a such behaviour, a poloidal magnetic field must be utilised. The stability is expressed by the safety factor q defined

$$q = \frac{\partial\Phi}{\partial\Psi} \overset{c.p.}{\approx} \frac{r}{R}\frac{B_T}{B_P}, \tag{1.31}$$

where Φ is the toroidal magnetic flux and Ψ is the poloidal magnetic flux, r and R are minor and major radius coordinate, respectively, 'c.p.' means circular plasma approximation.
However, the introduced poloidal component of the magnetic field together with the toroidal electric field (loop voltage) may cause a radial $E \times B$ drift that is very important for runaway electrons.

Curvature and ∇B drift

Curvature drift corresponds to the last term in (1.29). In tokamak, the magnetic field lines are curved strongly and therefore this drift plays a significant role. It may be understood as an effect of the centrifugal force. As it is connected with the parallel component of velocity the relativistic factor γ appears. This direction of the drift is dependent on the particle charge and it leads to the separation of charges.

As the name ∇B drift suggest, this type of drift is connected to the spatial changes of magnetic field magnitude. The second term of the relativistic drift equation (1.29) shows that this drift is connected with changes of magnetic field magnitude perpendicular to the direction of the magnetic field vector. This situation indeed occurs in tokamaks. Toroidal magnetic field decreases with the distance from the main axis. This is caused by the toroidal geometry as the toroidal field coils are closer to each other on the inner side of the torus. Poloidal field also varies radially. This type of drift is also dependent on the charge of the particle. Curvature and ∇B drift in tokamaks may be written using single expression [60]

$$\mathrm{v}_D = \frac{\gamma m}{eB} \frac{\mathbf{R}_c \times \mathbf{B}}{R_c^2 B} \left(\mathrm{v}_\parallel^2 + \frac{\mathrm{v}_\perp^2}{2} \right). \tag{1.32}$$

This combined drift velocity was derived using Maxwell equation div$\mathbf{B} = 0$ in cylindrical coordinates. Using this form, the ∇B term may be described using ther curvature radius $\mathbf{R_c}$ or the curvature κ. This description is possible in situations where the gradient of magnetic field is actually caused by the curvature, e. g. for field lines forming the torus. Note that the direction of both drifts is the same. This leads to the separation of charges mentioned in the $\mathbf{E} \times \mathbf{B}$ paragraph. The effect of these drifts is increased in the case of relativistic particles, due to the factor γ.

Other drifts

If we consider a slowly evolving magnetic field, the inertial drift may be introduced

$$\mathbf{v}_{in} = \frac{\mathrm{v}_\parallel}{\omega_C} \hat{b} \times \frac{\partial \hat{b}}{\partial t}. \tag{1.33}$$

A slowly varying electric field is responsible for polarisation drift with the velocity magnitude (as derived in Chapter 2 of book [60])

$$\mathbf{v}_p = \frac{m}{eB^2} \frac{\partial \mathbf{E}}{\partial t}. \tag{1.34}$$

This drift may be neglected for electrons due to their small mass.
Finally, the effect of finite Larmor radius in space-varying electric field leads to modification of (1.30)

$$\mathbf{v}_{Es} = \left(1 + \frac{1}{4} r_L^2 \nabla^2 \right) \mathrm{v}_{E \times B}. \tag{1.35}$$

Due to the plasma pressure gradient, the virtual diamagnetic drift is created. This is not a movement of particle gyrocentres, but rather dominant velocity direction in reference

area that appears in the MHD description. The velocity is calculated using equation [29]

$$\mathbf{v}_D = -\frac{\nabla p \times \mathbf{B}}{enB^2}. \tag{1.36}$$

1.2.5 Effects of toroidal geometry

We have described the most important drifts in the toroidal configuration. However, there are other important effects connected with the parallel velocity. If we go back to the equation (1.28), the two terms on the right-hand side with opposite signs may suggest, that there exist a stationary point for the parallel velocity and under some conditions it is even possible that the particle stops and starts to move backwards. For particles with high value of perpendicular component of velocity (hidden in μ) with respect to the parallel component, the effect of magnetic mirror occurs (trapped particles). Particles with high parallel velocity moves around whole poloidal cross-section (passing particles) with circular orbits slightly shifted due to drifts.

Trapped particles

In tokamak the particles may be trapped on the low field side (the outer part of the torus in radial direction) and move on the so called banana orbits. These trajectories are described in many publications, including [60] or bachelor thesis of author [12]. This is not generally the case of runaway electrons. The high parallel momentum of RE can be hardly switched to the perpendicular component due to the common collisions. However, the transition may be caused by the resonance braking on plasma wave, e. g. Parail-Pogutse instability that will be described in following chapters. Also the avalanche mechanism may produce the trapped electrons with large energy [46]. These electrons may runaway after redistribution of momentum. Some authors consider complicated mechanisms that can result in transition of trapped particle into the runaway region, e. g. including Ware pinch (the move of banana trajectory towards the magnetic axis) [19].

1.2.6 Betatron equilibrium

As mentioned above the RE dominated plasma in tokamak may be compared to betatron operation. In the history of accelerator physics even the stabilising toroidal field was used. Furthermore, the "plasma-assisted betatron" as an electron accelerator with background low density plasma ($n_i = 10^{16}\,\mathrm{m}^{-3}$) to lower the effects of space charge was proposed [36]. Traditional betatrons are characterised by a changing vertical field that is responsible for both acceleration and stable orbits. The accelerating electric field is determined by the Faraday's law and the stable orbit is based on the equilibrium of magnetic part of Lorenz force and the centrifugal force. These two relations lead to the famous Widerøe's (betatron) condition [24]

$$B(r_0) = \frac{1}{2}\frac{\Delta\phi}{\pi r_0^2}, \tag{1.37}$$

that is: magnetic field on the radial coordinate of the beam center r_0 is equal to the half of the change of magnetic flux through the circle enclosed by the beam $\Delta\phi$ divided by the area of this circle. This condition is automatically fulfilled when the acceleration and stabilisation is done by the same coils, unless the iron core is saturated or the flux is damaged by some error fields.

This condition may be possibly useful in the RE beam stabilisation and suppression. If some special waveform is used for the central solenoid and outer poloidal field coils, it should be possible to stabilise and even decelerate (or scatter) the RE beam. However, the plasma assisted modified betatron is affected by instabilities similar to these observed in tokamaks. [36] The stabilisation of RE beam is to be studied in following campaigns.

1.3 Statistical physics and kinetic approach

Once the interest is not focused on the trajectory of a single particle and we investigate the macroscopic behaviour of plasma, we have to use a more general attitude. The statistical physics is very powerful in the description of plasma and can be exceptionally useful in the RE description. From the single particle momentum we step to the distribution function (particle probability density function) $f(t, \mathbf{x}, \mathbf{v})$, defined as the probability of finding dN_α particles in the element of the phase space $(\mathrm{d}\mathbf{x}, \mathrm{d}\mathbf{v})$. This definition is described by the following relation

$$dN_\alpha = f_\alpha(t, \mathbf{x}, \mathbf{v}) d^3\mathbf{x} d^3\mathbf{v}, \tag{1.38}$$

where α denotes the type of the particle (ions in particular ionisation states, electrons,...). When integrating this equation over the whole phase space, the number of particles is obtained, while integrating (1.3) over the velocity part of the space results in the density of particles n_e. The evolution of the system of many particles is described primarily by the Liouville theorem [30]. This theorem states that the total derivative of the probability density function along the trajectory is zero in a system without any sinks or sources. The actual time development of the distribution function of specific type of particles is described by the Boltzmann transport equation (BTE) [29]. The total time derivative of the distribution function is equal to the change of the distribution function caused by collisions with different kinds of particles and to change caused by the sources and sinks

$$\begin{aligned} \frac{Df_\alpha}{Dt} &= \frac{\partial f_\alpha}{\partial t} + \frac{\partial f_\alpha}{\partial \mathbf{x}_\alpha}\frac{d\mathbf{x}_\alpha}{dt} + \frac{\partial f_\alpha}{\partial \mathbf{v}_\alpha}\frac{d\mathbf{v}_\alpha)}{dt} = \\ &= \frac{\partial f_\alpha}{\partial t} + (\mathbf{v}_\alpha \cdot \nabla_\mathbf{x}) f_\alpha + \frac{1}{m_\alpha}(\mathbf{F}_\alpha \cdot \nabla_\mathbf{v}) f_\alpha = \left(\frac{\partial f_\alpha}{\partial t}\right)_{col} + \left(\frac{\partial f_\alpha}{\partial t}\right)_s . \end{aligned} \tag{1.39}$$

The source (sink) term in the case of plasma may be connected with a loss to the walls, gas or impurity injection and many other processes that may be described with approximate models. The processes like ionisation or recombination may be covered either by the source term or by the collisional term and described using differential cross-sections. The sources that change the velocity part of the distribution function, e. g. the heating systems, have to be also incorporated into the equation to get the complete description of the system. The collisional term is harder to determine. In the Boltzmann equation,

this term is given by a very general "collisional integral", in the Vlasov equation for collisionless plasma the collisional term is equal to zero and the collisional term of the BGK equation corresponds to a simple approximation $\nu_c(f^\alpha - f_{LE})$, using the local equilibrium distribution function f_{LE} and the collisional frequency ν_c, defined in section 1.1.

1.3.1 Fokker-Planck equation

In the case of plasma with RE, the collisions are essential. Therefore the Fokker-Planck (Landau) collisional term, which is considered to be very accurate in a plasma, have to be used. The term will be briefly described below. The force $\mathbf{F}_\alpha$ from the equation (1.39) must be specified. The Lorenz force dominates and the equation takes form

$$\frac{\partial f_\alpha}{\partial t} + (\mathbf{v}_\alpha \nabla_{\mathbf{x}})\, f_\alpha + \frac{Q_\alpha}{m_\alpha}\left(\mathbf{E}_{(\alpha)} + \mathbf{v}_\alpha \times \mathbf{B}_\alpha\right) \cdot \nabla_{\mathbf{v}} f_\alpha = \left(\frac{\partial f_\alpha}{\partial t}\right)_{col} + \left(\frac{\partial f_\alpha}{\partial t}\right)_{s}. \tag{1.40}$$

Let us remind the assumptions of the classical Fokker-Planck approximation. Most of the assumptions are based on the qualitative properties typical for the Coulombic interaction (relatively fast decrease of intensity with distance, shielding)

- Every particle is affected by many small collisions, the overall change of velocity during the time period Δt is small.
- The collisions are elastic.
- Only the field of the particles in the Debye sphere is considered.
- The collisions with the large scattering angle ($> 90°$) are not considered as they are less probable.
- The collisions satisfy the Markov property, i. e. the process is 'memoryless'. Therefore, the probability of changing the velocity of the particle $\wp(\mathbf{v}, \Delta\mathbf{v})\mathrm{d}^3\mathbf{v}$ from the value $\mathbf{v}$ to the value $\mathbf{v} + \Delta\mathbf{v}$ during the time period Δt does not depend on time.

Based on these assumptions, the general Fokker-Planck equation may be derived using the Lagrange theorem for the time derivative of the distribution function related to the collisions in combination with the second order Taylor series of the integrand in the relation

$$f(t, \mathbf{x}, \mathbf{v}) = \int f(t - \Delta t, \mathbf{x}, \mathbf{v} - \Delta\mathbf{v})\wp(\mathbf{v} - \Delta\mathbf{v}), \Delta\mathbf{v})\mathrm{d}^3\left(\Delta\mathbf{v}\right), \tag{1.41}$$

where the function $\wp$ contains the properties of Coulomb interaction and will be specified below. The derivation is described in detail in [29] and many other plasma kinetic theory books. The final equation may be written using tensor formalism

$$\begin{aligned} \frac{Df_\alpha}{Dt} &= -\frac{1}{\Delta t}\nabla_{\mathbf{v}} \cdot \left(f_\alpha \langle \Delta\mathbf{v} \rangle\right) + \frac{1}{2\Delta t}\left(\nabla_{\mathbf{v}} \otimes \nabla_{\mathbf{v}}\right) : \left(f_\alpha \langle \Delta\mathbf{v} \otimes \Delta\mathbf{v} \rangle\right) \\ \langle \Delta\mathbf{v} \rangle &\equiv \int \Delta\mathbf{v}\wp\, \mathrm{d}^3\left(\Delta\mathbf{v}\right) \\ \langle \Delta\mathbf{v} \otimes \Delta\mathbf{v} \rangle &\equiv \int \Delta\mathbf{v} \otimes \Delta\mathbf{v}\wp\, \mathrm{d}^3\left(\Delta\mathbf{v}\right) \end{aligned}, \tag{1.42}$$

where the left-hand side may be written as in the equation (1.40) and the two terms on the RHS originate in the Taylor expansion mentioned above. The first term corresponds to the 'dynamic friction' and it can be described as a braking of the beam of supra-thermal particles penetrating into the thermal plasma. The second term is the 'diffusion term' corresponding to the scattering of the beam. That is identical to spreading of the distribution function in the velocity space. The specific form of the right-hand side ($\wp$) for the Coulombic collisions is described by the Rosenbluth potentials. Let us remind that the Rosenbluth potentials are derived for a non-relativistic situation without the strong magnetic field and therefore its precision is limited when applied for RE in tokamaks. The derivation of these potentials is based on the analysis of Coulombic collision of two particles in the centre of mass coordinate system. The most important quantity in the derivation is the relative speed $g = |\mathbf{v}_\alpha - \mathbf{v}_\beta|$. The exact derivation of Rosenbluth potentials is quite long and technical, therefore it will not be shown here. The derivation can be found in [29] or [30]. The final form of the equation is

$$\begin{gathered}
\frac{\partial f_\alpha}{\partial t} + (\mathbf{v}_\alpha \nabla_\mathbf{x})\, f_\alpha + \frac{Q_\alpha}{m_\alpha} (\mathbf{E}_\alpha + \mathbf{v}_\alpha \times \mathbf{B}_\alpha) \cdot \nabla_\mathbf{v} f_\alpha = S_{\alpha\beta} \\
S_{\alpha\beta} = K_{\alpha\beta} \ln \Lambda_{\alpha\beta} \left[-\frac{m_\alpha + m_\beta}{m_\beta} \nabla_\mathbf{v} \cdot \left(f_\alpha \nabla_\mathbf{v} H_{\alpha\beta} \right) + \frac{1}{2} (\nabla_\mathbf{v} \nabla_\mathbf{v}) : \left(f_\alpha \nabla_\mathbf{v} \nabla_\mathbf{v} G_{\alpha\beta} \right) \right] \\
H_{\alpha\beta}(\mathbf{v}_\alpha) = \int \frac{1}{g} f_\beta \mathrm{d}^3 \mathbf{v}_\beta \qquad G_{\alpha\beta}(\mathbf{v}_\alpha) = \int g f_\beta \mathrm{d}^3 \mathbf{v}_\beta \\
K_{\alpha\beta} = 4\pi \left(\frac{Q_\alpha Q_\beta}{4\pi\epsilon_0 m_\alpha} \right)^2 \qquad \ln \Lambda = \left(\frac{\lambda_D}{b_0} \right) \qquad b_0 = \frac{Q_\alpha Q_\beta}{4\pi\epsilon_0 \mu g^2}
\end{gathered} \tag{1.43}$$

where $m_\bullet$, $Q_\bullet$, $\mathbf{v}_\bullet$, $f_\bullet$ are mass, charge, velocity and distribution function of particles of the kind α or β. $H_{\alpha\beta}$ and $G_{\alpha\beta}$ are Rosenbluth potentials corresponding to the drag and diffusion in velocity space, respectively. Landau parameter b_0 corresponds to the 90 degrees scattering and Debye length corresponds to the maximum collisional parameter as it was defined in previous text. The constant $\mu = m_\alpha m_\beta/(m_\alpha + m_\beta)$ is reduced mass. The equation in this form is useful for the description of kinetic instabilities and RE.

1.4 Two-fluids magnetohydrodynamics of electrons

To describe phenomena connected with space rather than with velocity distribution of plasma particles, it is suitable to use even more simplified attitude. The MHD equations may be derived as the moments of the Fokker-Planck equation. Direct integration of the equation over velocity space results in the equation for the time evolution of particle density, integral of the equation multiplied by v_α or $m\mathrm{v}_\alpha$ is the equation of motion and second moment $\int \cdot m\mathrm{v}^2/2$ gives equation for the evolution of energy [30].
Multi-fluids magnetohydrodynamics is often used for multicomponent plasma in the terms of electrons, fuel ions and impurities, albeit it is also suitable for RE. Most MHD models consider RE as a different "fluid" in the background of thermal electrons. Using this attitude, it is natural to use runaway rates of various processes described below as source terms in the equation for the RE amount or density. The sinks are derived from statistical evaluation of particle losses due to different channels (drifts, magnetic field perturbation,...). Similar terms may be derived for conservation of momentum (velocity) and

energy, however, in these equations also the radiation processes play an important role. Interaction of runaways with background plasma is often neglected and the velocity of the RE fluid is often considered to be equal to the speed of light. Let us remind the definition relations for the most important quantities describing the fluids

$$n_\alpha(\mathbf{x},t) = \int f(\mathbf{x},\mathbf{v},t)\mathrm{d}^3\mathbf{v} \qquad \mathbf{u}_\alpha(\mathbf{x},t) = \frac{\int \mathbf{v} f(\mathbf{x},\mathbf{v},t)\mathrm{d}^3\mathbf{v}}{\int f(\mathbf{x},\mathbf{v},t)\mathrm{d}^3\mathbf{v}} \qquad \mathbf{j}_\alpha = Q_\alpha n_\alpha \mathbf{u}_\alpha, \quad (1.44)$$

that is particle density, mean velocity and current density respectively.

Chapter 2

Runaway Electrons Physics and Modelling

2.1 Generation of runaway electrons

RE in tokamaks may be generated by many processes that are divided into two groups - the primary and the secondary. The primary generation occurs when the electric field is present, the fast particles are not slowed down collisionally and therefore, acceleration prevails. Indeed, as will be shown in the further text, the collisional frequency decreases with the velocity raised to the power of minus three and fast enough electrons are further accelerated, while the tail of the thermal distribution is refilled from the bulk plasma by collisional diffusion in the velocity space. This leads to the rising number of RE. So called hot-tail mechanism is a modification of this process, occurring during the thermal quench of disruptions. During this process, the rapid cooling of the bulk plasma makes the fast tail of the former hot Maxwell distribution almost collisionless and the population of runaway electrons can be created. The secondary generation is different, as it is based on close collisions. Significant population of RE created by the primary mechanism (seed) may be multiplied by collisions with the thermal particles. Except of these dominant processes, there are some marginal channels that may also create the runaway seed. Among these are the tritium β decay, cosmic radiation, Compton scattering, etc. Actually, a more important source may be some instabilities and waves, namely the R-wave (resonant interaction on electron cyclotron frequency ω_C [29]), reconnection phenomena and kinetic instabilities.

2.1.1 Primary generation

The basic concept of the primary runaway electron generation will be described in the following text. This basic description is non-relativistic and without considering the magnetic field. The influence of relativistic effects on the runaway phenomenon will be discussed later, strong magnetic field changes namely the symmetry of this problem. We have to estimate the number of electrons that are not collisionally slowed down in a specific electric field. The presence of electric field creates the RE region in the velocity space. The number of the electrons in this region is not constant but rises due to the dif-

fusion of thermal electron distribution in velocity space.
Following detailed derivation is an expanded translation of the derivation conducted in Czech monograph on plasma theory [29]. This solution of the runaway problem is successfully compared with the results published in the famous Dreicer article [11] that is considered to be the first publication in the field of RE physics.
Derivation of the collisional drag is based on the solution of the equation (1.43). We have to choose the distribution functions f_α and f_β. Let the f_β be the Maxwellian distribution function of thermal plasma and f_α a mono-energetic beam

$$f_\alpha = n_\alpha \delta(\mathbf{v}_\alpha - \mathbf{v}(t)) \qquad f_\beta = n_\beta \left(\frac{m_\beta}{2\pi k_B T_\beta}\right)^{3/2} \mathrm{e}^{-\frac{m_\beta \mathrm{v}_\beta^2}{2k_B T_\beta}}. \tag{2.1}$$

The monochromatic beam does not diffuse because it is an equivalent of single particle in this attitude. Mathematically, the Dirac δ function allows only one value of velocity, the same for all particles of the beam. This means that only the potential $H_{\alpha\beta}$ must be determined in this case. In following derivation we will use $\mathrm{v}_{T\beta} = \sqrt{2k_B T_\beta / m_\beta}$. The expression for the potential $H_{\alpha\beta}$ (1.43) leads to the integral

$$H(\mathbf{v}_\alpha) = \frac{n_\beta}{\pi^{3/2}\mathrm{v}_{T\beta}^3} \int \frac{1}{|\mathbf{v}_\alpha - \mathbf{v}_\beta|} \mathrm{e}^{-\left(\frac{\mathrm{v}_\beta}{\mathrm{v}_{T\beta}}\right)^2} \mathrm{d}\mathbf{v}_\beta^3. \tag{2.2}$$

This integral have to be solved by expanding the denominator using the Legendre polynomials.

$$H(\mathrm{v}_\alpha) = \sum_{l=0}^{\infty} \iiint f_\beta(\mathrm{v}_\beta) \frac{\min^l(\mathrm{v}_\alpha, \mathrm{v}_\beta)}{\max^{l+1}(\mathrm{v}_\alpha, \mathrm{v}_\beta)} P_l(\cos\theta) \mathrm{v}_\beta^2 \sin\theta \, \mathrm{d}\phi \, \mathrm{d}\theta \, \mathrm{d}\mathrm{v}_\beta \tag{2.3}$$

where θ is the angle between $\mathbf{v}_\alpha$ and $\mathbf{v}_\beta$. The integration over ϕ gives 2π and for the given argument $\cos\theta$, only the first Legendre polynomial ($l = 0$) is non-zero and the integral over θ is 2. The difference in the denominator causes branching of the integral in the pole $\mathrm{v}_\alpha = \mathrm{v}_\beta$

$$H(\mathrm{v}_\alpha) = 4\pi \left[\frac{1}{\mathrm{v}_\alpha} \int_0^{\mathrm{v}_\alpha} \mathrm{v}_\beta^2 f_\beta \mathrm{d}\mathrm{v}_\beta + \int_{\mathrm{v}_\alpha}^{\infty} \mathrm{v}_\beta f_\beta \mathrm{d}\mathrm{v}_\beta \right]. \tag{2.4}$$

So far, the derivation was general and the particular distribution was not used. For Maxwell distribution the integral reads

$$H(\mathrm{v}_\alpha) = \frac{n_\beta}{\mathrm{v}_{T\beta}} \frac{4}{\sqrt{\pi}} \frac{1}{x} \int_0^x \xi^2 \mathrm{e}^{-\xi^2} \mathrm{d}\xi + \frac{n_\beta}{\mathrm{v}_{T\beta}} \frac{4}{\sqrt{\pi}} \int_x^\infty \xi \mathrm{e}^{-\xi^2} \mathrm{d}\xi, \tag{2.5}$$

where $\xi = \mathrm{v}_\beta / \mathrm{v}_{T\beta}$ and $x = \mathrm{v}_\alpha / \mathrm{v}_{T\beta}$. The second integral may be solved by simple substitution, while the first corresponds to the definition of so called Chandrasekhar function

$$\psi(x) = \frac{2}{\sqrt{\pi} x^2} \int_0^x \xi^2 \mathrm{e}^{-\xi^2} d\xi \tag{2.6}$$

This special function is connected with another one - the Error function $\phi(x)$ - by a simple algebraic relation

$$\psi(x) = \frac{\phi(x) - x\phi'(x)}{2x^2} \qquad \phi(x) = \frac{2}{\sqrt{\pi}} \int_0^x \mathrm{e}^{-\xi^2} d\xi. \tag{2.7}$$

Using the Chandrasekhar function the potential H may be written as

$$H(\mathrm{v}_\alpha) = \frac{n_\beta}{\mathrm{v}_{T\beta}} \left[2x\psi(x) + \frac{2}{\sqrt{\pi}} \mathrm{e}^{-x^2} \right]. \tag{2.8}$$

This form may be further simplified using (2.7) and we get the final result

$$H(\mathrm{v}_\alpha) = \frac{n_\beta}{\mathrm{v}_{T\beta}} \frac{\phi(x)}{x}. \tag{2.9}$$

Now we have to use the derived drag potential in the Fokker-Planck equation for the beam f_α. The distribution function f_α may have different form, e. g. the same Maxwell distribution as we have used for the f_β. The choice of mono-energetic beam will make the process and the role of the derived critical values for field and velocity more transparent. We will use the first moment of the equation (1.43) to derive the velocity evolution. Therefore, the equation is multiplied by $\mathbf{v}_\alpha$ and integrated over the velocity space. The second term on the left hand side (LHS) of (1.43) is zero, because the distribution function does not depend on the space coordinates. In the third term the electric field vector in the direction of z-axis is used

$$\int \mathbf{v}_\alpha \frac{\partial f_\alpha}{\partial t} \mathrm{d}^3\mathbf{v}_\alpha + \frac{Q_\alpha E_\alpha}{m_\alpha} \int \mathbf{v}_\alpha \nabla_\mathbf{v} f_\alpha \mathrm{d}^3\mathbf{v}_\alpha = -K_{\alpha\beta} \ln\Lambda_{\alpha\beta} \frac{m_\alpha + m_\beta}{m_\beta} \int \mathbf{v}_\alpha \nabla_\mathbf{v} \cdot (f_\alpha \nabla_\mathbf{v} H)\, \mathrm{d}^3\mathbf{v}_\alpha \tag{2.10}$$

Now we substitute the Dirac distribution $n_\alpha \delta(\mathbf{v}_\alpha - \mathbf{v}(t))$ for f_α and adjust the left hand side (LHS) and right hand side (RHS) of the equation separately:

$$\begin{aligned} \mathbf{LHS} = n_\alpha \int \mathbf{v}_\alpha \frac{\partial \delta(\mathbf{v}_\alpha - \mathbf{v}(t))}{\partial t} \mathrm{d}^3\mathbf{v}_\alpha + n_\alpha \frac{Q_\alpha E_\alpha}{m_\alpha} \int \mathbf{v}_\alpha \nabla_\mathbf{v} \delta(\mathbf{v}_\alpha - \mathbf{v}(t)) \mathrm{d}^3\mathbf{v}_\alpha = \\ = \frac{\partial}{\partial t} n_\alpha \int \mathbf{v}_\alpha \delta(\mathbf{v}_\alpha - \mathbf{v}(t)) \mathrm{d}^3\mathbf{v}_\alpha + n_\alpha \frac{Q_\alpha E_\alpha}{m_\alpha} \left[\mathrm{v}_\alpha \delta(\mathbf{v}_\alpha - \mathbf{v}(t)) \right]_{-\infty}^{+\infty} - \\ - n_\alpha \frac{Q_\alpha E_\alpha}{m_\alpha} \int \delta(\mathbf{v}_\alpha - \mathbf{v}(t)) \mathrm{d}^3\mathbf{v}_\alpha = n_\alpha \frac{\partial \mathbf{v}}{\partial t} - n_\alpha \frac{Q_\alpha E_\alpha}{m_\alpha}, \end{aligned} \tag{2.11}$$

where for the first term the order of derivative with respect to the parameter (time t) and integration over $\mathbf{v}_\alpha$ was changed and in the second term integration by parts was used. We have to restrict the electric field to a small value and direction given by $\mathbf{v}_\alpha$. For the RHS we have

$$\begin{aligned} \mathbf{RHS} = -n_\alpha K_{\alpha\beta} \ln\Lambda_{\alpha\beta} \frac{m_\alpha + m_\beta}{m_\beta} \int \mathbf{v}_\alpha \frac{\partial}{\partial \mathbf{v}_\alpha} \left(\delta(\mathbf{v}_\alpha - \mathbf{v}(t)) \frac{\partial H}{\partial \mathbf{v}_\alpha} \right) \mathrm{d}^3\mathbf{v}_\alpha = \\ = -n_\alpha K_{\alpha\beta} \ln\Lambda_{\alpha\beta} \frac{m_\alpha + m_\beta}{m_\beta} \left[\mathbf{v}_\alpha \left(\delta(\mathbf{v}_\alpha - \mathbf{v}(t)) \frac{\partial H}{\partial \mathbf{v}_\alpha} \right) \mathrm{d}^3\mathbf{v}_\alpha \right]_{-\infty}^{+\infty} + \\ + n_\alpha K_{\alpha\beta} \ln\Lambda_{\alpha\beta} \frac{m_\alpha + m_\beta}{m_\beta} \int \left(\delta(\mathbf{v}_\alpha - \mathbf{v}(t)) \frac{\partial H}{\partial \mathbf{v}_\alpha} \right) \mathrm{d}^3\mathbf{v}_\alpha = \\ = n_\alpha K_{\alpha\beta} \ln\Lambda_{\alpha\beta} \frac{m_\alpha + m_\beta}{m_\beta} \frac{\partial H(\mathbf{v})}{\partial \mathbf{v}}, \end{aligned} \tag{2.12}$$

where the integration by parts was used again and the Dirac function in the integral caused the transition from the variable $\mathbf{v}_\alpha$ to the variable $\mathbf{v}$. Now, using (2.9), the result for a

single particle of the beam is

$$\frac{\partial \mathbf{v}}{\partial t} - \frac{QE}{m} = K_{\alpha\beta} \ln \Lambda_{\alpha\beta} \frac{m_\alpha + m_\beta}{m_\beta} \frac{\partial H(\mathbf{v})}{\partial \mathbf{v}} \qquad H(\mathbf{v}) = n_\beta \frac{1}{\mathrm{v}} \phi \left(\frac{\mathrm{v}}{\mathrm{v}_{T\beta}} \right). \tag{2.13}$$

We should remind that both $\psi(x)$ and $phi(x)$ are functions of velocity magnitude, thus v is used in the argument. Finally, the derivative of the potential H must be found. The relation (2.7) is used again.

$$\frac{\partial}{\partial \mathbf{v}} \left(\frac{1}{\mathrm{v}} \phi \left(\mathrm{v}/\mathrm{v}_{T\beta} \right) \right) \frac{\partial \mathrm{v}}{\partial \mathbf{v}} = \frac{\phi' \mathrm{v}/\mathrm{v}_{T\beta} - \phi}{\mathrm{v}^2} \frac{\mathbf{v}}{\mathrm{v}} = -2\mathrm{v}_{T\beta}^{-2} \psi(\mathrm{v}/\mathrm{v}_{T\beta}) \frac{\mathbf{v}}{\mathrm{v}} \tag{2.14}$$

The overall form of the averaged Fokker-Planck equation for the electron acceleration ($Q = -e$, $E = (0, 0, -E)$) in plasma therefore is

$$\frac{\partial \mathbf{v}}{\partial t} = \frac{eE}{m_e} - 2 n_\beta K_{\alpha\beta} \ln \Lambda_{\alpha\beta} \frac{m_\alpha + m_\beta}{m_\beta} \mathrm{v}_{T\beta}^{-2} \psi(\mathrm{v}/\mathrm{v}_{T\beta}) \frac{\mathbf{v}}{\mathrm{v}}, \tag{2.15}$$

where the scalar function on the RHS (everything except of the $\mathbf{v}$) corresponds to the electron collisional frequency. Now, there is an important question: What are the particles that cause the collisional drag? In a the tokamak plasma, both electrons and ions should be taken into account. For electrons, the m_β in the equation (2.15) is equal to m_e and Q_β equals the elementary charge. For the ions m_β is nuclear mass and $Q_\beta = Ze$. The first term is of the order m_e/m_i in the case of ions and may be neglected. To sum up the effect of the electron and the ion drag force, the definition of an effective ion charge is used

$$Z_{\mathrm{eff}} = \frac{\sum Z_i^2 n_i}{n_e}, \tag{2.16}$$

where Z_i and n_i are charge numbers and density of all ion types present in plasma. Using this quantity, the drag force (last term in (2.15) times m_e) takes form

$$F_d = \frac{n_e e^4 \ln \Lambda}{4\pi\epsilon_0 m_e} \left[\frac{Z_{eff}}{\mathrm{v}_{Ti}^2} \psi \left(\frac{\mathrm{v}}{\mathrm{v}_{Ti}} \right) + \frac{2}{\mathrm{v}_{Te}^2} \psi \left(\frac{\mathrm{v}}{\mathrm{v}_{Te}} \right) \right]. \tag{2.17}$$

The factor in front of ψ is larger by (m_i/m_e) in the ion term, however, the function ψ has its maximum scaled towards smaller velocities by factor ($\sqrt{m_e/m_i}$). The overall effect of these transformation is displayed in figure 2.1. In the region of the supra-thermal velocities the contributions from ion and electron drag are comparable.

The equation (2.15), simplifying the constants in front of the Chandrasekhar function and specifying the direction of the acceleration, may be re-written as

$$\frac{\partial \mathrm{v}}{\partial t} = \frac{eE}{m_e} - \frac{2e}{m_e} E_D \psi(\mathrm{v}/\mathrm{v}_{T\beta}), \tag{2.18}$$

where E_D is the Dreicer field, denoted as the critical field in the original paper [11]; the factor 2 is caused by different normalisation used in the original paper. The result of our derivation corresponds to the conclusions of Dreicer.
Finally the relation for the Dreicer field is

$$E_D = \frac{n_e e^3}{4\pi\epsilon_0^2 k T_e} \ln \Lambda \qquad \ln \Lambda = \ln \left(\frac{\lambda_D}{b_0} \right). \tag{2.19}$$

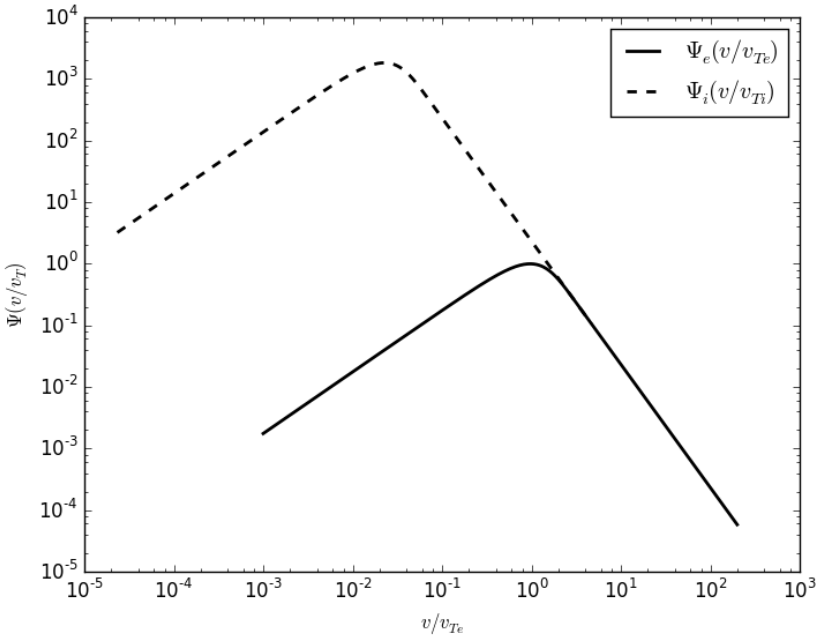

Figure 2.1: The logarithmic plot of the calculated ion (dashed line) and electron contributions to the drag force as a function of velocity normalised to thermal velocity of electrons (ions). Maximum of the electron drag is normalised to 1, maximum of ion drag is higher by factor m_i/m_e. In this figure $T_e = T_i$ and $Z_{eff} = 1$ is assumed.

If the electric field reaches the value of $E_D\psi(1) \sim 0.43E_D$ [11] all electrons are accelerated towards relativistic velocities, because the constant electric force reaches the maximum value of the collisional friction force. The Dreicer field depends on plasma electron temperature T_e and density n_e. This formula takes a slightly different form in the CGS unit system that is often utilised in theoretical papers, e.g. in [8]. The value of the Dreicer field is usually adjusted according to (2.17) to incorporate both the drag by electrons and ions and normalisation of the Chandrasekhar function, although in some formulas for runaway rates the role of Z_{eff} is accounted separately [8]. The most basic mechanism of RE generation is connected with the magnitude of Dreicer field. The Dreicer mechanism describes accelerating of some part of the electron distribution in the electric field stronger then the Coulomb friction force. At least some electrons are accelerated when the electric field is over so called critical field (current designation)

$$E_c = \frac{ne^3}{4\pi\epsilon_0^2 m_e c^2} \ln(\Lambda) . \tag{2.20}$$

The critical field is proportional to local minimum of the friction force, thus it is the threshold for electron acceleration in terms of the external electric field magnitude. The friction force reaches the minimal value for particles with their kinetic energy equal to their rest energy. Faster particles have smaller collisional frequency, but they are affected by relativistic effects, so the overall slowing down force rises for higher energies again. The situation is visualised in the figure 2.2, where the Chandrasekhar function and arbitrary accelerating electric field are plotted. Also the rising tail of the friction force

caused by the synchrotron radiation 2.3.1 is drawn in a dashed curve, albeit this is only illustration, not an exact function. However, the relation for the critical field lacks the dependence on temperature and in most experiments, the value of the real critical field (i. e. the field that presents the lower limit of runaway observation) proves to be higher [17]. The critical situation in a specific external field may be described by the critical velocity that can be derived from the Dreicer field immediately using the high velocity limit of the Chandrasekhar function

$$\frac{2}{\sqrt{\pi}x^2}\int_0^x \xi^2 \mathrm{e}^{-\xi^2} d\xi \longrightarrow \frac{1}{2x^2}. \tag{2.21}$$

Now, the equilibrium of the collisional friction force and the constant electric field corresponds to

$$E_D(2 + Z_{eff})\frac{\mathrm{v}_T^2}{\mathrm{v}_c^2} = 2E \tag{2.22}$$

This leads to the following relation for critical velocity

$$\mathrm{v}_c = \sqrt{\frac{ne^3(1 + Z_{eff}/2)}{4\pi\epsilon_0^2 m_e E}\ln\Lambda}. \tag{2.23}$$

Every particle that is moving with a velocity higher than $\mathrm{v}_c(E)$ along electric field E is accelerated to relativistic velocities. This quantity may help to estimate the number of possible RE in plasma with a Maxwell distribution. It should be reminded that we still use non-relativistic framework. Regarding the previous layout, the density of RE n_{RE} is approximately

$$n_{RE} = \int_{\mathrm{v}_c}^{c} n_e \left(\frac{m_e}{2\pi k_B T_e}\right) \mathrm{e}^{-\frac{m_e \mathrm{v}^2}{2k_B T_e}} \mathrm{d}\mathrm{v}. \tag{2.24}$$

The upper bound is chosen as c because the hypothetical contribution of larger values is negligible even for non-relativistic Maxwell distribution with reasonable temperatures. For smaller fields the result is usually several orders of magnitude below the electron density. However, this simple model does not predict the magnitude of RE population (Maxwellian plasma assumption at every moment), but rather helps to identify the conditions and discharge phases suitable for RE generation. This RE generation process is dominant for smaller machines and discharges with larger loop voltage (colder plasma with impurities) and lower density. In these tokamaks the electric field overcomes the critical field at least during the breakdown. Part of the runaway population can be directly lost but most of it is confined. The latter are subsequently lost via instabilities, during the disruptions or they can be partly slowed down by increasing plasma density. Furthermore, methods of RE mitigation are being searched for. The magnetic field perturbations, massive injection of noble gasses or cryogenic "killer" pellets are among the most promising mitigation methods [22].

If there is a permanent situation with electric field higher than the critical field, the population of RE grows in a non-linear manner due to the collisional diffusion in the velocity space and the tail of the distribution function expands in one direction. The efforts to estimate the growth rate of runaways can be traced down for many years. In this case, the steady state form of kinetic (Fokker-Planck) equation is usually transformed to new

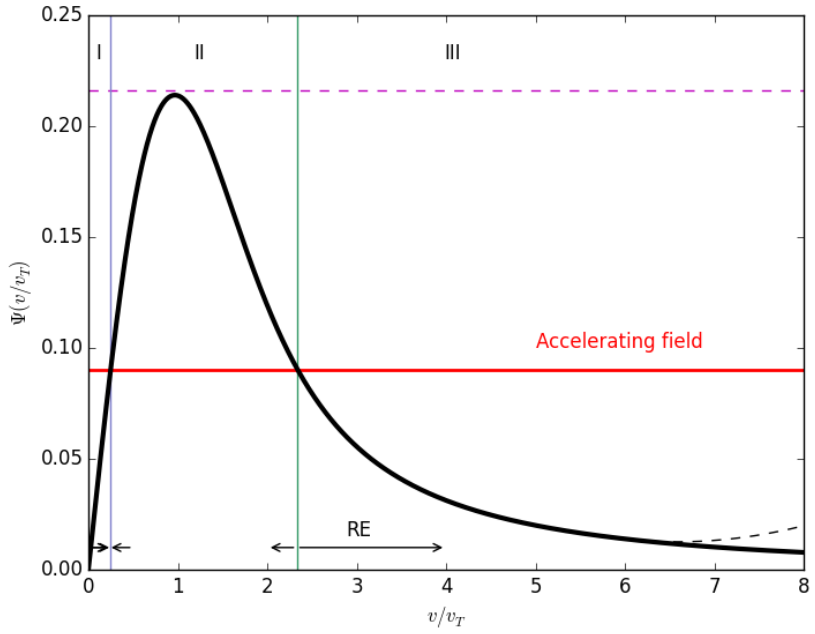

Figure 2.2: A graph of the Chandrasekhar function as an illustration of the Dreicer mechanism. The function marked by the thick black line corresponds to a friction force and the red line to constant accelerating force. This configuration generates three regions, the border of the regions I and II is stable (blue line), while the border of the regions II and III (green line) is unstable. All particles to the right from this border are accelerated to high energies. The magenta dashed line shows the maximum of the Chandrasekhar function proportional to the Dreicer field E_D. For higher velocities, synchrotron radiation drag force plays a role (illustrated by dashed rising tail of the function in the right corner).

coordinates that better reflect symmetry of this problem (i.e. toroidal magnetic field)[47]

$$\frac{eE_{\parallel}}{m_e}\left(\frac{\partial f}{\partial \mathrm{v}}+\frac{1-\xi^2}{\mathrm{v}}\frac{\partial f}{\partial \xi}\right)=\nu_{ee}\mathrm{v}_T^3\left[\frac{1+Z_{eff}}{2\mathrm{v}^3}\frac{\partial}{\partial \xi}(1-\xi^2)\frac{\partial f}{\partial \xi}+\frac{1}{\mathrm{v}^2}\frac{\partial}{\partial \mathrm{v}}\left(f+\frac{T_e}{m_e\mathrm{v}}\frac{\partial f}{\partial \mathrm{v}}\right)\right] \tag{2.25}$$

where v is magnitude of the velocity and $\xi = \cos\theta$ is the cosine of the pitch angle, i. e. the angle between the magnetic field line and velocity vector of the particle. Gurevich has solved this equation in his article [20] and improved original results of Dreicer, although the solution was still relevant only for small part of velocity space. In the following years this solution was improved by Lebedev and then by Kruskal and Bernstein (the improvements are summarised in [8]). Connor and Hastie managed to find the relativistic correction [8] of Kruskal-Bernstein work. The solution of the previous equation and its relativistic version were found as different expansions of distribution function in different velocity regions. The non-relativistic part of the growth rate (the flux of particles into the runaway region) is

$$S_{KB/NR}=C\nu_{ee}\left(\frac{m_ec^2}{2T_e}\right)^{\frac{3}{2}}\left(\frac{E_D}{E_{\parallel}}\right)^{\frac{3}{16}(Z_{\mathrm{eff}}+1)}\mathrm{e}^{-\frac{E_D}{4E_{\parallel}}-\sqrt{\frac{(Z_{\mathrm{eff}}+1)E_D}{E_{\parallel}}}}, \tag{2.26}$$

where C is a scaling factor of order unity. The relativistic correction has a form

$$S_R=S_{NR}\mathrm{e}^{-\frac{kT_e}{m_ec^2}\left[\frac{1}{8}\left(\frac{E_D}{E}\right)^2+\frac{2}{3}\left(\frac{E_D}{E}\right)^{3/2}\sqrt{1+Z_{\mathrm{eff}}}\right]} \tag{2.27}$$

This relation is used in most models as the source term for the Dreicer generation of runaway electrons. Integration of this rate in time should give directly the density of RE. A simple illustration of the Dreicer mechanism is in the top left picture of figure 2.3.

2.1.2 Hot-tail mechanism

The so called hot-tail mechanism is slightly different from the Dreicer mechanism. It is connected mainly with plasma disruptions. The disruption, i. e. rapid termination of the plasma current, may be initiated by numerous causes. The most important type of disruption for studies of RE generation is the radiative disruption. In these events, sudden rise of impurity level causes the thermal quench of plasma, followed by the current quench due to a loss of conductivity. It is often caused by intrusion of little parts of wall material into plasma. The radiative disruption may be also triggered intentionally by injecting high Z gas or pellets. This technique may be very important to mitigate the effects of more dangerous types of disruptions, e.g. vertical displacement event or fast ideal MHD disruption. If this kind of event is detected early enough, injection of gas may slow down the event and limit the tremendous forces induced in support structures of the tokamak due to fast disruptions. During the thermal quench, the bulk electron distribution is cooled down namely by ionisation and excitation of the impurity atoms. However, the faster the electrons are compared to the thermal velocity the smaller is their collisional frequency. This means that the fastest electrons are not slowed down during the thermal quench, because their collisional time τ is larger than the cooling time t_0 of plasma. The simplified models assume exponential decrease of temperature

$$T(t)=T_f+(T_0-T_f)\mathrm{e}^{-\frac{t}{t_0}}, \tag{2.28}$$

where T_f is the temperature after the thermal quench and T_0 is temperature of plasma before disruption [53]. Those fast electrons appear in the runaway region after the thermal quench, accelerated by the toroidal electric field which is increased due to the decreasing plasma current during the current quench. It is important to point out that this process of RE generation is not connected only with the increase of electric field but it is also influenced by the rapid plasma parameters change that leads to the change of the Dreicer field. In fact, the Dreicer field rises during the thermal quench (temperature is denominator in the term (2.19)), so the electric field accelerates only the fast electron population that remains above the value of critical velocity established during the current quench (→ "hot-tail mechanism"). The method to estimate the number of the RE created this way was proposed by Smith [52]. For the special temperature evolution according to 2.28, the approximate solution (velocity distribution) may be found directly as using the velocity moments of the F.-P. equation. The relative density of RE is then obtained with the critical velocity v_c as the lower integration limit (the electric field is introduced in this moment via v_c)

$$\frac{n_{ht}}{n_e} = \frac{4}{\sqrt{\pi}} \int_{\mathrm{v}_c}^{\infty} \left(1 - \frac{(u_c^3 - 3\tau)^{2/3}}{(u^3 - 3\tau)^{2/3}}\right) \mathrm{e}^{-u^2} u^2 \mathrm{d}u. \tag{2.29}$$

Here, $u = \mathrm{v}/\mathrm{v}_{T0} + 3\tau$, $u_c = \mathrm{v}_c/\mathrm{v}_{T0} + 3\tau$ and collisional time τ is obtained as a solution of differential equation in form $\tau(t) = (t - t_0)\nu c^3/\mathrm{v}_{T0}^3$, where ν is the collisional frequency of electrons **??**. Different temperature profiles lead to the different solutions which require more complex derivation. The illustrative scheme of this process is also in the figure 2.3. Quite a large population of RE can be generated by the described mechanism and further multiplied by the avalanche mechanism, see section 2.2. It can produce the RE also in the case of other instabilities connected with rapid cooling of plasma.

2.1.3 Other seed generation mechanisms

Except of the most important mechanisms described above, there are several minor channels that may lead to creation of the RE seed (small population that may be multiplied by secondary mechanism). In ITER, the tritium decay can be source of fast electrons. The number of electrons originating in the beta decay of tritium (half life over 12 years) may not be negligible during long experiments. However, the energy of the produced electrons is below 20 keV which is more or less the same as the electron temperature in ITER.
The other mechanism considered (e.g. in [15]) is the Compton scattering of gamma photons on free electrons. In the harsh environment of fusion reactors the presence of MeV photons could be caused by several mechanisms including the impact of RE on the wall and some nuclear reactions. Some of these high energetic photons may interact transmit their energy to plasma electrons.
Last but not least some instabilities (e.g. local rapid change of magnetic field) may be a source of RE. Most of the instabilities that are to create the RE could be considered as modified local versions of mechanisms described above. However this phenomena will be detailed in chapter 4.

2.2 Secondary mechanism of RE generation

The secondary mechanism of runaway electrons generation, which is often called the avalanche, is the most important way of production for large tokamaks and it will be crucial for ITER. This mechanism was firstly discovered by Sokolov and later described in detail by Rosenbluth and Putvinski [46]. It is called secondary mechanism, because it needs initial RE population (seed) which is further multiplied. The Dreicer mechanism was proven to be weak to generate large runaway populations that were observed in experiments with rather low electric fields. As the typical loop voltage in ITER (0.1 V) will be near the value of the critical field for this machine, the avalanche will be in fact much more important than the direct Dreicer mechanism. The avalanche is a cumulative effect of the so called knock-on collisions. These are close collisions (i. e. with a very small impact parameter) with large amount of parallel momentum being transformed. One RE can push several thermal electrons into the runaway region of the velocity space, while retaining enough momentum to stay in the region itself. These newly created RE are further accelerated by the electric field and then act the same way as the primary ones, so this is indeed an avalanche mechanism. Due to the effect of close collisions, the average energy of RE is reduced to 10-20 MeV for the population of primary electrons of energies up to 100 MeV [46] - the number of RE is increased by avalanche and the typical energy of RE is slightly decreased. Some of the high energy electrons may appear on the banana orbits after these collisions. Therefore, Rosenbluth and Putviski [46] used the relativistic bounce-averaged (average over poloidal cycle, see section 1.2.5) relativistic Fokker-Planck equation in dimensionless variables and were able to "interpolate" the solution for relatively wide range of conditions from limit solutions. The final relation for the growth rate of RE density due to the avalanche is

$$\gamma_A = \frac{\mathrm{d}n_r}{\mathrm{d}t} = \frac{n_r}{\tau ln(\lambda)} (E_r - 1) \sqrt{\frac{\pi\Gamma}{3(Z_{eff}+5)}} \left(1 - E_r + \frac{4\pi(Z_{eff}+1)^2}{3\Gamma(Z_{eff}+5)\left(E_r^2 + 4/\Gamma^2 - 1\right)} \right)^{-1/2}, \tag{2.30}$$

where $E_r = \frac{|E_\parallel|}{E_c}$ is the relative strength of the electric field, $\tau = \frac{m_0 c}{eE_c}$ and $\Gamma(\epsilon)$ is so called neoclassical function for large inverse aspect ration $\epsilon = a/R$, that describes the effects of the toroidal geometry

$$\Gamma(\epsilon) = \frac{3}{4} \int \frac{2\pi\lambda \mathrm{d}\lambda}{\oint \sqrt{1 - \lambda b(\theta)} \mathrm{d}\theta} \approx (1 + 1.46\sqrt{\epsilon} + 1.72\epsilon)^{-1}. \tag{2.31}$$

This equation is written using special coordinate system, where λ express the relative role of the perpendicular momentum component and $b(\theta)$ the dependency of magnetic field on the poloidal angle θ. The complicated equation (2.30) may take a more simple form in the limit $E_r \gg 1$, $Z_{eff} = 1$ and $\epsilon \to 0$

$$\gamma_A \approx \sqrt{\frac{\pi}{2}} \frac{n_r}{3\tau \ln\Lambda} \left(\frac{|E_\parallel|}{E_c} - 1 \right). \tag{2.32}$$

It has to be remembered that these conditions are not even close to a fulfilment in present tokamaks, albeit it could be useful in particular situations and for a approximate estimation.

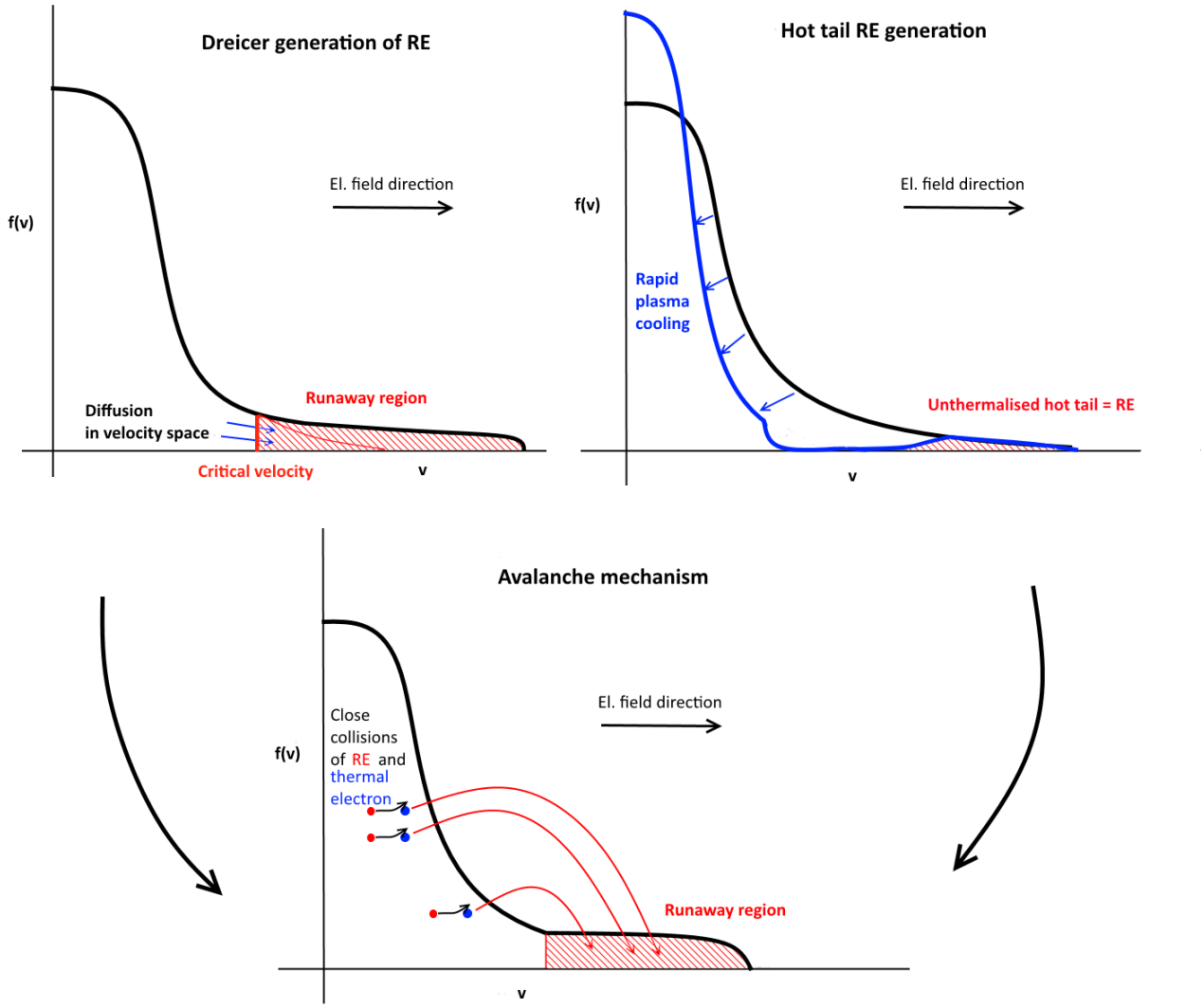

Figure 2.3: Schemes of the most important RE production mechanisms and its effect on the distribution function in the direction of the electric field. Primary mechanisms (top) may give the seed that is further multiplied by the avalanche process

It can be observed than even in fields just above critical field, avalanche can be very significant after long period of time because the growth rate (2.32) is linear function of $|E_{\parallel}|/E_c$, while (2.26) is exponentially small [47]. Furthermore, the rise of the number of RE in plasma with given parameters is exponential due to the avalanche mechanism while it is linear for Dreicer. This highlights the importance of avalanche in long discharges.

2.3 Radiation losses

The radiation losses present an important slowing-down mechanism for the relativistic electrons and also an important diagnostic tool to prove the RE presence and to measure their properties. In plasma, there are many types of radiation, albeit in our case, only two

types of radiating mechanisms are important: synchrotron radiation and bremsstrahlung (free-free collisions or braking radiation). An accelerated charged particle (with acceleration a) radiates with a total power

$$P = \frac{e^2 a^2}{6\pi\epsilon_0 c^3}. \tag{2.33}$$

The power of the specific radiation type then depends on the formula for the acceleration mechanism.

2.3.1 Synchrotron radiation

Generally, synchrotron radiation is a radiation of ultra-relativistic charged particles exposed to an acceleration perpendicular to the direction of their motion (e. g., in magnetic field). It is obvious that RE in tokamak produce this type of radiation. Generally, both velocity components - perpendicular and parallel to the direction of toroidal magnetic field - are important for the synchrotron radiation of relativistic particle in tokamak. The latter is usually called gyrocenter synchrotron radiation and it is more important for smaller machines. However, even synchrotron radiation caused by perpendicular motion is strongly peaked in the direction tangential to the trajectory of the particles due to the relativistic effects. The comparison of the gyro-motion contribution and the gyrocenter contribution is given in [1]. Synchrotron radiation may serve as an important diagnostics mechanism to infer the distribution function and space profiles of the RE beam in tokamaks, therefore it is an object of intensive modelling efforts. The role of the synchrotron radiation as an energy loss mechanism is significant only for very large energies (70+ MeV) [55], therefore it is not important in smaller tokamaks. However it could play a role for electric fields near the critical limit. The spectral density of synchrotron radiation power for high electron energies ($\gamma \gg 1$) in the case of straight magnetic field lines can be written as

$$\Pi(\lambda) = \frac{1}{\sqrt{3}} \frac{ce^2}{\epsilon_0 \lambda^3 \gamma^2} \int_{\lambda_c/\lambda}^{\infty} K_{5/3}(l)\mathrm{d}l, \tag{2.34}$$

where $\lambda_c = (4\pi c m_e \gamma_{\|})/3eB\gamma^2$ and $\gamma_{\|}$ denotes the Lorentz factor of the parallel component of velocity, while K_q is the modified Bessel function of the second kind. The equation (2.34) needs to be adjusted in the case of toroidal geometry to relation described in [55]. The overall spectral density of the synchrotron radiation from runaway population may be obtained by

$$P(\lambda) = \frac{2\pi}{n_r} \int_{\Omega_{RE}} f_{RE}(p,\xi)\Pi(p,\xi,\lambda)p^2 \mathrm{d}p\mathrm{d}\xi \tag{2.35}$$

where Ω_{RE} is the runaway region of momentum space, f_{RE} is the distribution function (in momentum magnitude and cosine of pitch angle) and Π is the single particle power spectral density described above.
The drag force of the synchrotron radiation is given by

$$F_S = \frac{2}{3}\frac{e^2}{4\pi\epsilon_0}\left(\frac{\mathrm{v}}{c}\right)^3 \gamma^4 \left\langle \frac{1}{R^2} \right\rangle \tag{2.36}$$

where γ is the Lorentz factor and the field line curvature averaged over the gyromotion is

$$\left\langle \frac{1}{R^2} \right\rangle = \frac{1}{R_0^2} + \frac{\sin\theta^4}{r_{LR}}, \tag{2.37}$$

that is the curvature given by the tokamak main radius R_0 and curvature by relativistic Larmor radius r_{LR} of particle with pitch angle θ.

2.3.2 Bremsstrahlung

Bremsstrahlung is also called particle braking radiation and in fact, synchrotron radiation is just a subset of this group of radiative processes. In the narrower sense, this word describes the process of radiation caused by the acceleration due to the Coulomb interaction between charged particles. Bremsstrahlung is also one of the energy loss channels for RE. Spectrum of bremsstrahlung radiation from single electron scattered on ion could be obtained using Fourier transform on time evolution of electric field between encountering particles like in [3]. The spectrum is dependent on particle velocity v, atomic number of the ion Z and collisional parameter b

$$P(\lambda) = \frac{4\pi^2}{3} \frac{Z^2 e^6}{m_e^2 c^3 b^2 \mathrm{v}^2} \mathrm{e}^{-\frac{4\pi c b}{\lambda \mathrm{v}}} \tag{2.38}$$

Thermal bremsstrahlung is the most important channel of radiation losses of plasma, the frequency of the radiation is usually in the soft X-ray range and the overall emissivity in $\mathrm{W/m^{-3}}$ is dependent on plasma density n_e and temperature T_e [60] according to the relation

$$\epsilon_b = 5.35 \cdot 10^{-37} n_e^2 T^{1/2} Z_{eff}^2. \tag{2.39}$$

The drag force due to the bremsstrahlung radiation of relativistic particles is equal to

$$F_B = \frac{4}{137} n_e (Z_{eff} + 1) m_e c^2 \gamma r_e^2 \left(\ln 2\gamma - \frac{1}{3} \right), \tag{2.40}$$

where $r_e^2 = \frac{e^2}{4\pi\epsilon_0 m_e c^2}$ is the classical electron radius [1]. On the contrary to the synchrotron radiation drag force, bremsstrahlung drag is independent of magnetic field. On the other hand it is strongly increased with the presence of impurities.

2.4 Runaway positron production

One of the most thrilling theoretical issues regarding RE in tokamaks is linked to the predicted creation of the electron-positron pairs. Large kinetic energy of RE suggests that the electron-positron pairs may be produced in the field of nuclei. The pair production caused by high energetic photons in material is a well-known process, observed for example in scintillation detectors. High energetic electrons in the field of ions may produce pairs either directly (the process is known as "trident process") or via bremsstrahlung photons.

The energy threshold for the pair production (1022 keV) is easily achieved by RE and the total cross section is [14],[18]

$$\sigma_{tot} = aZ^2 \ln^3 \left(\frac{\gamma_e + x_0}{3 + x_0} \right), \tag{2.41}$$

where a is a constant of the order μb and x_0 is a constant of the unit order. Notice the quadratic dependency on the charge of the nucleus Z. This means that the positron creation is in particular possible in plasmas with high Z impurity presence. A low temperature argon plasma with the RE beam after disruption triggered by gas injection represents the suitable environment.
The RE positrons are created with high initial velocity [14]. The positrons heading in the right direction may immediately runaway. These particles are almost collisionless, albeit in contrast to RE, they are moving in a direction corresponding to the direction of plasma current. The life time of runaway positrons may be quite long (in the order of seconds) according to theoretical estimation, enabling the outward drift and annihilation with particles of the first wall [33].
The detection of runaway positrons in tokamaks has not been successful yet. Annihilation radiation is weak in comparison to other sources. The possible detection method could rely on synchrotron radiation measurement, as it is strongly peaked in the direction of the particle flight [14]. This means that an IR camera opposing the direction of plasma current could see large runaway runaway positron population. Runaway positrons carry an imprint of the confined RE properties, therefore, the detection of positrons, if possible, could present useful diagnostic method for validation of the RE models. It seems that if the number of runaway positrons was indeed as large as the theoretical estimations predict, it would be also an important channel of the RE energy loss. This is a open topic that needs further theoretical work, incorporation to models and development of novel sensitive diagnostics.

2.5 RE confinement and losses

The confinement of runaway electrons in hot plasma is one of the topics that are not fully understood and several mechanisms have been proposed. It seems reasonable that the confinement of RE is better in diverted plasmas than in circular limited plasmas. However, the differences are large. If RE electrons are continuously accelerated, they should leave the plasma relatively early due to the radial drift velocity. In Compass, there is evidence that some part of the RE population is able to survive the whole discharge in the central plasma region. This may suggest that there is some kind of equilibrium possibly due to avalanche or synchrotron radiation, although estimated energies of the RE in COMPASS are below the level typical for equilibrium connected to this phenomenon. The mechanism of RE confinement within magnetic islands was also proposed and it is mentioned in many publications including [26].
The radial drift velocity may determine the time of RE crash into the plasma facing components. It was theoretically studied in publication [19] by the means of the relativistic Lagrange formalism for gyro-averaged equation that was briefly described in the first chapter of this thesis. The authors derived the relation for the drift velocity that resembles

the velocity of $E \times B$ drift (toroidal electric field and poloidal component of magnetic field). However, the effective electric field due to the synchrotron and bremsstrahlung radiation drag forces is also included.

$$\mathrm{v}_D = \frac{q(E + E_{\mathrm{eff}})}{B_T}, \tag{2.42}$$

where $eE_{eff} = F_S + F_B$ is effective electric field given by synchrotron and bremsstrahlung radiation drag force and q is the safety factor, that describes the magnitude of the magnetic field lines helicity.
In MHD models, the Rosenbluth-Rochester radial diffusion approximation for perturbed magnetic field is used frequently

$$\left(\frac{\mathrm{d}n_{RE}}{\partial t}\right)_{loss} = \frac{1}{r}\frac{\partial}{\partial r}\left(D_{RR}\frac{\partial n_{RE}}{\partial r}\right), \qquad D_{RR} = \pi q \mathrm{v}_{\|} R \left(\frac{\delta B}{B}\right)^2, \tag{2.43}$$

where $\mathrm{v}_{\|}$ is parallel velocity, usually considered to be near c, R is the value of major radius, q is the safety factor and $\left(\frac{\delta B}{B}\right)$ is relative value of the magnetic field fluctuation usually in the order of 10^{-5} - 10^{-2}. However, this diffusion term was derived for fully stochastic magnetic field lines and predicts very fast loss of all RE. The presence of magnetic surfaces with well defined magnetic topology can strongly suppress the losses. At this moment, general model of runaway electron confinement and losses is not available. The transport of supra-thermal electrons is described for example in Chapter 2 of thesis [51].

2.6 RE-wall interaction

The interaction of fast electrons with dense matter is dominantly carried out via collisional ionisation or excitation (interaction with electrons) and bremsstrahlung radiation (interaction with ions). Bremsstrahlung dominates for higher energies and higher atomic numbers. This means that for typical energies and materials of plasma facing components, the ionisation and excitation processes dominate [2]. As the density of particles in solid materials is many orders of magnitude larger compared to that of plasma, the electrons lose their energy very quickly when reaching the wall. With respect to the thickness of the vacuum vessel and other coatings, no runaway electrons manage to get out of the tokamak. Of course, other processes, like the direct pair production mentioned above, also take place in the material surrounding the plasma. However, the energy of the electrons is transformed dominantly to the hard X-ray (HXR)/gamma radiation that can be easily measured. The reconstruction of the properties of the RE beam (e.g. the distribution function) using this effect is difficult.

2.6.1 Photoneutron creation

If the energy of incident runaway electron is high enough, the HXR bremsstrahlung photon is able to interact with nuclei of the wall material. If the photon has energy that

exceeds the binding energy of nucleus ($\sim E_{th}$), giant dipole resonance occurs. During this process some particle is released and the nuclei is transmuted into the different isotope. Neutrons are able to leave the material of the wall easily, thus (γ,n) reactions are the most interesting regarding the diagnostics. However, for some materials (γ,p) and (γ,α) reactions are also possible. The most relevant photoneutronic reactions are these [16]

$$\begin{aligned} {}^{12}\mathrm{C}(\gamma,\mathrm{n})^{11}\mathrm{C} \qquad & E_{th} = 18\,MeV \\ {}^{13}\mathrm{C}(\gamma,\mathrm{n})^{12}\mathrm{C} \qquad & E_{th} = 4.9\,MeV \\ {}^{9}\mathrm{Be}(\gamma,\mathrm{n})^{8}\mathrm{Be} \qquad & E_{th} = 1.7\,MeV \\ {}^{2}\mathrm{D}(\gamma,\mathrm{n})^{1}\mathrm{H} \qquad & E_{th} = 2.2\,MeV \end{aligned} \tag{2.44}$$

2.7 Overview of important modelling tools

The efforts in modelling of the runaway electrons beam has been very intensive in the last decade. Although the experiments in smaller machines could contribute with ITER-relevant results they should be combined with modelling to improve our understanding of plasma physics. Moreover, we should be able to predict the behaviour of plasma and quantitative values of important parameters for ITER. The modelling of runaway electrons, namely their generation during the disruption is especially important for the safety of the machine.

The models in plasma physics can be generally divided into two groups - predictive and interpretative. The former try to infer the desired results from either first principles, complex theories or phenomenological relations, while the latter use the measured data to uncover the nature of processes behind this data. These attitudes are usually combined to get a truly reliable model.

The various models of runaway electrons generation and losses in tokamaks use all the attitudes described in the first chapter. To decide whether runaways are important in plasma of particular parameters, it is sufficient to use the fluid approximation and estimate the number of RE from their primary rate. If we want to know the distribution function or inspect the interaction with kinetic instabilities, the kinetic models based on the Fokker-Planck solvers are necessary. Then, to estimate the losses of runaway electrons in slightly perturbed magnetic field, the relativistic drift equation is the best option. Finally, if the changes of magnetic field are too large, we have to use full equations of motion.

In current models, the work is focused on the right implementation of synchrotron energy losses and energy limit that arise due to these losses. Further important topic is the right implementation of avalanche operator and pitch angle scattering into kinetic models. Let us summarise the most important models that have been frequently used and further developed lately. On the other hand there are many different models like ARENA or CLQ3D that are a bit older but still often used. CLQ3D was used for example in thesis [28].

LUKE

LUKE is very a complex RE dynamics code developed at CEA Cadarache.[9] It is based on Fokker-Planck solver with avalanche operator. Later, synchrotron radiation drag force

was also included and there is possibility to add source terms like radiofrequency heating, etc. This software is probably the best option for understanding the steady-state plasma with RE generation. There are two possible ways how to include parameters of plasma equilibrium - the first is directly based on measured data and the other uses plasma parameters of plasma equilibrium supplied by METIS/CRONOS codes. LUKE is connected with the databases of many tokamaks (JET, TCV, EAST,...) and it was coupled also with the COMPASS database in recent months.

CODE + SYRUP

CODE (COllisional Distribution of Electrons) is light, computationally effective software that deals with primary and secondary runaway generation and computes the electron distribution function from equilibrium between acceleration and drag force, while SYRUP computes the synchrotron radiation spectra for particular machine and electron distribution function. Together, CODE+SYRUP can describe the generation and acceleration of runaway electrons with high computational efficiency [32, 55].

GO

The GO code is a compact 1D fluid (MHD) model of cylindrical plasma designed to describe the RE electron generation during the disruptions. It contains many processes important for disruption analysis including electric field diffusion and radiation operators to solve the energy balance of electrons, ions and impurities.

Chapter 3

Runaway electrons in COMPASS and Golem tokamaks

3.1 Brief characteristics of the Czech tokamaks

3.1.1 COMPASS

The COMPASS (COMPact ASSembly) tokamak was originally built in United Kingdom and operated at Culham Centre for Fusion Energy as Compass-D during 1989-2001. It was offered to the Institute of Plasma Physics of the Czech Academy of Sciences after the spherical tokamak MAST was built and commissioned in Culham. The previous tokamak of the CSAV was rather small and obsolete (but unique in the new EU countries), so this was a great opportunity to make the fusion research in the Czech Republic more up to date. Transport of the tokamak to the newly constructed hall happened in 2007 [40]. Since 2012, COMPASS has operated in regular scientific campaigns including H-mode discharges. In the Table 3.1, main parameters of the machine are listed.

The ITER-like configuration and plasma shape (so called D-shape and single-null divertor (SND) configuration) makes COMPASS relevant for scaling experiments. Due to its size (probably the smallest tokamak to operate in the full H-mode), experiments are focused on plasma-wall interaction and diagnostics of the edge plasma. One of the

Major radius	R	0.56 m
Minor radius	a	0.23 m
Max. plasma current	I_p	400 kA
Toroidal magnetic field	B_t	0.9-1.3 T
Vacuum level	p_0	10^{-6} Pa
Plasma shape		D, SND, elipse, circular
Elongation	ϵ	1.8
Pulse length	t_p	$\sim$ 500 ms

Table 3.1: The basic parameters of tokamak COMPASS and its plasmas.

most important topics considering the plasma core are runaway electrons. The runaway electron experiments are conducted under the MST2 (Medium Size Tokamaks) project of EUROfusion, the coordinating body of the European fusion research centres.

3.1.2 Golem

Tokamak Golem was constructed among the first tokamaks in the USSR under the name TM1 and it has served many years at the Institute of Plasma Physics as CASTOR (Czechoslovak Academy of Sciences TORus). The research was focused on the edge plasma and Lower-hybrid waves then. After the opportunity to get COMPASS has appeared, CASTOR was moved to the Faculty of Nuclear Sciences and Physical Engineering of the Czech Technical University in 2009. The new name Golem is connected to the old Jewish legend as the building of the Faculty is situated in the former Jewish quarter.
The tokamak is now operated namely by students and it offers experiments for distant universities and other institutes via remote web-based control room. Although some of the systems are still under construction (e.g. feedback system), this device offers a remarkable opportunity to study the RE as its discharges are typically of low temperatures and large electric fields. Direct line averaged density measurement via interferometer was successfully installed recently. The parameters of this historic tokamak with modern control interface are in the Table 3.2.

Major radius	R	0.4 m
Minor radius	a	0.09 m
Max. plasma current	I_p	$\sim$ 2 kA
Toroidal magnetic field	B_t	$\sim$ 0.3 T
Plasma shape		circular
Pulse length	t_p	$\sim$ 10 ms

Table 3.2: The basic parameters of tokamak Golem and its plasmas.

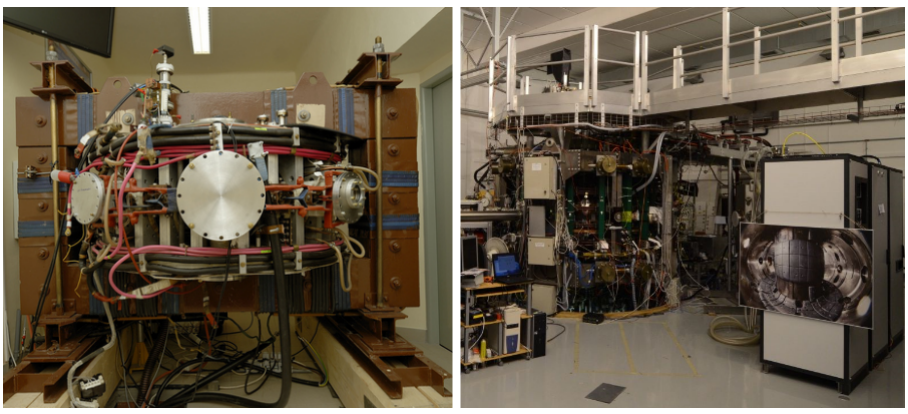

Figure 3.1: Photograph of tokamak Golem (left) [54] and tokamak COMPASS (veda.cz).

3.2 Runaway electrons in smaller tokamaks

Small tokamaks generally reach lower values of plasma parameters that are most important for runaway electron production - the electron density n_e and electron temperature T_e. Furthermore, the electric field that is required to plasma creation and sustainment of plasma current, is determined by the level of impurities expressed by the effective charge Z_{eff} defined in the previous chapter.

3.2.1 Role of plasma density

Maximum accessible plasma density n_e is determined by the value of toroidal magnetic field. To be more specific, the plasma density limit is proportional to square of the magnetic field. This relation follows from equilibrium of plasma the pressure and the pressure of the magnetic field that is essential for magnetic confinement. The parameter β is defined as the ratio of the pressures

$$\beta = \frac{< p >}{\frac{B^2}{2\mu_0}} = \frac{en_eT_e[eV]}{\frac{B^2}{2\mu_0}}, \tag{3.1}$$

where μ_0 is permeability of vacuum and e is elementary charge. Values of β are below 10% for tokamaks, the accessible values of density are slightly above $10^{20}\,\text{m}^{-3}$ for $B = 1\,T$ and temperatures around 1 keV. For COMPASS this means standard operation with densities in the order of $10^{19}\,\text{m}^{-3}$ and for Golem almost order of magnitude lower. Another density limit is rather phenomenological, the value of the Greenwald density

$$n_{G,20} = \frac{I_p}{\pi a^2}, \tag{3.2}$$

in this form depending on plasma current I_p in MA and minor radius a in m, presents the upper electron density limit in $10^{20}\,\text{m}^3$. Although this limit is not sharp, disruption usually occurs when it is exceeded. The Greenwald limit is very high for COPASS and near $10^{19}\,\text{m}^{-3}$ Generally speaking, this means, that the values of density in small tokamaks are more suitable for the RE creation.

3.2.2 Role of plasma temperature

Temperature T_e is very important as the Dreicer field and critical velocity are inversely proportional to its value. Therefore, higher temperature plasma generally means more RE. We can understand this in a simple way: typical time during which one particle is affected by the field of the other (Coulomb interaction between two particles) is lower as they are moving faster and this effectively lowers the drag force. In smaller tokamaks, temperature is lower than in larger machines and the experimental energy confinement time is also lower in small tokamaks. The reasons are practical - the ohmic heating starts to be ineffective around 1keV and for further increase of temperature, additional heating systems must be utilised. As the discharges in small tokamaks are generally shorter and additional heating systems are quite expensive both in terms of initial costs and operation,

the systems are used only for specific experiments and not on the regular basis (COMPASS - Neutral Beam Injection). The smallest machines are usually not equipped with such systems at all (Golem). In agreement with these facts, typical electron temperatures in COMPASS are 600 eV without NBI, 1200 eV with NBI and for Golem few tens of eV. The ion temperature T_i in small tokamaks with short discharges is lower than the electron temperature T_e because ion heating is slower and equilibrium of T_e and T_i is not established. We should remind that the optimal ion temperature T_i for deuterium-tritium fusion is 10-20 keV and small tokamaks are far from reaching these values. To sum this up, the temperature in smaller tokamaks is lower and according to this single parameter RE generation should be weaker in smaller tokamaks. The value of this parameter namely lowers the importance of the hot tail RE generation 2.1.2 that is partly responsible for the RE beam initiation during the disruptions. The sudden thermal quench which is necessary for this mechanism starts with more narrow distribution function and the collisional time of the particles from the tail of the distribution is longer for lower temperatures. This does not mean that the creation of the post disruption runaway beam is impossible, however, it is probable only with strong RE seed originating in the breakdown.

3.2.3 Role of plasma impurities

Runaway rate (2.27) is a strong function of Z_{eff}, so this is a crucial parameter. Unfortunately, the experimental measurements of this parameter are rather difficult and it is not fully integrated on COMPASS. In the case of Golem, the value of Z_{eff} could be only guessed from simple visible spectrometer data.
The impurities may originate in many sources including air (ineffective vacuum pumping), first wall and its treatment (little shards of material, boronisation, ...) or even intentionally inserted higher Z elements (disruptions mitigated or triggered by injection of Ar, ...). Tokamak Golem is currently equipped with quite ineffective vacuum pumping and Z_{eff} is very large (estimated above 5). On the other hand, COMPASS is a well maintained tokamak with scheduled baking in between the campaigns and glow discharge ideally after every experimental discharge or at least after 4 discharges. Therefore, Z_{eff} should match common levels (2-3).
The role of Z_{eff} should not be misinterpreted. It increases the friction force for all electrons, however this effect is important namely for the thermal electrons. Higher impurity level increases the plasma resistivity and this results in higher breakdown voltage and even the voltage during the later phase of the discharge. Thus, the probability of the RE creation is higher in impure plasma. This highlights the role of vessel conditioning. For example the discharge accompanied by HXR emission was repeated without HXR after the glow discharge in tokamak Golem.

3.2.4 Electric field - feedback vs. predefined

Electric field in modern tokamaks is usually predefined for breakdown phase, albeit in the later part of the discharge it is maintained by the feed-back based on the requested plasma current. This is also the case of COMPASS. This attitude may help to limit the RE population even for lower densities. Once the RE beam carries a significant part of

the current, the electric field goes down almost to zero and the number of RE is no longer increased by primary mechanism. The regime with majority of plasma current carried by RE is called slide-away regime. For discharges with higher densities the feed-back may also help to create plasmas without RE.
However, in tokamak Golem , the typical length of the discharge and time scales of instabilities are too short to use the feed-back. The electric field is predefined by the voltage and time constants of the capacitors. The electric field rises as a sine function while the decay is exponential. This means that the vacuum electric field is rising for significant part of the discharge. It should be mentioned that the typical length of the Golem discharge is comparable to the length of COMPASS breakdown phase (that is also predefined), therefore it may be comparable. The breakdown phase/current ramp-up phase is generally the largest source of RE in smaller tokamaks. The electric field is high and in the beginning the electron density is very low, as some of the atoms are not ionised and only a necessary amount of fuel is injected. In this situation the FP drag force is small and the role of the interaction of electrons with neutral atoms has to be calculated by Monte-Carlo algorithms.

3.2.5 Magnetic field

The magnitude of the magnetic field may probably influence the runaway generation in specific situation, albeit it affects namely runaway losses, synchrotron radiation spectra and thresholds for some instabilities connected with the RE beam. In COMPASS the toroidal magnetic field (1.3 T) is relatively low in comparison with other tokamaks. In Golem, the field is in the range 0.3-0.5 T. Lower value of magnetic field naturally means lower level of confinement and greater migration of particles across the magnetic field lines (most of drifts $\sim 1/B$). For RE with small pitch angle also the magnitude of vertical field plays important role (betatron approximation 1.2.6). Also, the synchrotron radiation spectrum is shifted towards lower energies with lower values of magnetic field (far IR in the case of COMPASS and sub-millimetre waves for Golem). Furthermore some of the instabilities are connected with the magnitude of cyclotron frequency and therefore with the magnitude of magnetic field (Parail-Pogutse instability also known as fan-like instability briefly described in section 3.5.2).

3.3 RE generation for typical plasma parameters

The growth rates and number of runaway electrons for given radial profiles of plasma parameters was estimated in thesis [28]. In this thesis, namely Kruskal-Bernstein relation for growth rate and several codes (for example CLQ3D) were used. We will use the more simple estimation of density of electrons with velocity higher than critical limit for given parameters (relation (2.24) derived in the second chapter). We should remind again that this relation can not provide the direct estimation of the overall number of runaway electrons in plasma, however it helps to identify the parameters and discharge phases that are suitable for the RE generation. The main advantage of this estimation method is its simplicity, it relies only on the derivation of runaway solution from the FP equation.

However, we should remind that the high velocity limit of the Chandrasekhar function was used and this estimate is becoming improper for velocities near the thermal velocity. All the graphs below display the order of magnitude of runaway electron density (color) as a function of temperature and electric field for typical range of these quantities. The plasma density is fixed.

3.3.1 COMPASS

Typical values of the electric field (in this approximation the value of the field is derived from the loop voltage on the position of the magnetic axis) in COMPASS are $0.1-0.7\,\mathrm{V/m}$ during flattop and $3-5\,\mathrm{V/m}$ during the plasma breakdown and fast disruptions. The typical temperature range was described above. The Z_{eff} is set to 2.5.

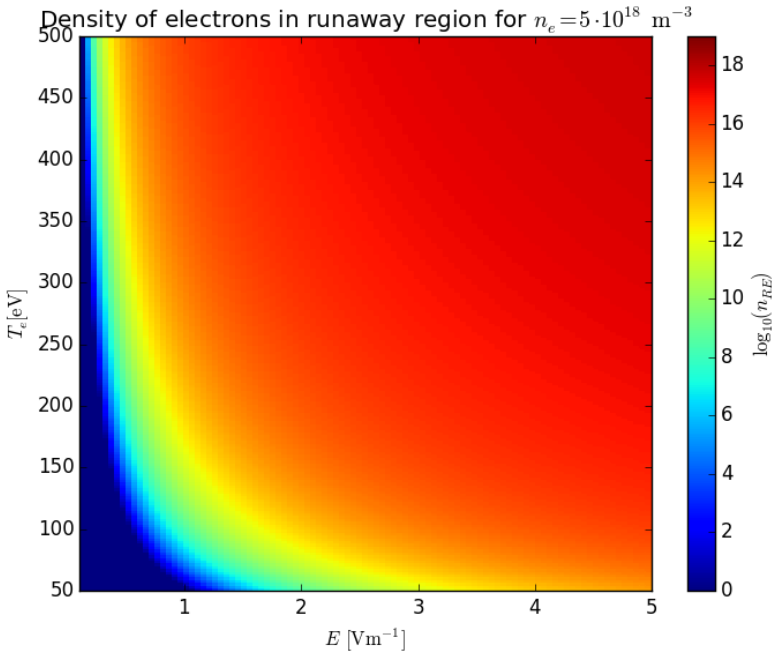

Figure 3.2: The density of electrons in the runaway region of velocity space for given range of plasma parameters typical for the plasma breakdown and low density discharges (dedicated runaway campaign) in COMPASS tokamak.

3.3.2 Golem

For Golem, typical values of the electric field are much higher,$3-4\,\mathrm{V/m}$ during the discharge. This is caused by a high impurity level. The breakdown field and the field during the fast plasma termination are not much higher, because the maximum field is limited by parameters of the capacitor bank. The electron temperature in Golem is estimated using simple visible spectrometry, its values usually vary from 10 to 20 eV. However most of the visible radiation comes from the plasma edge, the central temperature may be higher.

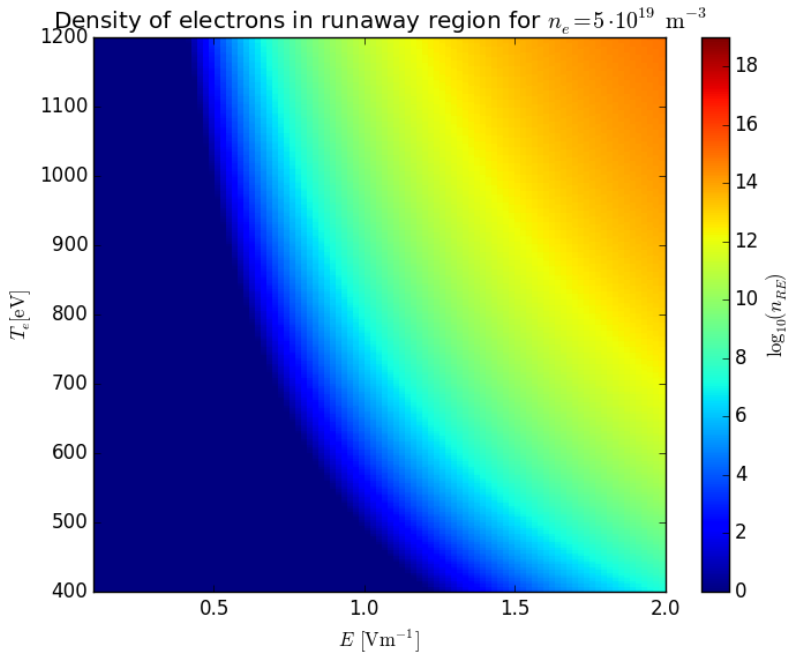

Figure 3.3: The density of electrons in runaway region of velocity space for higher density discharges and temperature up to the values accessible only with Neutral Beam Injection, tokamak COMPASS.

Thanks to the recent an re-installation of interferometer, the typical electron plasma density was measured to be in the range $3 - 8 \cdot 10^{18}\,\mathrm{m}^{-3}$. These densities are close to the Greenwald density limit for this small tokamak with relatively low plasma current. The value of Z_{eff} is set to 5.

3.3.3 The role of the avalanche mechanism

The previous sections were focused on the primary generation. However the avalanche mechanism can be very important namely in COMPASS. In COMPASS and Golem tokamaks, the electric field is several orders of magnitude higher than the critical field, but the discharges in tokamak Golem are very short and the confinement time of runaway electrons corresponds only to 1-2 ms, which is not favourable for the avalanche.
The situation for COMPASS is displayed in the figure 3.6, where the avalanche growth rate is calculated using equation (2.32) as a function of the seed runaway electron density and the applied electric field. The population of RE may be increased by several tenths of original number or even doubled during typical COMPASS discharge (300 ms) according to this simple calculation. A significant increase of RE number due to the avalanche is indeed observed in experiment.

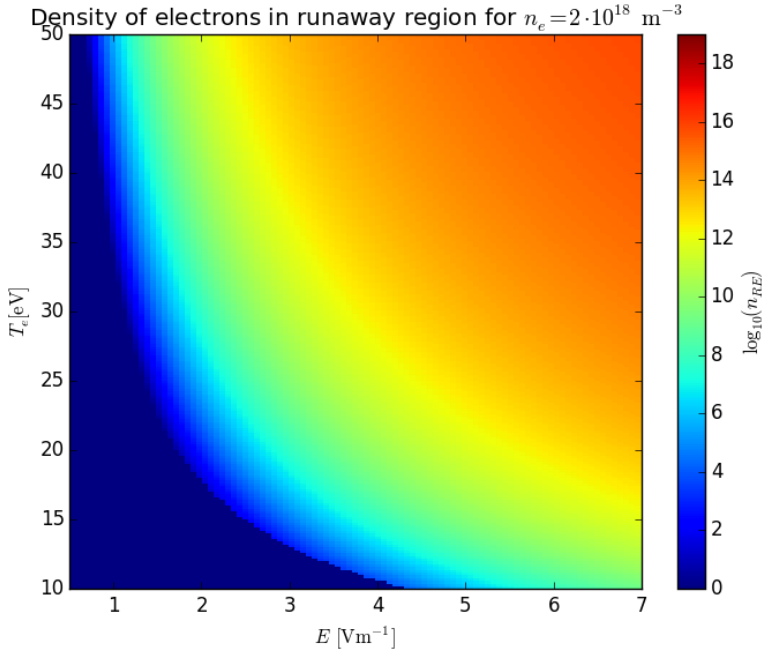

Figure 3.4: The order of magnitude of potential runaway electrons density for plasma parameters typical for breakdown and low density regimes in tokamak Golem.

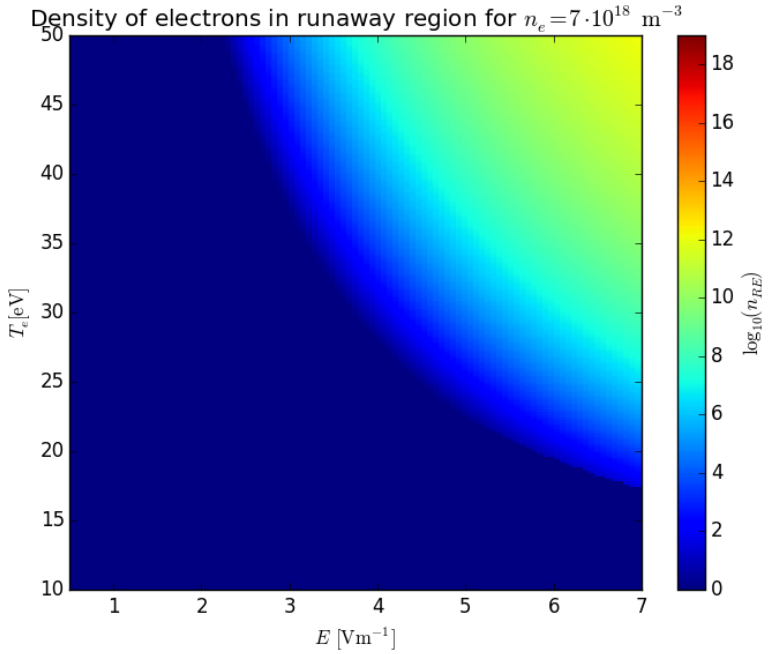

Figure 3.5: The order of magnitude of electron density in runaway region of velocity space for plasma parameters typical for standard stationary phase of the discharge in tokamak Golem.

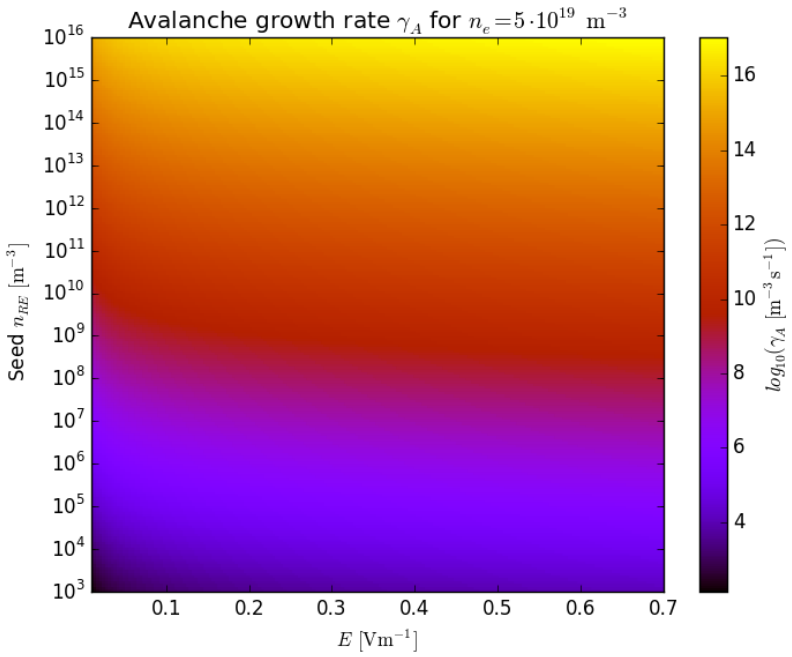

Figure 3.6: The order of magnitude of runaway electron density growth rate γ_A due to the avalanche in discharge with higher density (the electron density dependence of this mechanism is weak). The range of seed values covers estimated density of runaway electrons generated during the plasma breakdown and the range of electric fields is corresponding to typical values in the flat-top.

3.4 Diagnostic methods and standard scenarios

An overview of diagnostics methods suitable for RE detection is described in previous work [13]. Therefore, only diagnostic systems utilised on COMPASS and Golem will be described here. In following sections, also the discharge evolution and possible scenarios are described.

3.4.1 Diagnostic system on COMPASS

Although the systematic study of runaway electrons began last year on COMPASS, the machine was equipped with basic diagnostics confirming the presence of RE also during previous operation. Hard X-ray NaI(Tl) scintillation detector with 2" scintillation crystal and photomultiplier tube was installed from the very first shots of physics campaign. Later was added also plastic scintillation detector with increased sensitivity to neutrons and shielded by 10 cm of lead. However, during the first campaign it was proved that this detector measures also high energy photons (1-10 MeV), that have much higher intensity than photo-neutrons from the RE-wall interaction. In next sections, the diagnostics that gives some information about runaway electrons and that was in operation during the runaway campaigns is described.

HXR measurements

For the RE campaign, the HXR diagnostics system was enhanced using more scintillation detectors. In the first campaign, three dectectors were borrowed from the Department of Dosimetry FNSPE. Those were again 2" NaI(Tl) scintillation detectors with PMT working with positive input high voltage (HV). As these detecors were slightly older, they were equipped with external signal/HV separators. In the beginning of the campaign, there were some problems with noise (50 Hz) which was later identified as an effect of the common grounding on the data acquisition system.
One of the detectors mentioned above was borrowed also for the second campaign together with the detector from Golem tokamak that is mentioned in the next section. To extend the routine measurements of HXR radiation on COMPASS, 4 new CsI(Tl) scintillation detectors with semiconductor amplifying were installed. These detectors have many advantages namely considering the compactness and no need for the HV power source. On the other hand, this concept was proven to be very unsuitable for our usage. First of all, the time constant of the electronics had to be decreased ten times to get reasonable time resolution. After this adjustment, the detectors were able to measure only medium intensities. Due to the low signal to noise ratio, this type of detector fails to measure low intensities. It is also turning off in the case of saturated signal to prevent damage and therefore the detector is unable to measure also very high intensities. This effect can be partially prevented using lead bricks, however, the detectors are not as useful as traditional scintillators with PMT.

Other diagnostics affected by RE

The typical wavelength of RE synchrotron radiation should be in the infrared region of electromagnetic spectra. Regarding this, the slow IR camera (array of bolometers with filter) with wide wavelength range was attached to the co-current tangential port. During several shots strong signal that seemed to originate in plasma was measured. Furthermore, in some discharges, the reflected synchrotron radiation of the RE beam was probably measured.
Unfortunately, the IR spectrometer that was also installed in the tangential port, did not observe any IR radiation. It might be caused by too narrow spectral range in the transition of visual and IR region or unsuitable geometry.
The novel concept of Cherenkov detector was also tested during the first and third RE campaign with interesting results. This detector measures the lost energetic electrons directly. The principle was briefly described in [13]. The electron cyclotron emission diagnostics indicates high parallel momentum via measurements of intensity of the radiation emitted during the cyclic motion around the magnetic field line. It is installed in radial ports and therefore it detects only runaway electrons with large pitch angles. It can be especially useful for identification of particular instabilities, albeit it was not on-line during the first and second campaign. However, the ECE was tested on COMPASS and can be utilised for the edge plasma measurements in the third campaign.
SXR arrays on COMPASS were not constructed for measurements of RE, albeit for the purpose of this thesis, their ability to identify the saw-teeth instability is very useful. These detectors on COMPASS consist of semiconductor elements covered by $10\mu m$

beryllium foil. The measured energies should be in between 1 and 10 keV. There are more arrays on one poloidal cross section to enable the SXR tomography. During the low density discharges with high-energy runaways, the spiky signal appeared, corresponding to HXR emission due to the RE. Except of these spikes, the signal was almost zero in circular discharges. It is not clear if those spikes are caused by bremsstrahlung photons originating in plasma or rather by photons from interaction of runaways with plasma facing components. The latter option is more probable.
There are many other diagnostic systems that may give an evidence of runaway electron presence or that are necessary for the estimation of conditions suitable for RE generation. We should name plasma current I_p and loop voltage U_{loop} measurements, interferometer/Thompson scattering density n_e measurements, Thompson scattering temperature T_e measurements and spectroscopy among these. The toroidal magnetic field value B_T and the plasma shape and position reconstruction (calculated by EFIT) are also important. However this reconstruction program is designed for an equilibrium with plasma current carried by thermal particles and therefore the results for discharges with high number of RE are not reliable.

3.4.2 Diagnostics - Golem

Golem was also equipped with HXR scintillation probe during numerous discharges, although until autumn 2014 the fast HXR detector had been borrowed from the spectroscopic task of the Physics Practica of FNSPE. The width of the peak corresponding to a single gamma photon was approximately 5 μs for this detector, which was operated with positive input voltage using HV power source and a secondary amplifier between the detector and data acquisition system. In autumn 2014, another HXR NaI(Tl) scintillation detector was purchased. This new detector was more economic. It is designed for negative input voltage and the peaks are characterised by quick rise (1 μs) and long decay time ($\sim$ 150 μs). Due to these values, the number of pile-ups is very high. However the energy can be still estimated in some discharges from the height of the peak. Integrated signal can be also utilised to estimate the overall dose by comparing the area under the graph of the signal with the area of a single ^{137}Cs peak. The deposited energy obtained by this attitude have to be divided by the mass of the scintillation crystal (for 2" crystal the mass is approximately 200 g).

In-vessel TimePix detector for Golem

The Faculty of Nuclear Science and Physical Engineering of the Czech Technical University (CTU) is very active in the field of semiconductor particle detectors for various applications. Therefore, one of the small TimePix (sensor chip described for example on webpage [6]) detectors designed and developed in the framework of specialised research project will be tested in the environment of tokamak Golem. The semiconductor matrix device will be placed on the manipulator inside the vacuum chamber. The detector is sensitive to supra-thermal electrons and γ radiation with energies in the range of several tens or hundreds of keVs. This is suitable for RE detection in Golem and in small tokamaks. This attitude can offer an option to the Cherenkov detector that also measures the RE in-

side the tokamak. However, this is a long term project and only preparatory works have started so far. The technical aspects of this project are topic of the PhD thesis of Tomáš Benka from the Faculty of Electrical Engineering of CTU.

3.4.3 Evolution of the COMPASS discharge

The COMPASS tokamak data are typically displayed as a function of time in milliseconds with discharge initiation (plasma breakdown - BD) occurring slightly before 960 ms ($t = 0$ ms correspond to switch-on of the toroidal magnetic field). Plasma density at the beginning of the discharge (920-970 ms) is controlled by pre-set waveform of the gas puff (GP) valve and then it is usually kept on the desired value by a feedback system (sensor: interferometer, actuator: gas valve). The rise of the plasma current (ramp-up phase) usually lasts 60-80 ms. The part of the discharge with constant current of desired value is called flat-top (FT). The discharge preferably terminates in a controlled way called ramp-down. COMPASS is able to operate with circular plasmas (this is the case for low density discharges with high RE density), elongated and diverted plasmas. Also, the operation in high energy confinement regime (H-mode) is possible. In this regime hot central plasma is isolated by edge transport barrier that is characterised by the typical pedestal in plasma pressure profile and lower level of emitted radiation. COMPASS is able to transit into the H-mode using only Ohmic heating, however, the transit can facilitated by Neutral Beam Injection. When describing the H-mode, we should also mention ELMs (edge localised modes) - operation in H-mode is usually connected with quasi-periodic emission of plasma bunches. According to present physical models ELMs are connected to relaxation of the edge transport barrier and may be observed as a spiky signal on H_α radiation measurements during the H-mode experiments.

3.4.4 Discharge evolution - Golem

The time axis of graphs visualising the Golem data is labelled in milliseconds, too. The data are acquired for 40 ms and the plasma breakdown usually occurs 1 or 2 ms after the initiation of the electric field (the exact time can be set, the timestamps 10 or 15 ms are the most common values, switch-on of the toroidal field is absolutely independent). The evolution of the plasma current is usually of a parabolic shape sometimes with signs of a flat-top or sudden termination.

3.5 Achievements of COMPASS RE campaigns

The three campaigns conducted so far in the framework of MST2-9 EUROfusion project were successful and many remarkable results were achieved. Let us mention here the most interesting achievements.

3.5.1 RE plateau after Ar induced disruption

The post-disruptive RE beam can be the most dangerous event for ITER. This appeared as a possibly dangerous issue during disruptions triggered by Argon massive gas injection at JET [44], DIII-D [22] and other machines. Argon triggers thermal quench and sudden drop of conductivity leads to the increase of the loop voltage and better conditions for RE generation, the hot-tail mechanism probably playing a significant role. However, in small and medium size tokamaks, it is difficult to produce the RE beam during the rapid plasma termination. The most promising results were achieved on Tore Supra [50], where Argon injection in the current ramp-up phase (high loop voltage) was optimised. In the second dedicated RE campaign, the described scenario was also reached in COMPASS [59]. This type of discharge was repeated several times, however, at this moment, COMPASS is far from obtaining this beam regularly. The role of the wall conditioning and the gas recycling is obvious. The plasma parameters evolution for the discharge with strong RE beam are in figure 3.7 and the beam is visualised by argon line radiation on series of frames from fast visible camera in figure 3.8.

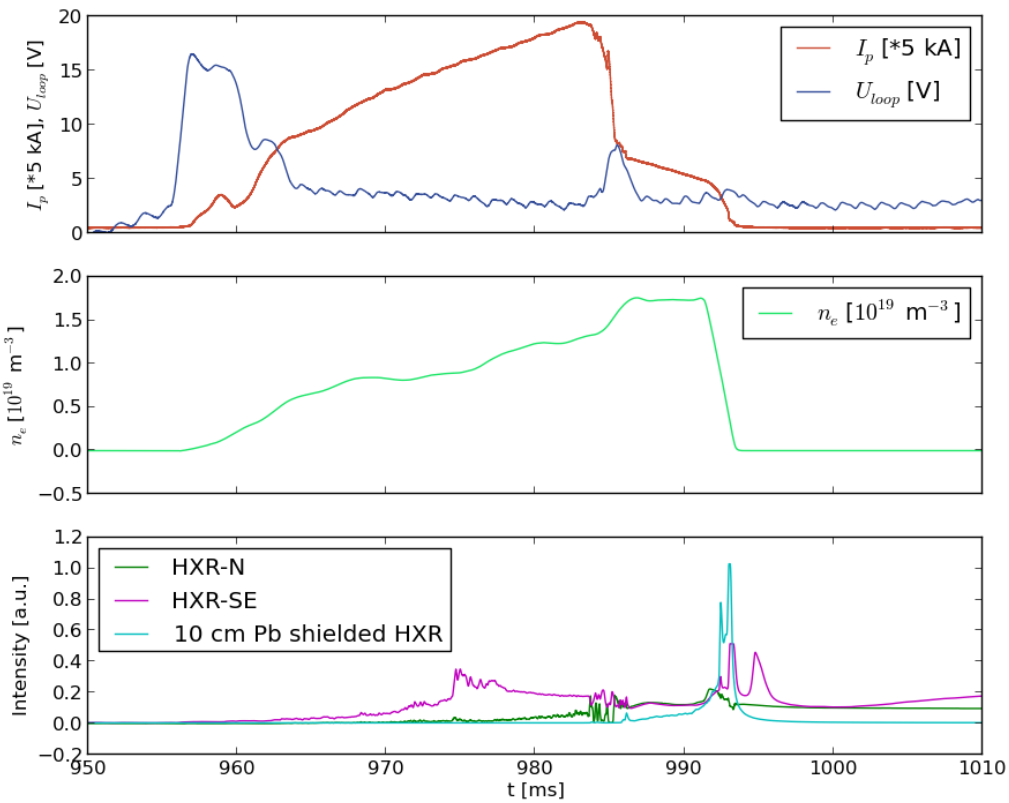

Figure 3.7: The most important plasma parameters (plasma current I_p and loop voltage U_{loop}, electron density n_e and signals from HXR detectors.) for the discharge #8585 with RE plateau after the argon induced disruption.

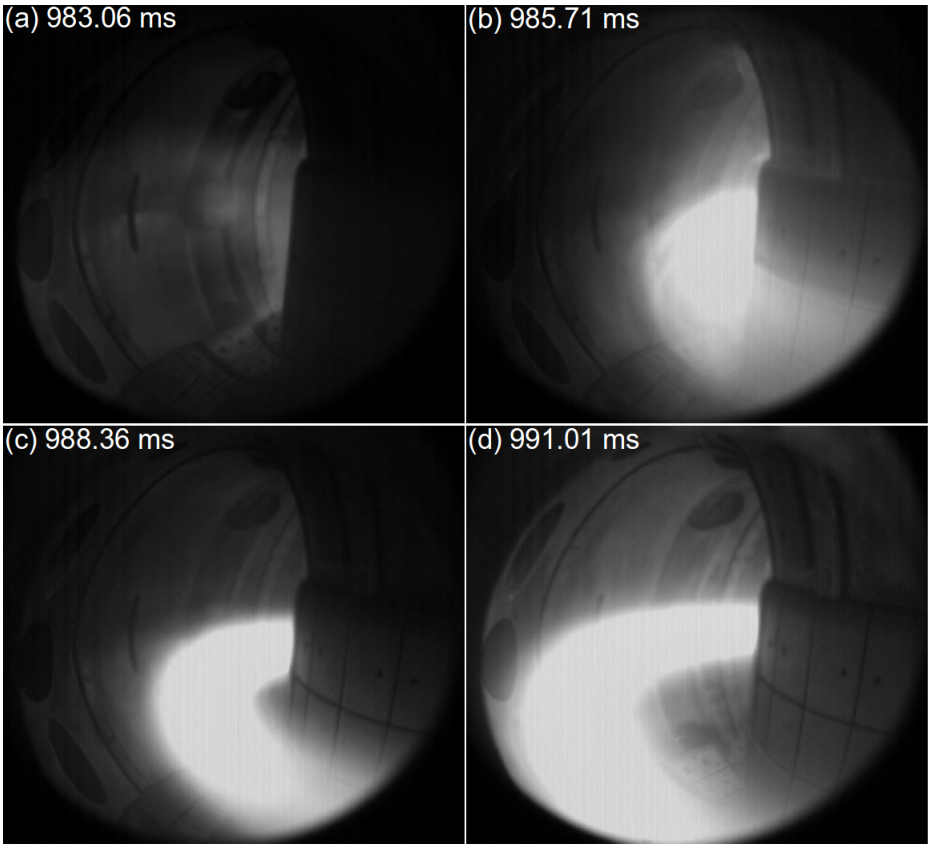

Figure 3.8: Images from visible camera showing clearly the RE beam after the Ar-induced disruption in discharge #8585, the radial expansion may be observed. Courtesy Miloš Vlainič and the Visible camera team.

3.5.2 Low density discharges with Parail-Pogutse instability

Circular discharges with very low density ($1 \cdot 10^{19}$ m^{-3} and lower) were characterised by production of RE during the whole discharge. In this case, the specific fan instability was probably achieved. This phenomenon is also called Parail-Pogutse(-Kadomtsev) instability (PPI) [45] after Russian scientists that provided the theoretical description. The nature of this instability is a resonance interaction between RE beam in plasma and a plasma wave. The RE beam may generate magnetised Langmuir wave via anomalous Doppler effect. This wave is then responsible for scattering of high energy electrons which results in truncation of distribution function above some velocity limit and fast loss of those particles with increased perpendicular component of velocity. However, the wave is damped by Landau damping (the mechanism of the damping is also described in [29]) when the distribution function is perturbed by the scattered RE. Finally, electrons reach the velocity limit again and the process is periodically repeated. The Landau damping on electrons is sufficient for distribution functions with high slope, thus it prevents the growth of the PPI in discharges with Maxwellian plasma and, on the other hand, it is unable to stop the instability growth in the case of distribution function with the flat runaway region [51]. The necessary conditions for evolution of this instability may be summarised as follows

$$\omega_{Ce} > \omega_{pe} \qquad v_b > 3\left(\frac{\omega_{Ce}}{\omega_{pe}}\right)^{3/2} v_c, \tag{3.3}$$

the first condition is satisfied at low densities for a given magnetic field. The second condition gives minimal beam velocity as a critical velocity (defined in section 2.1.1) multiplied by some factor and therefore, it can be satisfied in the case of strong primary RE generation. In some publications, third condition for collisional frequency is added. The most important parameters of the discharge 8559 together with the validation of the first condition are presented in figure 3.9.

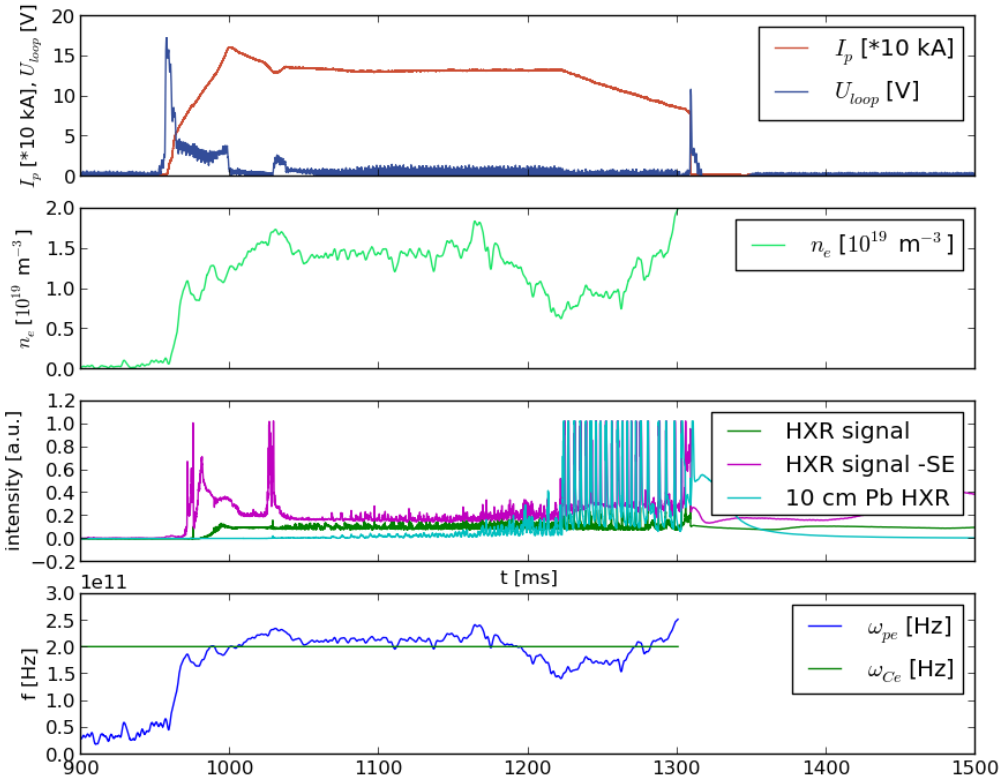

Figure 3.9: The most important plasma parameters (plasma current I_p and loop voltage U_{loop}, electron density n_e and signals from HXR detectors.) for the discharge #8559 with strong periodic HXR emission that is probably caused by Parail-Pogutse instability, validation of the frequency condition for magnetic field on axis and interferometric density data is displayed in the last graph (notice that the low value of plasma frequency ω_{pe} after 1200 ms corresponds to the increased spiky signal of HXR detectors, the lead shielded detector included).

3.5.3 Ultra-long discharges

During the second campaign, interesting results regarding the pulse length were also achieved. In the slide-away regime, where most of the current is carried by RE, it is possible to keep loop voltage very low. This in turn means slower increase of the current in primary windings and a longer time to reach its limit. Using this advantage, the record discharge with length $t_p = 968\,\mathrm{ms}$ was produced. During these discharges, the signal from shielded HXR detector was rising and RE were probably produced and lost continuously. The parameters of the longest discharge are in figure A.1 in the Appendix. Unfortunately, most of the data acquisition channels were not prepared for this extended length of discharge.

3.6 Interpretation of RE production and losses in Golem

In the Golem tokamak [54], runaway electrons were observed in many discharges. Generally, when the quality of vacuum is worse, RE are present in most discharges. As the increased level of HXR radiation should be prevented due to the safety reasons, we will analyse the discharges with strong HXR production and give some suggestions how to avoid them. Two different types of discharges with HXR emission were observed.

3.6.1 Discharges with RE generation in the breakdown

The first type is characterised by HXR emission in the middle of the discharge. The HXR emission starts a few milliseconds after the plasma breakdown. The fact that RE losses usually terminate before the end of the discharge would suggest that these electrons originate in the breakdown, are accelerated to energies in the order of hundreds of keVs and drift to the wall. The basic plasma parameters for the discharge 18900 with very good plasma position stabilisation are displayed in figure 3.10. In this figure, the stable position may be observed on the image from fast visible camera (based on rolling shutter principle) that observes the radial position of plasma through one of the top ports. In the third graph of this figure, the Kruskal-Bernstein runaway rate of the Dreicer process is displayed together with the method used in the previous sections (density of particles in runaway region at given time). Both quantities are high in the very beginning of the discharge. This supports our hypothesis. However, the absolute values of these estimates are not completely reliable as the Z_{eff} and T_e values are considered to be constant.

3.6.2 Discharges with RE generation at the end

The other type of the discharge may be quite different in terms of the HXR emission. The group of discharges, that we now analyse, is connected with plasma position instability. The basic parameters of the discharge are displayed in the figure 3.11 and accompanied by simple estimate of runaway generation at a given time as in the previous figure. Also the image from a visible camera suggests that plasma collapses towards the high field side

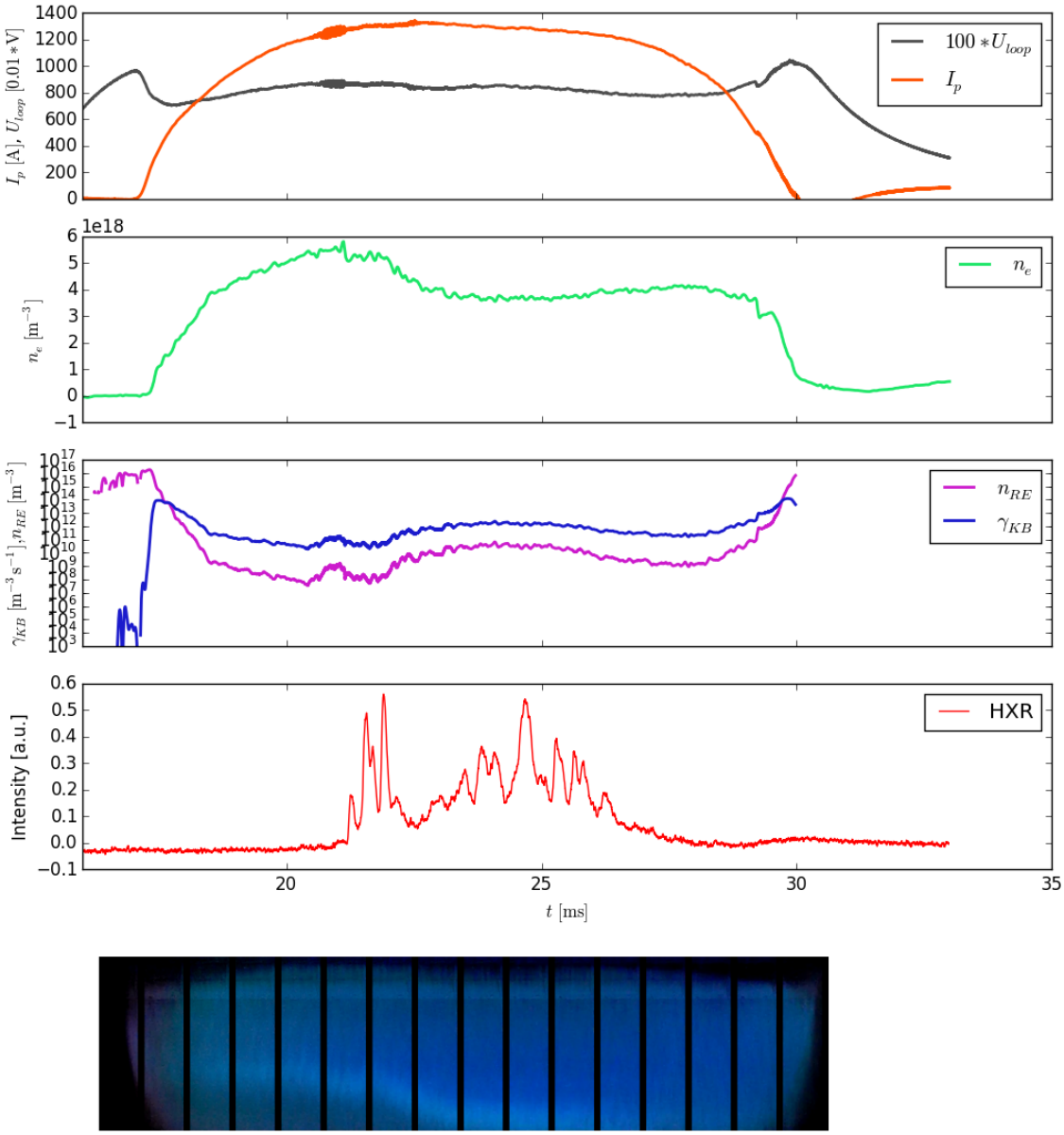

Figure 3.10: The main parameters of the discharge #18900 (from top: plasma current I_p and loop voltage U_{loop}, electron density n_e, HXR signal and top visible camera image) with plasma position stabilisation working properly. The measured quantities are accompanied by a rough estimate of possible number of runaway electrons at given time n_{RE} and the Kruskal Bernstein rate γ_{KB} for high $Z_{\text{eff}} = 6$ and estimated constant temperature $T_e = 10\,eV$.

(i.e. the direction towards the major axis) at the end of the discharge. This effectively lowers the density in the central part of the chamber and creates electric field higher that the measured one during the breakdown. The estimated value of RE under these conditions

confirms that the peak in HXR measurements is caused by electrons generated due to the position instability. The most suitable conditions for the RE creation are indeed towards the end of the discharge just before the peak in the HXR signal.

3.6.3 Other regimes and practical considerations

The two types of discharges described here can be combined, of course. If the vertical or radial kicks (fast movements) are applied using stabilisation coils, the conditions that were described in the previous paragraph can be repeated several times during the discharge. The sudden drop in density and rise in the electric field due to position instability is usually followed by HXR emission.
The largest issue for the RE generation is the bad quality of vacuum that causes extremely high loop voltage. In agreement with this statement, the series of discharges with the same pre-set parameters and long glow discharge before the first discharge were characterised by increasing level of HXR in subsequent discharges. This means that there is a lot of impurity atoms adsorbed on the walls and entering the plasma during standard operation. This effect is very different in larger machines with higher vacuum, where glow discharges usually make more favourable conditions for RE as it limits the recycling of deuterium gas (the level of impurities is much lower due to the better vacuum pumping and lower leakage rate). The recycling of deuterium may increase the density and create conditions less favourable for RE generation.
Golem operation without RE is preferable. To reach this, it is necessary to improve the vacuum pumping (maximum $p = 10^{-3}$ Pa before fuelling), operate at reasonable flat-top densities ($3 - 6 \cdot 10^{18}\,\mathrm{m}^{-3}$) and keep the plasma position stable. These steps should lower the breakdown voltage and also the flat-top voltage - for reasonable voltage on CD capacitors - below the threshold level for RE generation in present discharges.
Maximum energies of electrons can not be directly estimated using the detector currently installed as the decay time of pulse is too long and many peaks are integrated. However, the calculation presented in figure 1.1 suggest that the energy obtained by electrons in the Golem discharge can be hardly higher than 3 MeV. It is rather several hundred keVs or around 1 MeV as the impact on the wall usually comes 2-4 ms after the breakdown or 1-2 ms after the electric field ramp-up due to the position instability. Data from faster HXR detector used in former experiments [28] also confirm that the energies are in this range. Hopefully, Golem will be equipped with much faster scintillation detector in the future.

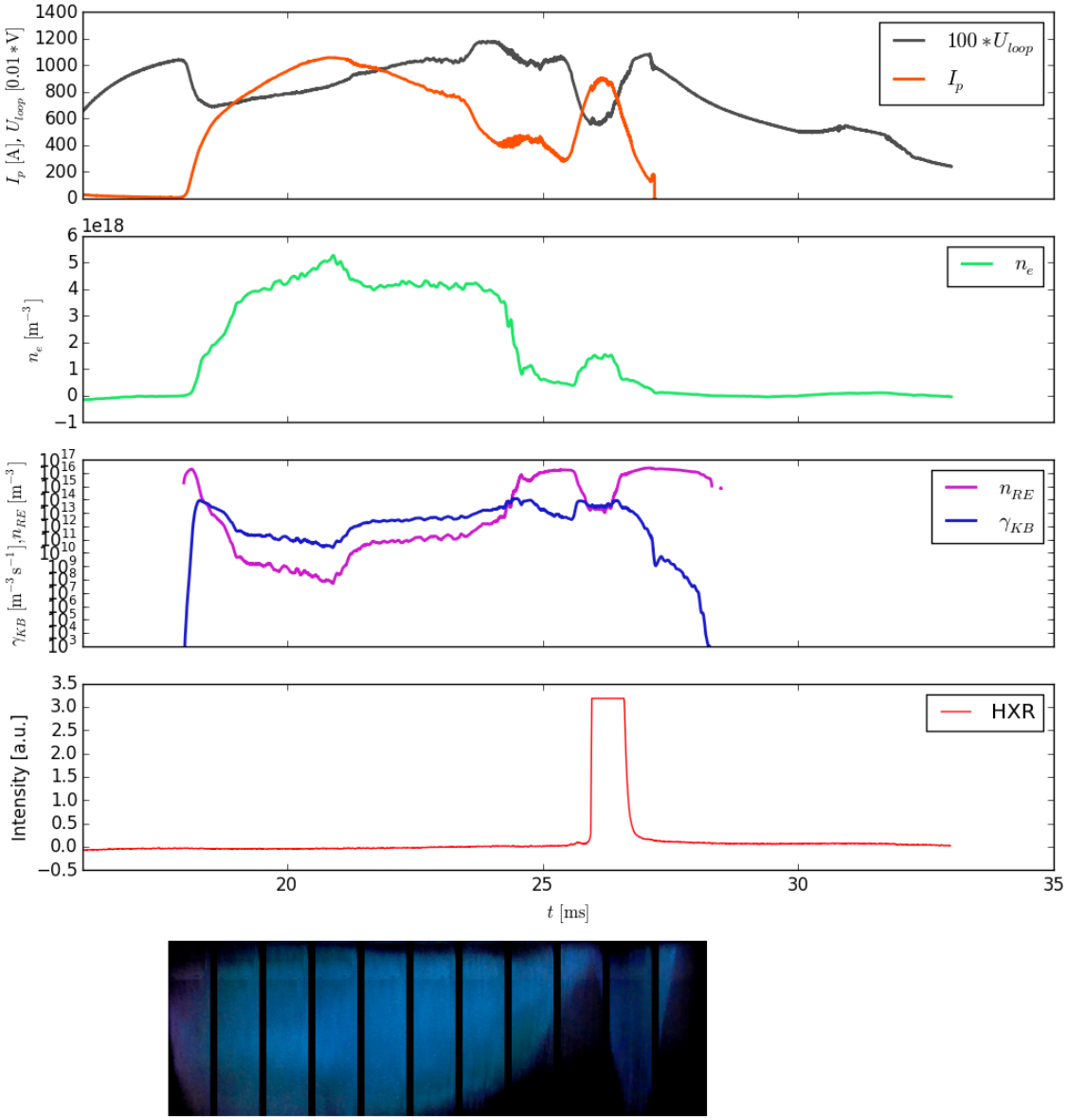

Figure 3.11: The main parameters (plasma current I_p, loop voltage U_{loop}, density n_e and measured HXR radiation intensity and top visible camera image) of Golem discharge #18950 with plasma position instability that leads almost to the termination of the discharge. The measured quantities are accompanied by a rough estimate of possible number of runaway electrons at given time n_{RE} and the Kruskal Bernstein rate γ_{KB} for high $Z_{\text{eff}} = 6$ and estimated constant temperature $T_e = 10\,eV$.

Chapter 4

Saw-tooth instability and runaway electrons in COMPASS

A clear coincidence of the saw-teeth instability with HXR emission (RE de-confinement) was observed during many discharges with the D-shape configuration on COMPASS. One session of the second runaway campaign was dedicated to investigate this phenomenon in further detail. Let us firstly describe the nature and properties of this instability.

4.1 Saw-tooth instability and COMPASS

Saw-tooth instability (STI) is one of the typical instabilities of tokamak plasmas [60]. It was observed at every present-day tokamak, with the exception of the smallest, low temperature machines. The observation on COMPASS and analysis of the correlations with other plasma events was published recently [25]. On JET it was even found that the period and intensity of this instability may be controlled by additional heating systems. STI, if frequent and relatively small, might be desirable due to its ability to clean the plasma center from impurities. On the other hand, massive ST may trigger neoclassical tearing modes (NTM) at some conditions. Such behaviour should be avoided [4, 60]. Although the experimental occurrence is well documented, the theoretical nature of this instability is not yet fully understood. However, saw-teeth instability is one of the phenomena of resistive magnetohydrodynamics and it is accompanied by the reconnection of magnetic field lines. This instability may be easily identified by periodic signal of soft X-ray detector observing the plasma centre. This signal consist of slow rise and sudden crash - the shape of the signal is where the name of the instability comes from. The signal of the detector observing the outer regions of plasma seems like the inversion of the signal from plasma center, while the signal of some channel observing the region in between is almost constant with typical spike during the crash (see Figure 4.1). Because the SXR detectors measure namely slightly supra-thermal bremsstrahlung radiation that is proportional to the square root of temperature, these signals are interpreted as the periodical rise of temperature in central plasma and sudden flux of the hot plasma to the outer regions. According to this interpretation, there has to be also some "inversion radius", where the temperature remains unchanged before and after the crash. This corresponds to the signal

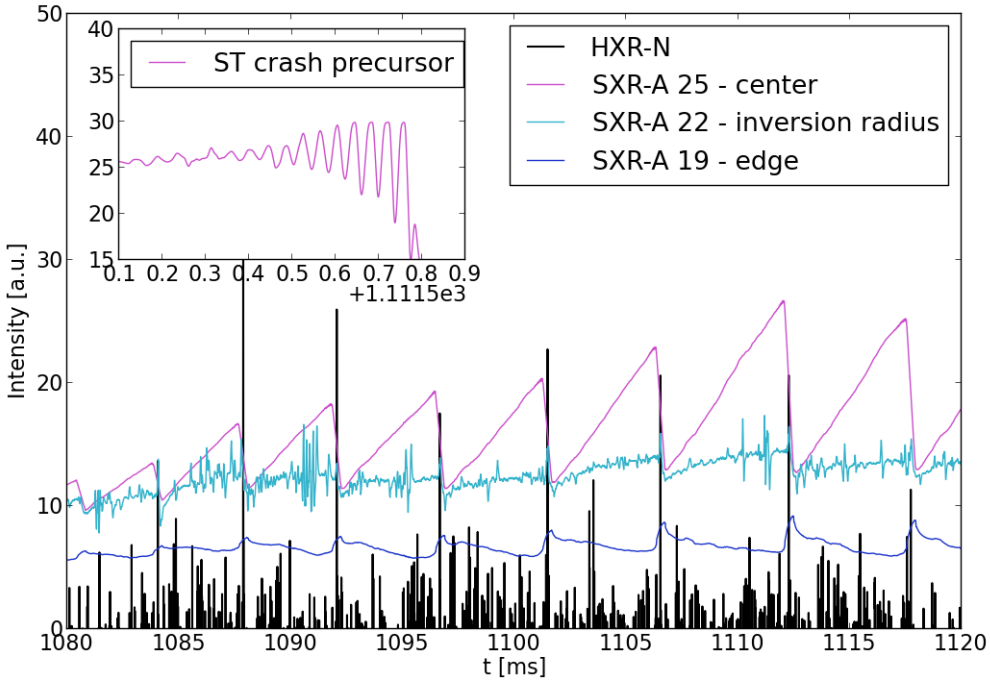

Figure 4.1: The typical signal of three soft X-ray detector channels during the saw-tooth instability and bursts of HXR radiation during the ST crashes. The detail of the precursor of the ST crash - massive internal kink (top left). Discharge 4420, very large ST due to NBI heating (full power).

of the channel 22 in 4.1, where the peak is caused by the hot plasma passing through the region. The amplitude and period of the STI in the shot displayed was increased due to the NBI heating, the usual period of STI in Ohmic regime is 2-3 ms and the amplitude is several times smaller.
The phenomenon of the increased HXR emission during the ST crash is documented in figure 4.1 and statistically analysed in 4.2. Although the ratio of ST ramp-up time to ST crash time is very high, a significant part of HXR radiation is released during the crashes and moreover, higher amplitudes of peaks dominate. However, the amplitude is related rather to intensity than to energy of particles in the case of our measurements.

4.2 Internal kink and Kadomstev ST crash model

The mechanism of the internal kink is thought to be responsible for the initial phase of the STI. Let us remind the relation for calculation of the safety factor q (1.31) that was defined in the first chapter. Due to the higher heating efficiency in central plasma region the strong peaking of the current is observed in some discharges. This increases the value

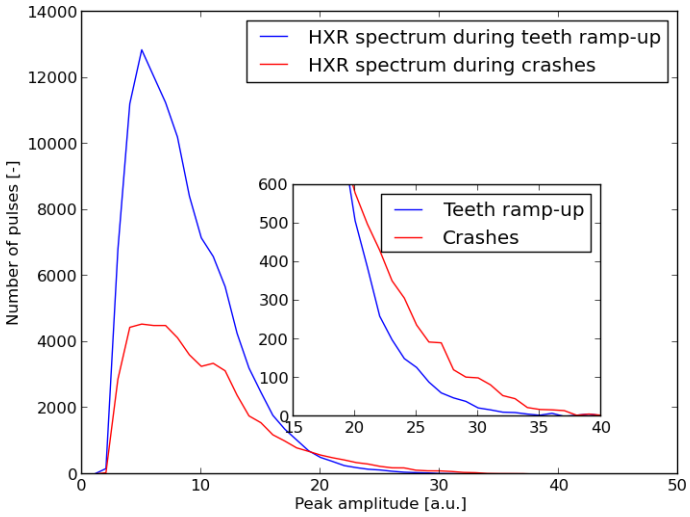

Figure 4.2: Comparison of the HXR peak height spectra during the teeth crashes and teeth ramp-ups for 25 shots with the described phenomenon. The very high peaks were detected dominantly during the crash. However, the signal is characterised by large number of pile-ups, thus higher peaks are probably caused by integration of peaks due to increased intensity rather than due to higher energy.

of the poloidal field and the value of the parameter q drops below one in the central plasma region. On the radius $q = 1$, the MHD instability with poloidal mode number $m = 1$ and toroidal mode number $n = 1$ occurs. This event is similar to the $m = 1$ (kink) instability of plasma cylinder observed in pinches and described in [29]. It can be considered as the displacement of hot central plasma. The transfer of the heat between the region inside the surface $q = 1$ and the region outside is incomplete and the temperature in the center rises and resistivity drops even more. The growth of the kink instability in the form of ST crash precursor may be identified as the oscillating SXR signal in the figure 4.1. According to the Kadomtsev model, this situation becomes unstable sooner or later, the displacement of region undergoing the kink instability results in crowding of magnetic field lines and subsequent creation of X-point via the magnetic reconnection [4]. The cooler $m = 1$ magnetic island is created and grows unless it fills entire volume of plasma centre and all the hot plasma is expelled from the center to outer regions. The reconnection is completed and new equilibrium with rising temperature in the center is established.

4.3 Possible explanations

A dedicated session of COMPASS RE experiments was focused on the phenomenon described in this chapter. Its aim was to investigate the origin of runaway electrons in these discharges. Before the session, three hypotheses were considered, although some of them were less probable

1. Generation of RE during by standard mechanisms during the flat-top and losses enhanced by the ST instability

2. RE originating in the plasma breakdown and ramp-up phase thrown out of the plasma dominantly during the ST crash

3. RE electrons accelerated during ST crashes in the electric field created by the reconnection phenomena

4.3.1 Constant acceleration

Regarding the results in section 3.3.1, the first option can be theoretically excluded as the density was up to $8 \cdot 10^{19}\mathrm{m}^{-3}$ in some discharges where the phenomenon was observed. At the same time, the electric field (proportional to the loop voltage) was rather small and no runaway electrons should be created by Dreicer mechanism during the flat-top.

4.3.2 Losses of ramp-up RE

Based on the fact that the conditions for runaway electron generation are satisfied only in the current ramp-up in high-density discharges, this option looks promising. However, in circular discharges density seems to be the limiting factor for the RE confinement (RE are mitigated in densities as low as $n_e = 3 \cdot 10^{19}\,\mathrm{m}^{-3}$ in COMPASS). The described phenomenon was observed in shaped discharges, usually with much higher density (up to $n_e = 8 \cdot 10^{19}\,\mathrm{m}^{-3}$) and HXR radiation was emitted during the whole discharge. This is surprising and it indicates that the confinement is much better in shaped plasmas. The reason could be connected with different structure of magnetic islands and other MHD activity.

4.3.3 Acceleration by reconnection-induced electric field

On the other hand, the third option was considered in many publications from various machines including TCV [27], T-10 [48] and DIII-D [49]. Notice that in these articles, supra-thermal electrons, not necessarily runaway electrons, are considered. Let us describe the idea of this mechanism briefly.
As described in the previous sections, the saw-tooth instability is connected with magnetic reconnection according to models currently accepted by the fusion community. During the reconnection the fast change of the magnetic field $\mathbf{B}$ may create the electric field $\mathbf{E}$ according to the Faraday law

$$\nabla \times \mathbf{E} = -\frac{\partial \mathbf{B}}{\partial t}. \tag{4.1}$$

In our case the toroidal electric field is important in order to accelerate the runaway electrons and therefore the change of the poloidal magnetic field is of interest. Moreover, the fast change is connected with the poloidal component of magnetic field due to the change

in the plasma current profile. We can make a rough estimate of electric field magnitude by simplifying the differential equation to linear variations of desired components

$$\frac{\delta E_t}{\delta r} \sim -\frac{\delta B_p}{\delta t}. \tag{4.2}$$

The characteristic length δr is the radius of the $q \leq 1$ area which is equal to 10 cm maximum in COMPASS, while the time of the crash δt is in the order of tens μs (we will use the value 100 μs). The change of the poloidal field will be estimated using the assumption that the safety factor on axis is changed from the value before the crash q_0 to 1 after the crash. The value of q_0 in discharges is hard to obtain for small ST because the EFIT is not able to reconstruct the plasma current profile accurate enough and sometimes shows value rather higher than 1. However, we can estimate the value as 0.95 which is typical for ohmic ST on other machines according to [49]. This difference must be multiplied by the value of poloidal field on the $q = 1$ radius which is possible to get from the approximation for circular plasma (1.31) and the magnitude of the toroidal magnetic field on axis. This approximation gives $B_{p1} = 0.2\,\mathrm{T}$. We can estimate the induced field using the final relation [49]

$$E_t \sim (1 - q_0)\delta r \frac{B_{p1}}{\delta t} \sim 10\,\mathrm{V/m}. \tag{4.3}$$

This value is much larger than the electric field due to the loop voltage. Furthermore, the value is further increased for faster crash or stronger plasma current peaking. On the other hand, the author of the text [49] used vacuum approximation, the reality in plasma will be much more complicated due to complex reaction of surrounding plasma to the locally induced electric field. Finally, such a field is generated in a rather small reconnection region and relatively low number of electrons can be affected. In the technical report [49] this field is used in simple one-dimensional model that utilises Kruskal-Bernstein primary generation term (2.26), simplified avalanche generation term ($\tau_A^{-1} = \frac{eE}{2m_e c \ln\Lambda}$) and diffusive loss term due to the perturbed field $\tau_{loss}^{-1} = f\left(\frac{\delta B}{B_T}\right)$. The author is using Rechester-Rosenbluth diffusion term [49] which was mentioned in the second chapter but it is not fully appropriate for this case. The model equation reads

$$\frac{dn_r}{dt} = \gamma_{KB} + \frac{n_r}{\tau_A^{-1}} - \frac{n_r}{\tau_{loss}^{-1}}. \tag{4.4}$$

We believe that the use of this model in this case is very inappropriate. For the fields near or above the Dreicer field (this is the case according to the report) the Kruskal-Bernstein runaway rate should not be applied. In this case, all the population of electrons should run away in the region of the high electric field. On the other hand, it is not possible to say how many times the electrons cross the reconnection region before they are deflected. In the text of the report, no hard limit on the number of electrons that are allowed to runaway is specified. Our re-implementation of the model was not successful and there is a question, how the author was able to get the reasonable values of RE density. Nevertheless, although there is some inconsistency in the technical reports on this topic, the acceleration during reconnection phenomena must be considered as a potential source of RE seed.

	#8632	#8633	#8634	#8636	#8637	Data source
I_p [kA]	165.99	163.21	167.5	163.33	164.11	Rogowski coil
$n_{e,FT}$ [10^{19} m^3]	7.5	8	8	8	8	Interferometer
T_e [eV]	-	500-600	600-700	600-700	-	Thomp. scatt.
U_{loop} [V]	1.67	1.74	1.77	1.76	1.76	Flux loop 02
B_{T,R_0} [T]	-1.15	-1.15	-1.15	-1.15	-1.15	Tor. flux loop
q_{95}	4.8	4.9	4.9	4.9	4.9	EFIT
GP 940ms [%]	20	20	30	20	30	Waveform
GP 960ms [%]	20	50	70	20	70	Waveform
$n_{e,975}$ [10^{19} m^3]	0.60	0.84	1.65	0.80	1.10	Interferometer
ST period [ms]	2	2	2	2	2	SXR-A
HXR emission	Strong	Medium	Weak	Strong	Weak	HXR-N

Table 4.1: Comparison of important plasma parameter values and other relevant quantities for five ST-RE dedicated shots. Parameter values correspond to the flat-top phase of the discharge, if not stated otherwise. GP means deuterium gas puff (fuel injection).

4.4 Comparing discharges

To find out which of the hypothesis described above is valid in our case, we decided to prepare a dedicated experimental session. An optimal scenario was to mitigate the electrons from breakdown and see if some HXR signal still follows the ST crashes. The optimal way how to do this is to change the waveform of the initial gas puff and limit the conditions for RE production during the ramp-up. A series of discharges with the same pre-set parameters was conducted. The parameters of the most relevant discharges from the dedicated session are summed up in the table 4.1. It is obvious that all the discharges were very similar in general. The different gas puff waveforms for the beginning of discharge are also displayed in the figure 4.3. Notice that slightly changed conditions during the breakdown resulted in complete suppression of HXR emission during the whole discharge. The comparison of the two discharges with different initial gas puff is in figure 4.4. Although ST instability is still present, no HXR emission is observed in the second discharge. The different gas puff waveform changed the initial density significantly as is obvious from the small graph. This is clear confirmation of the second considered option explained in section 4.3.2. The initial number of RE is crucial for the whole discharge. To increase the reliability, this pair of discharges was repeated after very long glow discharge. The result can be seen in the figure 4.4. There are some minor differences in HXR emission comparing to the first pair of discharges, however, generally speaking, the discharges were successfully repeated. The response of the density to the gas puff has changed slightly, however this is probably caused by recycling of gas. In one of the discharges, also third type of waveform with smaller increase during the breakdown was used (see the figure A.2 in the Appendix). This resulted in weaker HXR emission with respect to discharges 8633 and 8636.

Now, the nature of the phenomenon is uncovered and it is useful to find out if we can explain the difference between the discharges using the estimation for the density of elec-

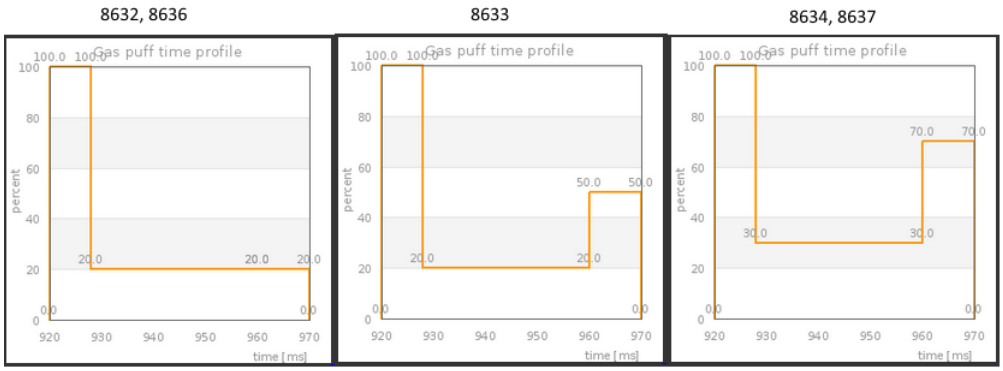

Figure 4.3: The initial fuelling waveforms used in the compared experiments. Plasma breakdown occurs slightly before 960. The plasma density response to the increased puff is several microseconds delayed and may be observed with microwave interferometer.

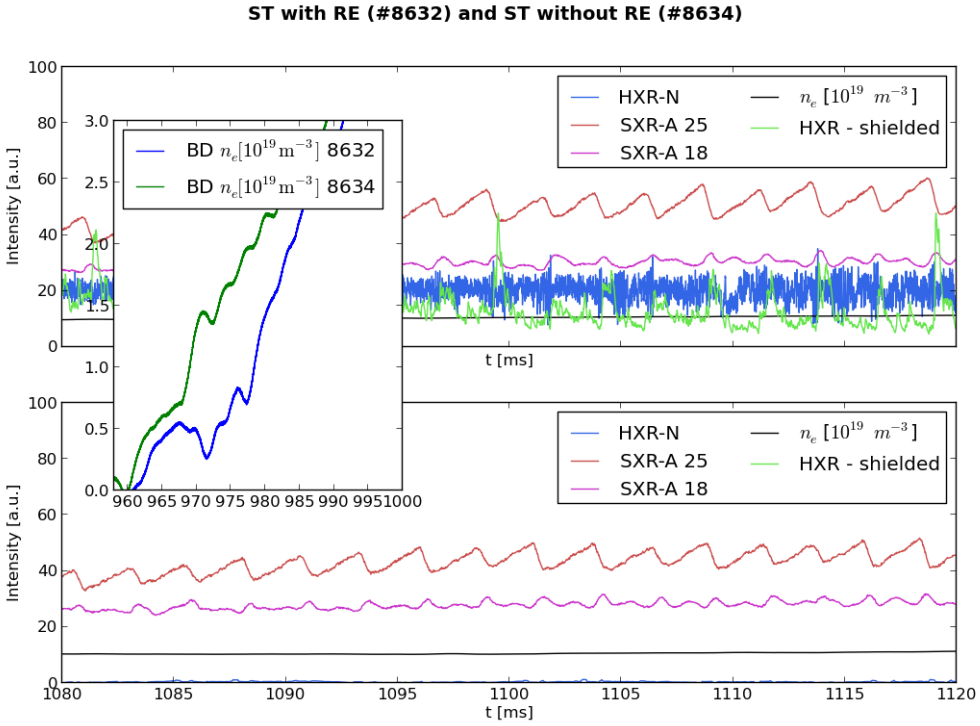

Figure 4.4: Main graphs: Graphical comparison of relevant signals for first pair of discharges with different initial fuelling. In shot #8632 the strong presence of runaway electrons losses were detected - standard HXR detector is saturated (blue curve), but the shielded one (green) sees increased emission during crashes. On the other hand in the shot #8634, no high energy photons appeared. Inserted graph: comparison of actual density during the first part (breakdown) of the discharges.

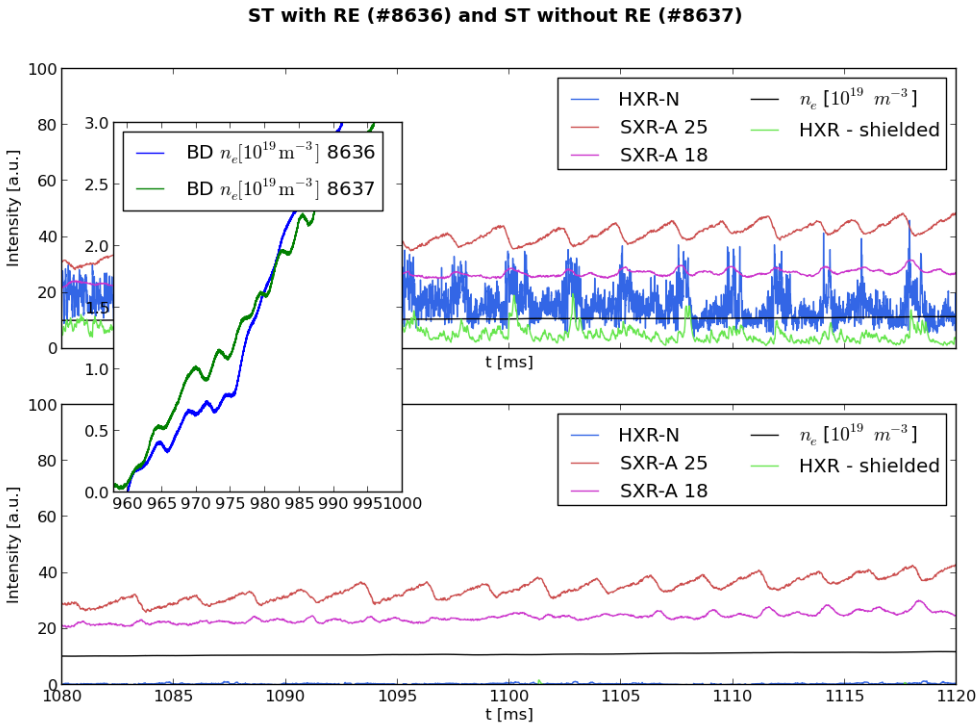

Figure 4.5: Successful repetition of the discharges #8632 and #8634 after long glow discharge.

trons in the runaway region for the ramp-up phase. We will again use the relation (2.24). The resulting estimation for the first 30 ms of the selected discharges are in figure 4.6. The differences between the HXR signal in the flat-top are well correlated with the differences in the prediction namely in time range 965-980 ms. The number of electrons being generated in later part of the discharge is negligible - as it is calculated in the figure A.3 in Appendix. To enrich the statistical significance of these results, several tens of similar discharges were analysed. In figure 4.7, the correlation between the mean value of the number of particles in runaway region n_{RE} during the ramp-up and averaged HXR signal in later phases of the discharge is displayed. The positive correlation is clear, however, points namely in the right part of the figure are very scattered. This can be caused by many factors, including the imperfections of standard HXR detector or imprecision of density measurements. We should also remind that our model is very simple. A question arises, whether the avalanche mechanism can contribute to the sustainability of the RE population in the plasma. According to the simple estimation using the flat-top parameters, the contribution of avalanche mechanism is not negligible, however it can add just several tens of percents to the seed population.

Let us briefly sum up the results of the dedicated session. It was found out that the increased HXR emission during the crashes of saw-teeth instability in the flat-top is caused by the losses of RE generated during the breakdown and plasma current ramp up. Reconnection processes in COMPASS plasma seem not to be able to create RE population of detectable level. Creation of supra-thermal electrons that cannot be detected by HXR detectors is not excluded.

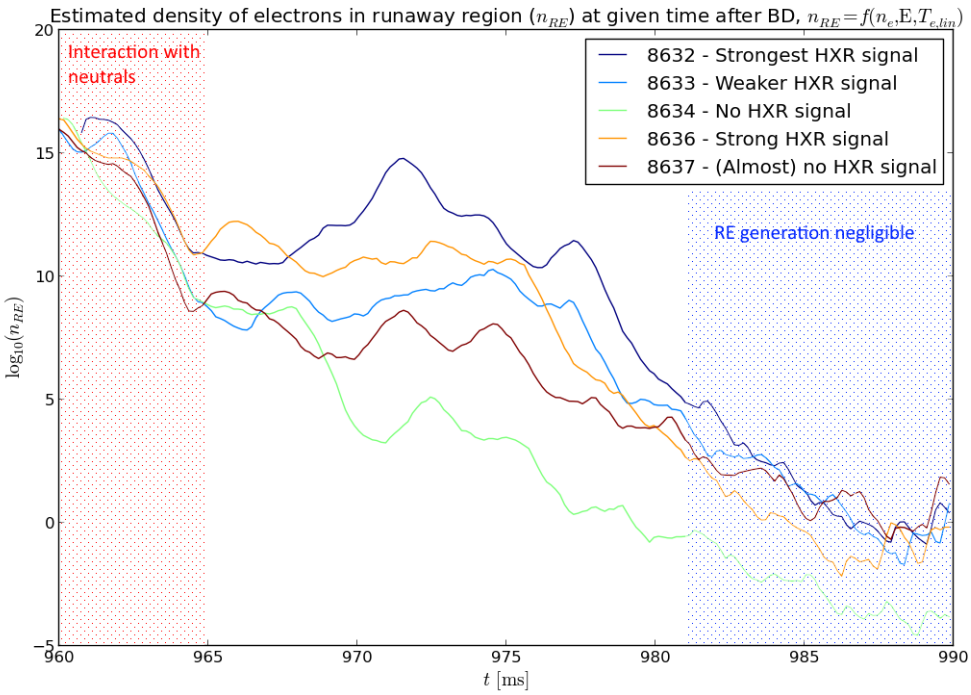

Figure 4.6: Analytical estimation of number of electrons in runaway region in the beginning of the discharge. The same linear increase of temperature and $Z_{\text{eff}} = 2.5$ is assumed for all discharges, however this assumptions change only the absolute value and not the relative differences between the curves. The comments on HXR intensity in the legend are related to the flat-top of the discharge. The intensity of HXR in the flat-top seems to be very well correlated to the estimated number. The regions that seem not be crucial for RE electron generation are dashed.

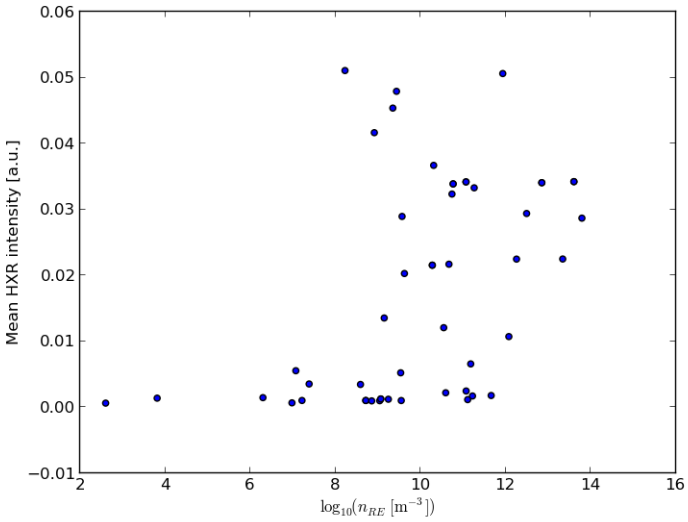

Figure 4.7: Correlation of averaged density of electrons in the runaway region in the beginning of the discharge (960-990 ms) calculated using relation (2.24) as in figure 4.6 and mean HXR signal in later phase of the discharge. Approximately 50 discharges with similar parameters were analysed. It is obvious that the generation of RE in the beginning affects whole discharge. On the other hand, the correlation seems not to follow a particular function dependence as it has rather a threshold character. However this could be caused by detector imprecision and other reasons.

4.5 Third campaign - validation and additional results

In the third campaign, which was conducted in the end of April 2015, the results were confirmed again. However, the response to the gas puff change was not so sharp this time. Furthermore, due to the changes in the interferometer signal (hardware filter removed), the density data from the beginning of the discharges have to be smoothed and compared very carefully with older data. It was proven that increased puff is able to suppress RE generation also in circular discharges with medium density ($n_e = 3 \cdot 10^{19}\,\mathrm{m}^{-3}$, discharge number #9910 with RE and #9911 without RE). According to the new data it also seems that the standard timing for increased puff (960-970 ms) is optimal because it reaches the plasma in the phase when it is already hot and the loop voltage is still high. Postponing of the increased puff results in lower efficiency of RE suppression.

4.6 Dependence of losses on plasma current and possible role of magnetic islands

In the third campaign it was also noticed that high current can result in earlier termination of the HXR radiation, i.e. RE electron confinement is worse. This confirms that MHD instabilities in general (not just ST) are crucial for RE confinement and losses. The comparison of four discharges with different plasma current is in figure 4.8. This comparison together with significant correlation of RE losses with rapid changes in the MHD mode structure (observed on spectrograms of the Internal Partial Rogowski Coils signals) is favourable to the hypothesis that the RE electrons may be confined in magnetic islands (partially isolated magnetic structures with possibly different values of plasma parameters). The decay of these structures then leads to increased losses according to [26] and many other publications. The losses in the flat-top of the discharge are dominantly periodic (with period around 1 ms), even without observable saw-teeth instability. This behaviour may also indicate the influence of some MHD activity. Furthermore, the correlation of the RE presence in plasma with different, high frequency modes (around 1 MHz) is currently under investigation on COMPASS.

4.7 RE losses during ELMs

Stable and highly reproducible H-mode discharges were achieved on COMPASS in recent months. During the improved confinement in the H-mode, there is a periodical emission of HXR radiation in some discharges. The peaks in the HXR signal seem to correspond to edge instabilities (ELMs) in the H_α signal. However, only the first few ELMs just after the L-H transition and the L-H transition itself are usually accompanied by these HXR bursts. After a more detailed analysis it was found that these ELMs coincide with saw-tooth crashes. Furthermore, according to the plasma current scan presented earlier it can be concluded that RE are released rather due to the MHD instabilities connected with high current than due to the transition to the H-mode here.

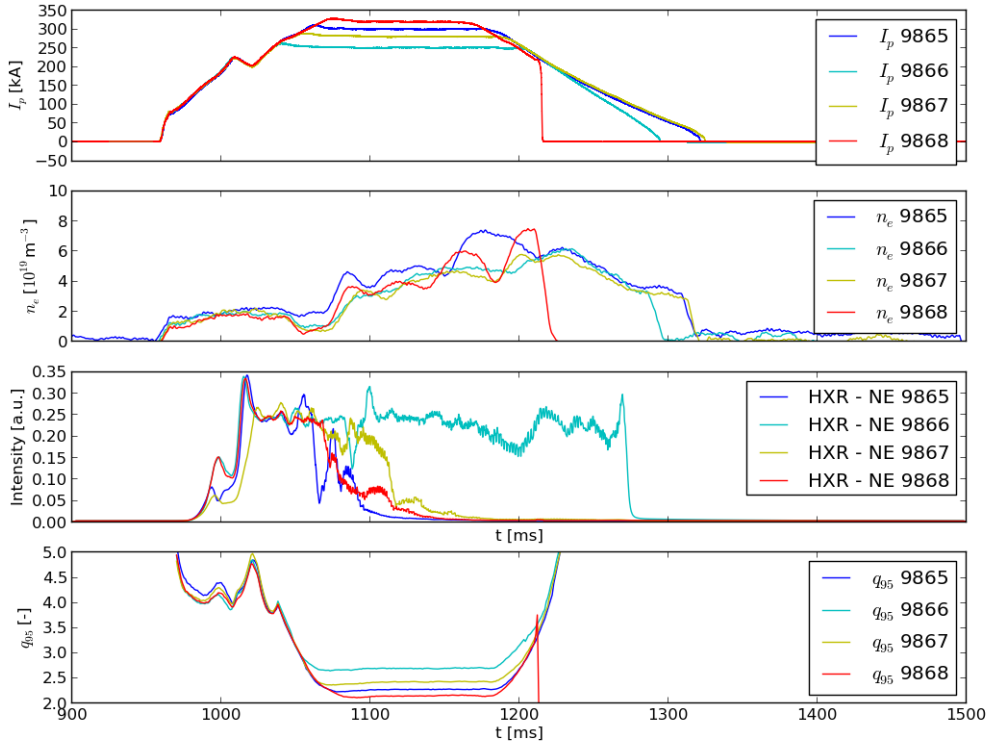

Figure 4.8: The comparison of four discharges with different plasma current I_p, the plasma electron density n_e for these discharges and a strongly smoothed HXR signal are displayed. The value of parameter q near the plasma edge shown in the third graph may suggest what modes are suspicious to be involved in RE confinement and losses. For example mode $m/n = 5/2$ could appear in discharge 9865, but not in others, and the HXR emission is also very different compared to others.

Summary and outlook

With ITER under construction, the controlled nuclear fusion for electricity generation is now closer than it has ever been before. However, there are many opened questions and challenges that we have to face and answer before the giant "box for the star" is commissioned. The safe operation of the machine has to be secured. This, among other issues, means that generation of the RE should be completely avoided as these fast particles can seriously damage the inner wall. Therefore, runaway electron generation, confinement, radiation, losses and mitigation must be studied on all present tokamaks, including COMPASS.

This thesis first summarises the theoretical model of runaway electron generation, transport and energy losses due to radiation processes. Furthemore, the relevant diagnostic methods are briefly described. The listed or derived relations for the RE generation are subsequently used to estimate significance of the RE for COMPASS and Golem tokamaks and interpretation of RE experiments conducted on both tokamaks with special interest in the RE electron bursts during the saw-tooth crashes.

In the first chapter, the physics background necessary for the RE description is introduced step by step. The chapter begins with the relativistic equation of motion for single particle in external field then turns to the relativistic drift equation, which is more useful to track a relativistic electron. Subsequent sections are focused on statistical plasma physics that is the most suitable instrument to treat the runaway electrons in plasma and simplified view of RE as a separate fluid in the thermal plasma.

The second chapter utilises the attitudes listed in the first chapter to the description of runaway phenomenon. In the beginning, the runway electron solution is derived from Fokker-Planck equation for electrons with electric field acceleration term and collisional term. This results in the definition of critical parameters for RE generation. Furthermore, complicated rates of primary and secondary generation (avalanche) are listed. The text continues with brief description of synchrotron and bremsstrahlung radiation of runaway electrons, losses due to the drift and radial diffusion and interaction of fast particles with the wall.

The third chapter is more practical, as the two Czech tokamaks and their typical discharges are described. The conditions for runaway electron generation in these devices are evaluated: the approximate number of electrons in runaway region is estimated for the breakdown and flat-top plasma and also the avalanche growth rate is considered. In the next part of the chapter the diagnostic tools related to runaway electrons and used on COMPASS and/or Golem are described. The chapter is concluded by analysis of interesting discharges in these tokamaks.

In the fourth - and final - chapter, namely the phenomenon of the RE bursts hitting the wall during the crashes of the saw-teeth instability is investigated. The possible explanations are considered and the dedicated session is described. It is concluded that this phenomenon may be suppressed by mitigating runaway electron generation in the beginning of the discharge with additional deuterium puff. This means that only losses and no primary generation of relativistic particles was observed during the reconnection phenomena. The differences between the discharges are explained using the estimation of RE generation during the ramp-up based on the simple relation derived in the second chapter. The results of the third dedicated runaway campaign confirm that both resistive and ideal MHD instabilities are very important for the confinement and losses of RE.

To conclude, we should remind that this thesis was partly elaborated in the framework of MST2-9 EUROfusion project and it was focused on runaway electron experiments in COMPASS and Golem tokamaks. The author of this thesis became the member of the runaway electron team and actively participated in the three RE campaigns that were conducted on COMPASS up to this time. In parallel to the work on COMPASS, runway electron discharges were also analysed on educational tokamak Golem, where intensive tests of new detectors are planned. The MST2-9 project will continue on COMPASS as the fourth campaign is scheduled for October. The comparison with results of other European tokamaks will be hopefully possible due to the scheduled participation in experiments on ASDEX-Upgrade, TCV and JET.

References

[1] BAKHTIARI, M.; KRAMER, G. J.; WHYTE D. G. *Momentum-space study of the effect of bremsstrahlung radiation on the energy of runaway electrons in tokamaks* Phys. Plasmas 12, 102503, 2005.

[2] BUSHBERG, T. J.; SEIBERT, J. A.; LEILDHOLDT, E. M.; BOONE, J. M. *The Essential Physics of Medical Imaging.* Chapter 3. Lippincott Williams & Wilkins, 2011.

[3] BAKER, J. *Free-Free (Bremsstrahlung) Radiation.* Astrophysics. Penn State University, Pennsylvania. http://www2.astro.psu.edu/~niel/astro485/derivations/baker-brem.pdf [4.3.2015]

[4] CHAPMAN, I. T. *Controlling Sawtooth Oscillations in Tokamak Plasmas*

[5] CARNEVALE, D. *A first approach to runaway electron control in FTU.* Fusion Engineering and Design 88 1109-1112, 2013.

[6] *CERN-Medipix collaboration.* Webpage. http://medipix.web.cern.ch/medipix/ [1.4.2015]

[7] COMMEAUX, N., et al. *Novel Rapid Shutdown Strategies or Runaway Electron Suppression in DIII-D* Nucl. Fusion 51 103001, 2011.

[8] CONNOR, J.W.; HASTIE, R.J. *Relativistic limitations on runaway electrons.* Nucl. Fusion 15, 1975.

[9] DECKER, J.; PEYSSON, Y.; BRIZARD, A. J.; DUTHOIT, F.-X. *Orbit-averaged guiding-center Fokker–Planck operator for numerical applications* Physics of Plasmas 17 112513, 2010.

[10] DIGHE, A.; *Lectures - Electrodynamics.* National Programme on Technology Enhanced Learning, India. http://www.nptel.ac.in/courses/115101004/downloads/module3/ed-3-1-2-new.pdf[14.2.2015]

[11] DREICER, H. *Electron and ion runaway in a fully ionized gas, I*.* Physical Review, vol. 115, 1959.

[12] FICKER, O. *Dekonvoluce dat z aktivačních sond jako metoda pro studium energií ionisujícího záření v tokamacích.* Bakalářská práce (Bachelor thesis), FNSPE CTU in Prague, 2013. http://fttf.fjfi.cvut.cz/StPrace/Bakalarky/2013/BP_FI_FTTF_13_ficker.pdf [13.12.2014]

[13] FICKER, O. *Runaway electrons on COMPASS and Golem tokamaks.* Research task, FNSPE CTU in Prague, 2014. http://physics.fjfi.cvut.cz/publications/FTTF/VU_Ondrej_Ficker.pdf [8.4.2015]

[14] FÜLÖP, T.; PAPP G. *Runaway Positrons in Fusion Plasmas.* Phys. Rev. Letters, 108, 225003, 2015.

[15] FEHÉR, T.; et al. *Simulation of Runaway Electron Generation During Plasma Shutdown by Impurity Injection in ITER.* Plasma Phys. Control. Fusion 53 035014, 2011.

[16] GALLMEIER,F.X. *General Purpose Photoneutron Production in MCNP4A.* Technical report. ORNL, 1995.

[17] GRANETZ, R. et al. *An ITPA joint experiment to study runaway electron generation and suppression.* Physics of Plasmas 21, 072506, 2014.

[18] GRYAZNYKH, D. A.; KANDIEV, Y. Z.; LYKOV, V. A. *Estimations of electron-positron pair production at high-intensity laser interaction with high-Z targets.* ArXiv. http://arxiv.org/pdf/physics/9909034.pdf [10.3.2014]

[19] GUAN, X.; QIN H.; FISH N.J. *Phase-space dynamics of runaway electrons in tokamaks* Physics of Plasmas 17, 092502, 2010.

[20] GUREVICH, A. V. *On the theory of runaway electrons.* Soviet Physics JETP, Vol. 12, Nr. 5, 1961.

[21] HOLMANN, E. M., et al. *Measurement of RE f(E) evolution following MGI into RE plateau.* REM Workshop, Gothenburg, 2014.

[22] HOLMANN, E.M., et al. *Control and dissipation of runaway electron beams created during rapid shutdown experiments in DIII-D.* Nucl. Fusion 53 083004, 2013.

[23] HUBA, J.D. *NRL Plasma Formulary.* Plasma physics Division, Naval Research Laboratory, Washington, 2013.
http://www.nrl.navy.mil/ppd/sites/www.nrl.navy.mil.ppd/files/pdfs/NRL_FORMULARY_13.pdf

[24] HUMPRIES, S. *Principles of charged particle acceleration.* University of New Mexico, Albuquerque, 1999.

[25] IMRÍŠEK, M.; WEINZETTL, V.; MLYNÁŘ, J., ODSTRČIL, T.; ODSTRČIL, M.; FICKER, O.; PINZON, J. R.; EHRLACHER, C.; PÁNEK, R.; HRON, M. *Use of soft x-ray diagnostic on the COMPASS tokamak for investigations of sawteeth crash neighborhood and of plasma position using fast inversion methods.* Rev. Sci. Instrum 85, 11E433, 2014.

[26] JASPERS, R.; et al. *Relativistic Runaway Electrons in TEXTOR-94.* 18^{th} Fusion Energy Conference, Sorrento, 2000. http://www-pub.iaea.org/mtcd/publications/pdf/csp_008c/pdf/exp2_06.pdf

[27] KLIMANOV, I.; FASOLI, A.; GOODMAN, T.P. and the TCV team. *Generation of suprathermal electrons during sawtooth crashes in a tokamak plasma.* Plasma Phys. Control. Fusion 49, 2007.

[28] KOCMANOVÁ, L. *Runaway electrons in the tokamak and their detection*. Master thesis, FJFI ČVUT v Praze, 2012. `http://fttf.fjfi.cvut.cz/StPrace/Diplomky/2012/KocmanovaLenka.pdf` [3.9.2014]

[29] KULHÁNEK, P. *Úvod do teorie plazmatu*. AGA, Praha, 2013.

[30] KRACÍK, J.; ŠESTÁK, B.; AUBRECHT, L. *Základy klasické a kvantové fyziky plazmatu*. Academia, Praha, 1974.

[31] LACKNER, K.; et al. *Fusion physics.* IAEA, 2012. ISBN 978-92-0-130410-0, chapter 3.

[32] LANDREMAN, M.; STAHL, A.; FÜLOP, T. *Numerical calculation of the runaway electron distribution function and associated synchrotron emission.* Computer Physics communications Vol. 185, Is. 3, 2014.

[33] LIU, J.; et al. *What is the fate of runaway positrons in tokamaks?* PHYSICS OF PLASMAS 21, 064503, 2014.

[34] LONGWEN, Y.; BINGREN, S.; YIMING, J. *Sawtooth-induced loss of runaway electrons in tokamaks.* Plasma physics and fusion technology, Vol. 33, Iss. 18, 2001.

[35] LOARTE, A., et al. *Magnetic energy flows during the current quench and termination of disruptions with runaway current plateau formation in JET and implications for ITER* Nucl. Fusion 51 073004, 2011.

[36] MANHEIMER, W. M. *The plasma assisted modified betatron.* Report. Naval Research Lab. Washington D.C. 1984.

[37] MARTIN, G. *Runaway electrons from Tore-Supra to ITER* Proc. 25th EPS Conf. on Controlled Fusion and Plasma Physics, Praha, 1998, pp. 651–654

[38] MARTÍN-SOLÍS, J.R.; et al. *Inter-machine comparison of the termination phase and energy conversation of the tokamak disruptions with runaway current plateau formation and implications for ITER.* Nucl. Fusion 54 083027, 2014.

[39] MLYNÁŘ, J. *Fyzika tokamaků (Physics of tokamaks).* Lectures, FNSPE, Czech Technical University, Prague.

[40] PÁNEK, R., et al. *Reinstallation of the COMPASS–D Tokamak in IPP ASCR* Czechoslovak Journal of Physics, Vol. 56, Suppl. B, 2006.

[41] PAPP, G.; DREVLAK, M.; FÜLÖP, T.; HELANDER, P. *Runaway electron drift orbits in magnetostatic perturbed fields.* Nucl. Fusion 51 043004, 2011.

[42] PAPP, G. *The role of magnetic perturbations in runaway electron and sawtooth dynamics.* Doctoral thesis. Chalmers university, Gothenburg, 2013.

[43] PLYUSNIN, V.V., et al. *Latest progress in studies of runaway electrons in JET.* 24th IAEA Fusion Energy Conference, San Diego, 2012.

[44] PLYUSNIN, V.V., et al. *Study of Runaway Electron Generation During Major Disruptions in JET.* Nuclear Fusion, 2006, 46.2: 277-284.

[45] PARAIL, V. V.; POGUTSE, O. P. *The kinetic theory of a runaway electron beam instability in a tokamak.* Nucl. Fusion 18 3, 1978.

[46] ROSENBLUTH, M.N.; PUTVINSKI, S.V. *Theory for avalanche of runway electrons in tokamaks.* Nucl. Fusion 37, 1997.

[47] RYDÉN, J. *Monte carlo simulation of runaway electrons.* Master thesis, Chalmers University of Technology, 2013. `http://ft.nephy.chalmers.se/JakobRyden_thesis_final.pdf` [3.9.2014]

[48] SAVRUKHIN, P. V.; TSAUN, S. V. *Sawtooth Instability and Magnetic Reconnection in Tokamak Plasma.* 19th IAEA Fusion Energy Conference, Lyon, 2002.

[49] SAVRUKHIN, P. V.; STRAIT, E. G. *Observation of suprathermal electrons during magnetic reconnection at the sawtooth instability in DIII-D tokamak.* General Atomics report GA-A24 144, San Diego, 2002

[50] SAINT-LAURENT, F. *Disruption and runaways electron mitigation studies on Tore Supra* EXS 2: 16, 2010.

[51] SCHOKKER, B. C. *Supra-thermal electrons in tokamak plasmas.* Doctoral thesis, Eindhoven University of Technology, 1996.

[52] SMITH, H. M.; et al. *Runaway electron generation in tokamak disruptions.* Plasma Phys. Control. Fusion 51 124008, 2009.

[53] SMITH, H.; Verwichte, E. *Hot tail runaway electron generation in tokamak disruptions.* 35th EPS Conference on Plasma Physics, Hersonissos, 2008

[54] SVOBODA, V.; et al. *Golem-wiki* Web encyclopedy of tokamak GOLEM. `http://golem.fjfi.cvut.cz:5001/`

[55] STAHL, A.; LANDREMAN, M.; PAPP, G.; HOLLMANN, E.; FÜLÖP, T. *Synchrotron radiation from a runaway electron distribution.* Physics of Plasmas 20, 2013.

[56] TRONCHIN-JAMES, A. N. *Investigations of runaway electron generation, transport, and stability in the DIII-D tokamak.* Doctoral thesis. University of California, San Diego, 2013.

[57] ÚLEHLA, I.; SUK, M.; TRKA, Z. *Atomy, jádra, částice*. Academia, Praha, 1990.

[58] VLAÍNIČ, M.; MLYNÁŘ, J.; WEINZETTL, V.; PAPŘOK, R.; IMRÍŠEK, M.; FICKER, O.; VONDRÁČEK, P.; HAVLÍČEK, J. *First dedicated observations of runaway electrons in COMPASS tokamak.* Submitted for publication in Nukleonika. 2014

[59] VLAÍNIČ, M.; MLYNÁŘ, J.; CAVALIER, J.; WEINZETTL, V.; PAPŘOK, R.; IMRÍŠEK, M.; FICKER, O.; NOTERDAEME J.-M. and the COMPASS TEAM *Post-Disruptive Runaway Electron Beam in COMPASS Tokamak.* Submitted for publication in Journal of Plasma Physics. 2015. http://arxiv.org/abs/1503.02947 [10.4.2015]

[60] WESSON, J. *Tokamaks*. Oxford University Press, New York, 2004.

[61] *World Energy Outlook* International Energy Agency, 2011. http://www.worldenergyoutlook.org/resources/energydevelopment/accesstoelectricity/

Important terms

Appendix

Appendix A

Additional figures

Ultra-long discharge

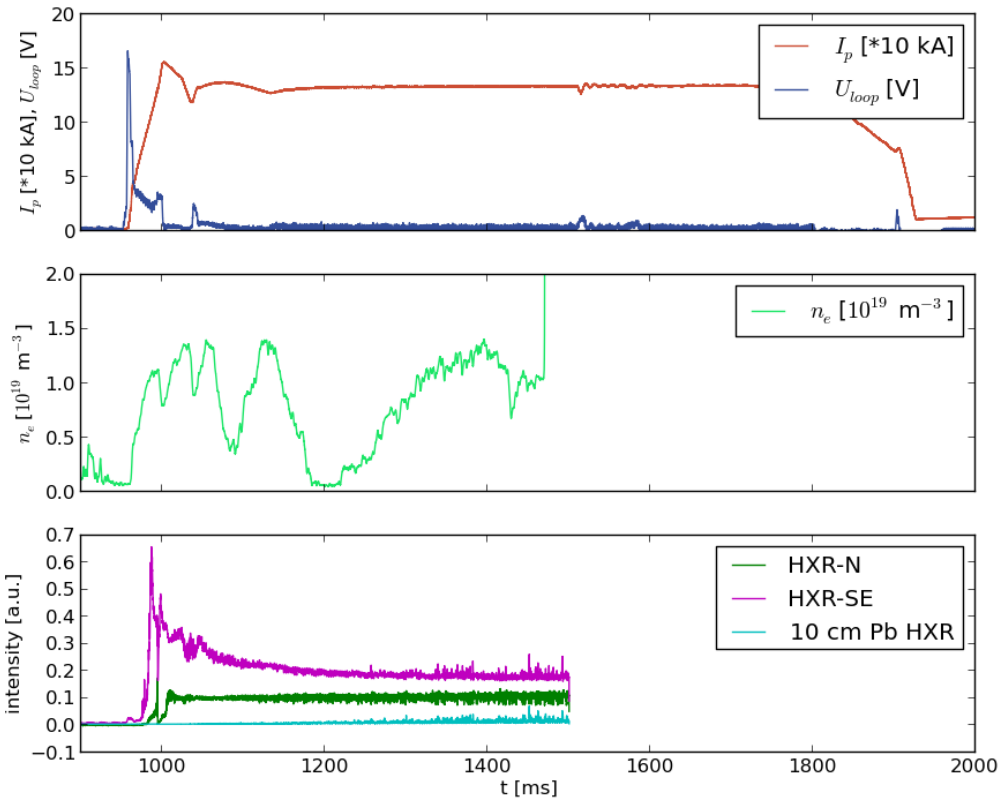

Figure A.1: The most important plasma parameters for the record-length discharge 8682. Unfortunately, data acquisition was not prolonged and therefore the graphs for electron density n_e and HXR measurements are not complete.

Partially and totally mitigated ramp-up RE emission during the saw-teeth instability

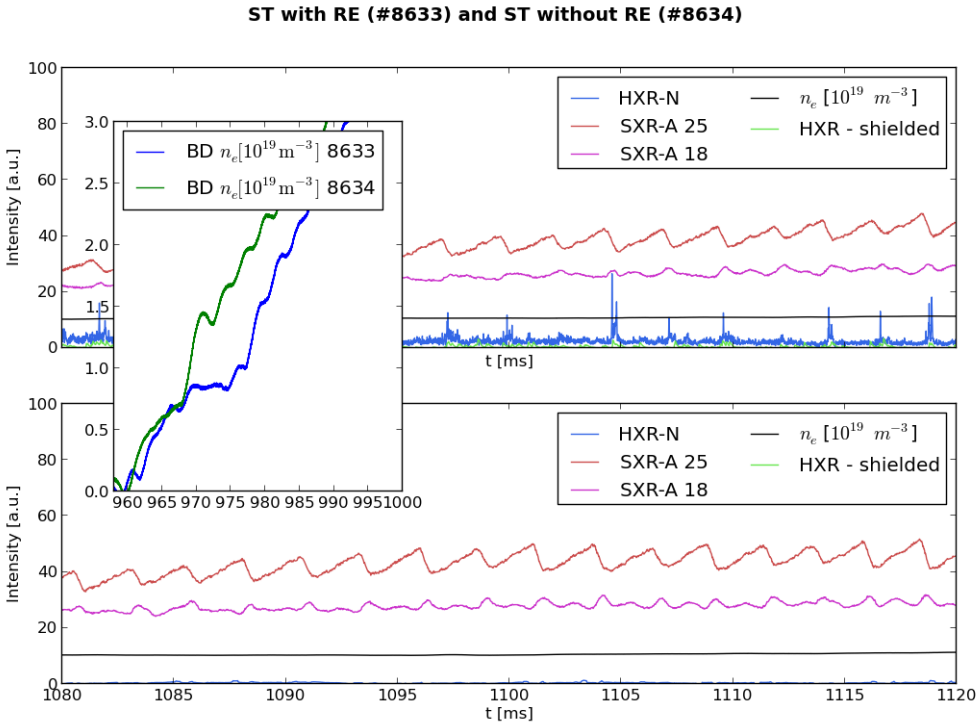

Figure A.2: Main graphs: Graphical comparison of relevant signals for first pair of discharges with different initial fuelling. Discharge 8632 with increased runaway electron losses during the STI. On the other hand, in the shot 8634 no high energy photons appeared. Inserted graph: comparison of actual density during the starting phase of the discharges.

No primary generation of RE for high density Maxwellian plasma in the flat-top of compared discharges

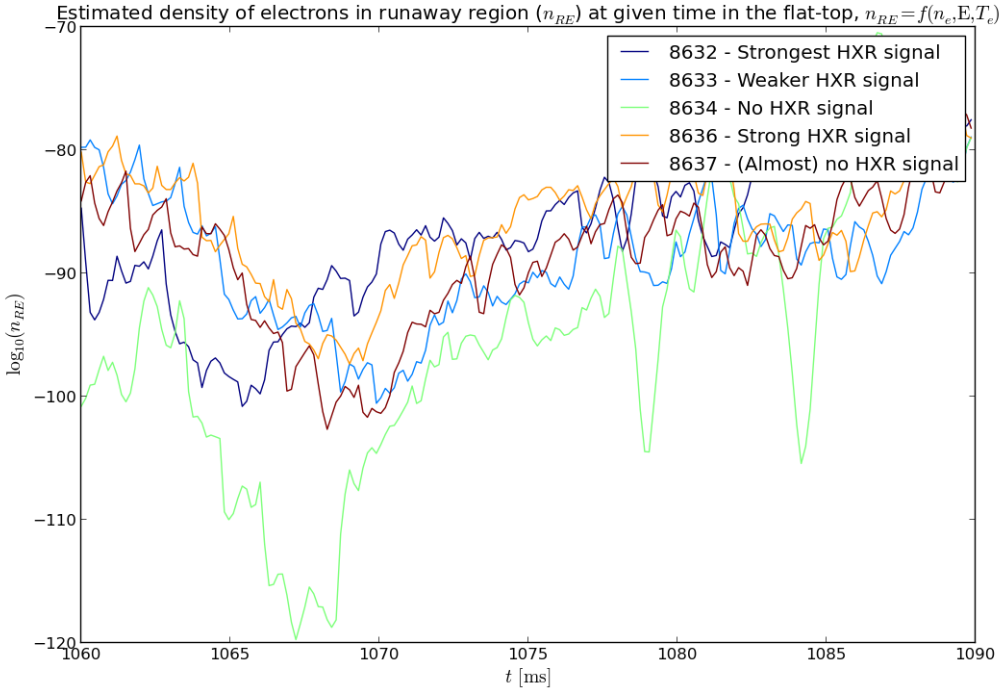

Figure A.3: The order of magnitude of number of electrons in runaway region at given time in the flat-top phase of the discharges described in chapter 4. The number is by far negligible for all discharges.

Appendix B

Cloud storage content

Electronic version of this document, some scripts that were used for model calculations, data analysis and plotting and working files are available at Google Drive `https://drive.google.com/folderview?id=0Bz7wTD2cnvNHSEFTNTZTXzZReFU&usp=sharing`.

Table of contents of this folder:

`DP.pdf`		electronic version of this thesis
`DP_x.pdf`		eventual extended versions of the document
`\Python`		scripts in Python
	`BB.py`	relativistic code for particle motion in EM field
	`NRE_est.py`	calculation of possible RE density for given range of plasma parameters
	`Golem_exp.py`	the previous script applied on measured Golem data
	`REC_model.py`	The model of RE generation and losses during reconnection events based on reference [49]
`\graphs`		figures used in the text

Scripts designed for the processing of publicly unavailable COMPASS data may be provided on demand.